TÉCNICO LISBOA

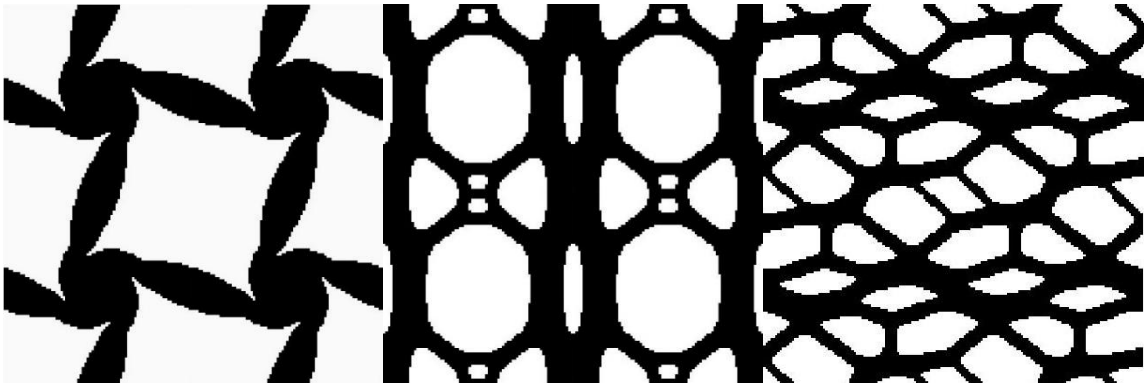

# Topology Optimization of Microstructures with Constraints on Average Stress and Material Properties

**Alexandre Manuel de Almeida Monteiro**

Thesis to obtain the Master of Science Degree in

**Aerospace Engineering**

Supervisors: Prof. José Arnaldo Pereira Leite Miranda Guedes

Prof. Hélder Carriço Rodrigues

**Examination Committee**

Chairperson: Prof. Fernando José Parracho Lau

Supervisor: Prof. José Arnaldo Pereira Leite Miranda Guedes

Member of the Committee: Prof. João Orlando Marques Gameiro Folgado

**November 2017**

Dedicated to my family and friends

# Acknowledgements

Firstly, I would like to express my gratitude to my supervisors. Professor José Miranda Guedes and Professor Hélder Rodrigues for their support, guidance, patience, advice and motivative input during this last year.

Secondly, a special thanks to Professor Krister Svanberg for his kind replies to my questions and for lending me his $MMA$ code that was essential to the completion of this thesis.

Thirdly, but most importantly to my family, for their unconditional love, support and trust throughout my life even in the bad moments.

Lastly, to all my friends, that have given me the motivation, happiness and companionship that I needed.

# Resumo

Otimização de topologia é uma abordagem comum no design de materiais estruturados. Trabalhos prévios centraram-se em problemas com constrangimentos de volume ou em problemas de minimização do volume com constrangimentos nas propriedades dos materiais. Um modelo computacional baseado em elasticidade linear é proposto para o design de materiais, combinando problemas de constrangimento de volume e propriedades materiais. Isto inclui, problemas de Maximização de Rigidez, de Módulo Volumétrico, de Módulo de Cisalhamento, e minimização do número de Poisson, com constrangimentos nos Critérios de Tensão de Von Mises ou nas Tensões Direcionais ou Propriedades do Material. Neste trabalho, o problema de densidades intermédias em otimização de topologia é abordado através dos modelos $SIMP$ e $RAMP$, as propriedades elásticas do material são calculadas usando ou um método de homogeneização baseado em condições de fronteira de periodicidade ou um método baseado na equivalência da energia média de extensão, e a otimização do problema é resolvida usando o esquema $OC$ ou o $MMA$. Para resolver o problema de tabuleiro de xadrez (checkerboard) um filtro de sensibilidades foi incorporado.

O programa foi codificado no software $MATLAB$, usando elementos finitos Bilinear de 4 nós. Apresenta várias opções de entrada, e foram apresentados numerosos resultados, com tempos de análise reduzidos, incluindo resultados não simétricos e auxéticos para uma variada gama de constrangimentos.

Contudo, alguns problemas relacionados com os constrangimentos nos Critérios de Tensão foram identificados. Discutivelmente, esses problemas advêm da formulação do problema, uma vez que a Rigidez é quase equivalente aos critérios de Tensões médias.

**Palavras-Chave:** Otimização de Topologia, Homogeneização, Microestruturas, $MATLAB$, Propriedades Elásticas dos Materiais.

# Abstract

Topology Optimization is a common approach used in the design of material structures. Previous works focused on mass constrained problems or minimization of mass with material properties constraints. A computational model for the design of linear elastic materials is proposed, combining both mass constrained problems with material constraints. This includes Maximization of Compliance, Bulk and Shear Modulus, and minimization of Poisson number with average stress criteria, single average stress parameters and material properties constraints.

In this work, the intermediate density problem of topology optimization is tackled with two different interpolation models, $SIMP$ and $RAMP$, the effective material properties are calculated using either a periodic boundary condition homogenization or a strain energy based approach, and the optimization problem is solved using an Optimality Criteria or $MMA$ schemes. Also, to solve the mesh-dependency problems and the checkerboard problem caused by lower order finite elements, a sensitivity filter is used.

The program was coded using the $MATLAB$ software, implementing the topology optimization problem with a Bi-linear 4-node finite element structured mesh.

Various user inputs and its influence were tested and discussed, and the results were overall satisfactory. The program presented numerous results with fast convergence times, including auxetic and non-symmetric materials with a varied set of constraints. However, problems with Maximum Stiffness Materials with average Stress Criteria's constraints were found. Arguably, those problems stem from the formulation of the optimization problem, since the stiffness is almost equivalent to the average Tension Criterias.

**Keywords:** Topology Optimization, Homogenization, Microstructure, $MATLAB$, Elastic Material Properties.

# Contents

# List of Figures

# Nomenclature

Greek symbols

| | |
|---|---|
| $\boldsymbol{\beta}$ | Optimality Criteria gradient parameter; |
| $\boldsymbol{\gamma}$ | Shear Strain, Finite Element aspect ratio; |
| $\boldsymbol{\varepsilon}$ | Strain tensor; |
| $\bar{\boldsymbol{\varepsilon}}$ | Average Strain Tensor; |
| $\boldsymbol{\varepsilon^0}$ | Unit Test Strain Fields |
| $\boldsymbol{\eta}$ | Damping coefficient in Optimality Criteria |
| $\boldsymbol{\kappa}$ | Bulk Modulus |
| $\boldsymbol{\lambda}$ | Lagrangian Multiplier |
| $\boldsymbol{\rho}$ | Density |
| $\boldsymbol{\sigma}$ | Stress tensor |
| $\bar{\boldsymbol{\sigma}}$ | Average Stress Tensor |
| $\boldsymbol{\upsilon}$ | Poisson Number |
| $\boldsymbol{\phi}$ | Compliance or Energy of Elastic Deformation |
| $\boldsymbol{\chi}$ | Nodal displacements corresponding to the strain test fields |
| $\boldsymbol{\Gamma}$ | Domain Boundaries |
| $\boldsymbol{\Omega}$ | Design domain |

Roman Symbols

| | |
|---|---|
| $\boldsymbol{B}$ | Finite Element Strain-Displacement Matrix |
| $\boldsymbol{C}$ | Stiffness Tensor from the Constitutive equations |
| $\boldsymbol{E}$ | Young's Modulus |
| $\boldsymbol{F}$ | Applied Forces Vector |
| $\boldsymbol{G}$ | Shear Modulus |
| $\widehat{\boldsymbol{H}}$ | Mesh Independent Convolution |
| $\boldsymbol{K}$ | Stiffness Matrix from the $FEM$ |
| $\boldsymbol{m}$ | Volume fraction |
| $\boldsymbol{mv}$ | Move Limit |
| $\boldsymbol{p, q}$ | $SIMP$ and $RAMP$ penalizations respectively |
| $\boldsymbol{r}$ | Filter Radius |
| $\boldsymbol{U}$ | Nodal Displacements Vector |
| $\widetilde{\boldsymbol{U}}$ | Arbitrary Vector from the adjoint equation |
| $\boldsymbol{u}$ | Displacement field |
| $\boldsymbol{u_e}$ | Macroscopic Displacement field |

Subscripts

| | |
|---|---|
| $\boldsymbol{e}$ | Element |
| $\boldsymbol{i, j, k, m, p, q, r, s}$ | Indexes |
| $\boldsymbol{mat}$ | Solid Material |
| $\boldsymbol{min}$ | Minimum or Residual |
| $\boldsymbol{VM}$ | Von Mises stress Criteria |
| $\boldsymbol{H}$ | Hydrostatic Stress |

Superscripts

| | |
|---|---|
| $*$ | Constraint |
| $\boldsymbol{H}$ | Homogeneous |
| $\boldsymbol{T}$ | Transpose |

# Glossary

| | |
|---|---|
| $FEM$ | Finite Element Method |
| $MATLAB$ | Matrix Laboratory. Multi-paradigm numerical computing environment from Mathworks, Inc. |
| $MMA$ | Method of Moving Asymptotes |
| $OC$ | Optimality Criteria |
| $RAMP$ | Rational Approximation of Material Properties |
| $SIMP$ | Solid Isotropic Material with Penalization |

# Chapter 1

# Introduction

The usual structural optimization practice has been to take an existing material and try to utilize it in the best conceivable way by varying the structures dimensions or shape. Nowadays all sectors of industry make use of computer-aided structural design when designing and developing new products. However, with the introduction of fiber reinforced composites, ways to design better structures were possible. After all, designing the right material for the right application can present numerous pay-offs, including higher stiffness to weight ratios, improvement of thermal or dynamic response to name a few.

Looking at any material through a microscope, a microstructure will be seen if the magnification is strong enough. The topologies and compositions of the individual microstructural levels are crucial for the effective properties of the material, thus, assuming a repetitive microstructure in the material, then its properties can be fully described by an analysis of the smallest repetitive unit.

This work intends to discuss the methods that apply the ideas of topology optimization, originally developed for structural optimization problems, to the design of materials, considering problems of maximum stiffness, prescribed material properties and average stress constraints, with the objective of implementing an efficient and simple computational model that can be effortlessly used by the academic community for further investigations.

## 1.1 Motivation

Topology optimization of structures is a rapidly growing field of particular interest to the automotive and aerospace industries. The cost of energy drives the need for more efficient solutions to the structural challenges that these industries face. Topology optimization, as opposed to shape optimization and sizing optimization can be used without a-priori assumption of the structural shape and connectivity, and allows the introduction of holes or cavities in structures which usually results in great savings in weight or improvement of structural behaviour such as stiffness, strength or dynamic response.

With the introduction of composite and cellular materials in industry, a new particular approach to the design of microstructures has recently gained some attention by the science and engineering community. It suggests that to produce the most efficient structures, not only should the specific structure be designed to match the needed application, it also suggests that the structure's material should be tailored for the local loading conditions.

In Aeronautics particularly, cellular and fiber reinforced composite materials represent a growing piece of the aerospace material pie. Once only considered for light structural pieces or cabin

components, composites' aerospace application range now reaches into true functional components such as wing and fuselage skins, engines, and landing gear. Composite components can be formed into complex shapes that, for metallic parts, would require machining and the creation of joints which are potential failure points within the aircraft.

Following this assertion, mathematical models that can efficiently evaluate and design structured materials with different properties are a necessary tool for the industrial and academic solution of problems yet to come.

For example, Negative Poisson Materials or Auxetic, which expand instead of shrinking when stretched, have been demonstrated to have enhanced shear resistance, indentation resistance and fracture toughness. Moreover, they have been shown to possess extraordinary damping, acoustic and dynamic crushing properties, hence making them have potential applications in the most diverse fields.

It is this enormous potential presented by exotic materials that drives the need for continuous research and experimentation in this subject.

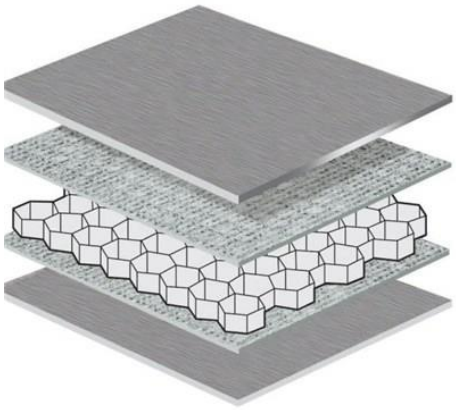

*Figure 1.1 – Honeycomb Sandwich Panel*

## 1.2 Overview

Even though Topology Optimization has been a debated subject for many years and can be traced back to 1904, Mitchell [1], the big preponderance it has gained started with the landmark paper in 1988 by Bendsøe and Kikuchi [2], who proposed a Structural Topology Optimization method based on a homogenization approach, using finite elements, where microscopic holes are created in the structure, resulting in a distribution of porous material. In 1989, Bendsøe [3] further developed this method to remove the microstructures and Rozvany et al. [4] later terms this novel approach with the designation of $SIMP$ method.

Using the $SIMP$ approach, Topology optimization methods have been demonstrated to be an attractive design approach in many fields covering mechanical and structural engineering, fluid dynamics, optical engineering and more [5]. Some structural problems include stiffest structure design subject to volume constraints [6, 7, 8], problems with multiple loading conditions [9], natural frequency

maximization [10, 11], compliant mechanism design [12, 13], and photonic crystal structures for low loss waveguide [14], structure volume minimization subject to stress constraints [15, 16, 17, 18, 19], and others.

Topology optimization has also shown its applicability to create novel materials with enhanced properties. In this way, material properties are tailored through a redistribution of the material layout in the microstructure, making it possible to create materials with exotic properties that are very attractive for modern technology. Using homogenization approaches to determine the material properties and sensitivities [20], material with high Bulk and Shear Modulus [21], Negative Thermal Expansion [22, 23], Negative Poisson Ratio [22, 24, 25, 26], novel piezoelectric properties [27] can be designed.

## 1.3 Objectives

A new problem is proposed in this work, in which the objective is the design of materials with certain properties, be it maximum stiffness or negative Poisson, while at the same time introducing different constraints than just the usual volume fraction constraint. The new constraints that are to be implemented are Stress Criteria constraints, Single Directional Stress Constraints and Stiffness Tensor Constraints.

To achieve that purpose a computational model is to be implemented. The program should be simple to use, require low computational resources and capable of implementing the most various type of constrained optimization problems.

To verify the viability of the implemented program, the influence of the user inputs should be studied for simple test analysis in order to understand and gain a certain sensibility to the program and which parameters should be used to reach the best results. Following, a study of the final results should be done, to understand in which problems did computational model excel or fail, and what can be changed in future work to attenuate those issues.

## 1.4 Outline

For an easier read and better organization of the topics of this work, it was decided to divide this thesis in 5 chapters.

The theoretical background was divided between Chapter 2 and 0, Chapter 4 will focus on the practical aspects of the mathematical model implementation, Chapter 5 will focus on result presentation and discussion, and Chapter 6 will be the conclusion.

In Chapter 2, Topology Optimization theory will be discussed. Methods of intermediate density penalization will be referred and the whole structural optimization process will be described including sensitivity analysis, optimization algorithms and filtering of sensitivities.

In 0, elastic material properties evaluation will be discussed, and how should the homogenization theories be applied in conjunction with Topology Optimization to the design of microstructures. Two methods of material properties evaluation will be discussed. One will be based on the homogenization theories and assumption of periodic boundary conditions and the other will be based on the classical micromechanics theory on the equivalence between average and micro strain energy.

The Chapter 4's theme is the implementation of computational model and how it works. Here, the finite element problem will be described and the boundary condition's implementation will be discussed.

In Chapter 5 the results will be presented and discussed. Starting with an explanation of the influence of the user inputs in the overall results, this chapter will then present the results to the constrained optimization problems that were the objective of this work.

Chapter 6 will be the conclusion for this work. A summary of the work and results, and the evaluation of completed objectives will be critically done. Also, future modifications and possible improvements to the present work will be proposed.

# Chapter 2

# Topology Optimization

## 2.1 Problem Formulation

Topology Optimization Goal is to maximize/minimize an objective function while at the same time satisfying several constraints, making it possible to obtain a final distribution of material within a certain domain. The final design is a combination of both spaces filled with material and empty spaces.

The design domain Ω is discretized by *N* finite volume elements, each of those is assigned a design variable $\rho_e \in [0,1]$ that represents its relative density, $e = 1, \dots, N$ .

Each element stiffness is dependent upon its element density $K_e[\rho_e]$, which in turn makes the assembled global stiffness matrix dependent on the overall distribution of densities across the domain, $K(\rho)$.

By the governing equilibrium equations

$$K(\rho) \cdot U = F, \tag{2.1}$$

Where $K$ represents the Global Stiffness Matrix, $U$ the displacement vector and $F$ the external loads.

In the design of the Topology of a structure the interest is to determine the optimal placement of a given isotropic material in space. To do so, one must find which of the elements in the discretized domain Ω, should remain void and which should be material, thus finding a rough description of the continuum structure boundaries. In discrete form, this corresponds to a black and white representation of the geometry with pixels given by the finite element discretization.

This approach implies that the constitutive material tensor for each element is characterized by

$$C_{ijkl} = 1\Omega_{mat} C_{ijkl}^{mat} \, , 1\Omega_{\mathrm{mat}} = \begin{cases} 1 \, , x \in \Omega_{mat} \\ 0 \, , x \in \Omega \backslash \Omega_{mat} \end{cases} \, , \tag{2.2}$$

Where $C_{ijkl}^{mat}$, is the constitutive tensor of the base material and

$$\int_{\Omega} 1\Omega_{mat} \cdot d\Omega = Vol(\Omega_{mat}) \leq V \, , \tag{2.3}$$

Represents the volume of the base (solid) element available, which is smaller than the total design volume $V$. This is the volume constraint that is commonly used in minimum compliance design problems.

## 2.2 Intermediate Density Problem

The definition of admissible $C_{ijkl}$ means that we have formulated a discrete valued design problem $(0-1\,problem)$.

To solve this problem, the most common approach is to replace the integer variables with continuous variables with some form of intermediate density's penalization that steers the solution to discrete $0-1$ values. The design problem becomes a continuous problem by modifying the stiffness matrix so that it depends continuously as a function which is interpreted as a density of material.

The required results consist of almost entire regions of material or no material and they are obtained by using common approaches such as $SIMP$ (Solid Isotropic Material with Penalization) [3] or $RAMP$ (Rational Approximation of Material Properties) [28].

On $SIMP$ approach, the material properties of the intermediate densities are given by:

$$E_e(\rho) = \rho_e^p \cdot E_{mat}\,, \quad 0 < \rho_e \leq 1, \quad p \geq 1 \tag{2.4}$$

Where $E_{mat}$, is the Young's Modulus of the solid material and $p$ is the penalization power.

The intermediate densities are penalized since while the cost volume only increases linearly with $\rho$, the stiffness of intermediate densities is very small for $p \geq 1$.

On $RAMP$ approach, the material properties are given by:

$$E_e(\rho) = E_{min} + \frac{\rho_e}{1 + q \cdot (1-\rho_e)} \cdot (E_{mat} - E_{min})\,, \tag{2.5}$$

In this way, the stiffness of intermediate densities penalised by the $q$ penalization coefficient.

If the purpose of the interpolation model is to be related to a composite made of two different materials, then $E_{min}$ relates to the Young's Modulus of the least stiff material.

For $SIMP$ one of the material phases is zero, $E_{min} = 0$ , but we can also derive the corresponding expression by

$$E_e(\rho) = E_{min} + \rho_e^p (E_{mat} - E_{min})\,, \tag{2.6}$$

However, if the goal of the design is a two-material structure, the $RAMP$ model is in a sense more physical than the $SIMP$ approach. The latter will always violate the Hashin-Shtrikman bounds [29] for small density values while $RAMP$ has a whole range of $q$ values for which the bounds are satisfied [28].

The Figure 2.1 and Figure 2.2 show the relationship between the relative stiffness and the volume density for both $SIMP$ and $RAMP$ with different $p$ and $q$ values.

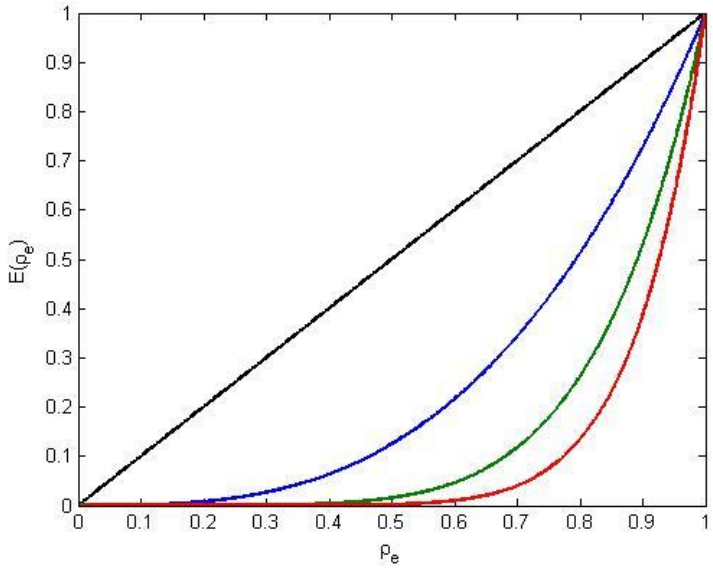


*Figure 2.1 – SIMP. Black: $p = 1$. Blue: $p = 3$. Green: $p = 6$. Red: $p = 9$*

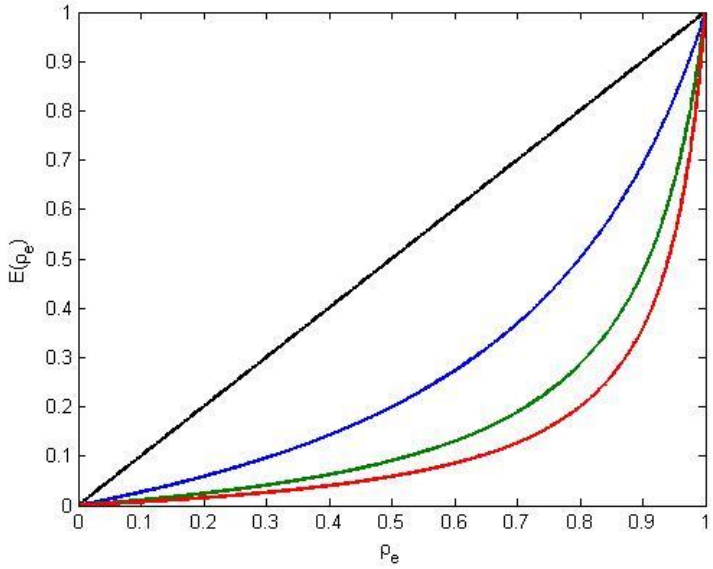


*Figure 2.2 – RAMP. Black: $q = 1$. Blue: $q = 3$. Green: $q = 9$. Red: $q = 15$*

By using a penalized Young's Modulus, the element stiffness matrix can be obtained for isotropic materials as

$$K_e(\rho) = \left[\frac{E_{min}}{E_{mat}} + \rho_e^p \left(1 - \frac{E_{min}}{E_{mat}}\right)\right] \cdot K_{mat}\,, \tag{2.7}$$

Where $K_{mat}$ is the element stiffness matrix that uses the solid isotropic material's Young's Modulus $E_{mat}$.

Similarly, for $RAMP$

$$K_e(\rho) = \left[\frac{E_{min}}{E_{mat}} + \frac{\rho_e}{1 + q \cdot (1 - \rho_e)} \cdot \left(1 - \frac{E_{min}}{E_{mat}}\right)\right] \cdot K_{mat}\ , \tag{2.8}$$

# 2.3 Minimum Compliance

One common objective for topology optimization is the minimization of the compliance while constrained by a volume fraction. The goal is to design a structure with maximum stiffness by minimizing the compliance for certain applied loads, while distributing a given amount of material.

The problem can be described by

$$\begin{aligned} minimize \quad & \phi = U^T \cdot K(\rho) \cdot U, \\ w.r.t. \quad & \rho_e, \rho = [\rho_{e=1}, \dots, \rho_{e=N}], \\ such\ that \quad & m(\rho) = \sum_{e=1}^{N} \rho_e \leq m^*, \\ & K \cdot U = F, \\ & 0 < \rho_{min} \leq \rho_e \leq 1. \end{aligned} \tag{2.9}$$

Where $U$ is the global displacement and $K$ the stiffness matrix and $\rho_{min}$ is a minimum relative density, which is non-zero to avoid singularities in the stiffness matrix [30]. When $\rho_e = \rho_{min}$, it represents a void element. $m(\rho)$ is the calculated volume fraction by summing every element density and $m^*$ is the volume fraction constraint.

It is also possible to give a residual stiffness to a void element so that instead of having $\rho_e \geq \rho_{min}$, it becomes $\rho_e \geq 0$ but a singular stiffness matrix is still avoided [5, 31].

The appropriate changes to the $SIMP$ and $RAMP$ approaches are as follows,

For $SIMP$

$$K_e(\rho_e) = \left[\frac{E_{res}}{E_{mat}} + \rho_e^p \cdot \left(1 - \frac{E_{res}}{E_{mat}}\right)\right] \cdot K_{mat}\ , \tag{2.10}$$

Forr $RAMP$

$$K_e(\rho_e) = \left[\frac{E_{res}}{E_{mat}} + \frac{\rho_e}{1 + q(1 - \rho_e)} \cdot \left(1 - \frac{E_{res}}{E_{mat}}\right)\right] \cdot K_{mat}\ , \tag{2.11}$$

The advantage of the latter method is that no volume fraction will be wasted on void elements. $E_{res}$ is the same as $E_{min}$ only in this case it is considered that $E_{min} \ll E_{mat}$ to simulate a void element.

## 2.4 Optimization

To compute the optimal distribution, over the reference domain, of the design variable $\rho$, it is necessary the application of an iterative process updated by an optimization method, that for a previously computed design point and its associated displacements, updates the design variables at each new point.

There are numerous optimization methods, such as the Optimality Criteria ($OC$) [32], Sequential Linear Programming ($SLP$), Sequential Quadratic Programming ($SQP$), Method of Moving Asymptotes ($MMA$) [33, 34], Convex Linearization Method ($CONLIN$) to name some. In this work both the $OC$ and $MMA$ methods will be used.

The $OC$ method is an iterative process based on satisfying the necessary conditions of optimality, that come from the Lagrange function.

In this way, the optimization problem

$$\begin{aligned} minimize \quad & \phi = U^T \cdot K(\rho) \cdot U, \\ w.r.t. \quad & \rho_e, \rho = [\rho_{e=1}, \dots, \rho_{e=N}], \\ such\ that \quad & m(\rho) = \sum_{e=1}^{N} \rho_e \leq m^*, \\ & K \cdot U = F, \\ & 0 \leq \rho_e \leq 1. \end{aligned} \tag{2.12}$$

Is translated to

$$\begin{aligned} \mathcal{L}\left(U, \tilde{U}, \rho, \lambda, \lambda^+_{e=1}, \dots, \lambda^+_{e=N,} \lambda^-_{e=1}, \dots, \lambda^-_{e=N,}\right) = \phi - \tilde{U}^T (K \cdot U - F) \\ - \lambda \cdot (m(\rho) - m^*) - \sum_{e=1}^{N} [\lambda^+_e \cdot (\rho_e - 1)] - \sum_{e=1}^{N} [\lambda^-_e \cdot (0 - \rho_e)], \end{aligned} \tag{2.13}$$

Where $\tilde{U}$, $\lambda$, $\lambda^+_e$ and $\lambda^-_e$ are the Lagrangian Multipliers for the constraints of the optimization problem and the necessary conditions for optimality are a subset of the stationarity conditions for the Lagrange function. $\tilde{U}$ belongs to the set $U$ of kinetically admissible displacement fields.

With the switching conditions,

$$\lambda^+_e \geq 0, \qquad \lambda^-_e \geq 0, \qquad \lambda^+_e \cdot (\rho_e - 1) = 0, \qquad \lambda^-_e \cdot (0 - \rho_e) = 0, \tag{2.14}$$

This means that for intermediate densities

$$\lambda^+_e = 0, \qquad \lambda^-_e = 0, \tag{2.15}$$

Then the Optimality Criteria Scheme [5, 30] can be formulated as

$$\rho_e^{new} = \begin{cases} \max(0\,, \rho_e - mv) & if \quad \rho_e \cdot \beta_e^{\eta} \leq \max(0\,, \rho_e - mv) \\ \rho_e \cdot \beta_e^{\eta} & if \quad \max(0\,, \rho_e - mv) < \rho_e \cdot \beta_e^{\eta} < \min(1\,, \rho_e + mv) \\ \min(1\,, \rho_e + m) & if \quad \min(1\,, \rho_e + mv) \leq \rho_e \cdot \beta_e^{\eta} \end{cases}, \tag{2.16}$$

Where $mv$ is a positive move limit, $\eta$ is a numerical damping coefficient and $\beta_e$ is found from the optimality condition from the Lagrange equation as

$$\beta_e = -\frac{\frac{\partial \phi}{\partial \rho_e}}{\lambda \cdot \frac{\partial m(\rho)}{\partial \rho_e}}\,, \tag{2.17}$$

Note that $\rho_e^{new}$ depends on the present value of the Lagrange multiplier $\lambda$ , which should be adjusted to satisfy the volume constraint. It is also, readily seen that the volume is a continuous and decreasing function of the multiplier $\lambda$, thus allowing the use of a bi-sectioning algorithm in an inner iteration loop to satisfy the active volume constraint.

The values of $mv$ and $\eta$ can be chosen by experiment, to obtain a suitable rapid and stable convergence of the iteration scheme.

Although heuristic, this type of scheme is very effective and efficient and can be used for many design studies. However, when constraints are not physically intuitive, unlike the volume fraction constraint, a mathematical programming method is a more direct way to obtain results.

One such method of mathematical programming is the $MMA$, which is based on a special type of convex approximations.

The $MMA$ updating scheme has the advantage of working with more than one constraint, and since it uses not only the sensitivity information at the current iteration point, but also some iteration history, it works very well for physically unintuitive constraints. Compared to the $OC$ method, $MMA$ provides an added flexibility, since it avoids the development and coding of new algorithms for each new problem. For simple compliance optimization problems, $MMA$ may be a bit slower than the $OC$ method, but for more complicated problems involving several constraints $MMA$ stands for excellent convergence properties.

## 2.5 Sensitivity Analysis

Since the update schemes are updated based on the element sensitivities of the design problem, then it is necessary to calculate compliance sensitivities.

Using the adjoint method,

$$\phi(U,\rho) = F^T \cdot U - \widetilde{U}^T(K \cdot U - F), \tag{2.18}$$

where $\widetilde{U}$, is any arbitrary but real vector that belongs to the set $U$ of kinetically admissible displacement fields. After rearrangement of terms

$$\frac{\partial \phi}{\partial \rho_e} = \left(F^T - \widetilde{U_e}^T \cdot K\right) \cdot \frac{\partial U_e}{\partial \rho_e} - \widetilde{U_e}^T \cdot \frac{\partial K}{\partial \rho_e} \cdot U_e, \tag{2.19}$$

In turn, when $\widetilde{U}$ satisfies the adjoint equation

$$F^T - \widetilde{U}^T \cdot K = 0, \tag{2.20}$$

Then

$$\frac{\partial \phi}{\partial \rho_e} = -\widetilde{U_e}^T \cdot \frac{\partial K}{\partial \rho_e} \cdot U_e, \tag{2.21}$$

For the compliance, it is directly obtained that

$$\widetilde{U} = U, \tag{2.22}$$

Then for $SIMP$

$$\begin{gathered} \frac{\partial \phi}{\partial \rho_e} = -U_e^T \cdot \frac{\partial K_e(\rho_e)}{\partial \rho_e} \cdot U_e \\ \frac{\partial \phi}{\partial \rho_e} = -U_e^T \cdot \left[p \cdot \rho_e^{p-1} \cdot \left(1 - \frac{E_{res}}{E_{mat}}\right) \cdot K_{mat}\right] \cdot U_e \end{gathered}, \tag{2.23}$$

And for $RAMP$

$$\begin{gathered} \frac{\partial \phi}{\partial \rho_e} = -U_e^T \cdot \frac{\partial K_e(\rho_e)}{\partial \rho_e} \cdot U_e \\ \frac{\partial \phi}{\partial \rho_e} = -U_e^T \cdot \left[\left(\frac{q+1}{\left((\rho_e - 1) \cdot q - 1\right)^2}\right) \cdot \left(1 - \frac{E_{res}}{E_{mat}}\right) \cdot K_{mat}\right] \cdot U_e \end{gathered}, \tag{2.24}$$

To simplify the code, and since the $\left(1-\frac{E_{res}}{E_{mat}}\right)$ term is transversal to every sensibility for each element, a scaling of the sensibilities can be introduced without interfering with the update results, since the only value that is affected is the Lagrangian Multiplier $\lambda$.

For $SIMP$

$$\frac{\partial \phi}{\partial \rho_e} = -U_e^T \cdot \left[p \cdot \rho_e^{p-1} \cdot K_{mat}\right] \cdot U_e, \tag{2.25}$$

And for $RAMP$

$$\frac{\partial \phi}{\partial \rho_e} = -U_e^T \cdot \left[\left(\frac{q+1}{\left((\rho_e - 1)\cdot q - 1\right)^2}\right) \cdot K_{mat}\right] \cdot U_e, \tag{2.26}$$

## 2.6 Complications – Checkerboard and Mesh-Dependency

Two important issues that significantly influence the computational results that can be obtained with the material distribution based topology design procedure are the appearance of checkerboards and the mesh-dependency of results. The former refers to the formation of regions of alternating solid and void elements ordered in a checkerboard like fashion and is related to the discretization of the original continuous problem. Mesh-dependence concerns the effect that qualitatively different optimal solutions are reached for different mesh-sizes or discretizations.

The appearance of checkerboard patterns, is directly related to the artificial high stiffness that such lay-outs of materials present when analysed in square Bi-linear 4-node ($Q4$) elements discretizations. In a uniform grid of these elements, a checkerboard pattern presents a stiffness comparable to the stiffness of a $\rho = {}^1/_2$ variable thickness sheet, for any prescribed loads [5]. Thus, for minimum compliance problem, is not surprising that the optimization problem has the checkerboard version as an optimal design. The use of higher order finite elements for the displacement function is a viable method to avoid the checkerboard problem. Checkerboards are typically prevented when using 8 or 9-node quadrilaterals, although, the use of higher order finite elements in topology design results in a substantial increase in CPU-time which can be avoided by employing alternative and computationally more economical methods.

The mesh dependency effect is a numerical instability where a larger number of holes appear when a finer finite element mesh is employed. That is, refining the finite element mesh for the reference domain ultimately leads to a generation of a fine-scale internal structural lay-out. The reason is that the efficiency of a given structure, generally increases with the introduction of more holes without changing the

structure volume. Given an enough fine mesh, one can obtain a fine-scale internal structural lay-out similar to a microstructure.

Computational experience has shown that filtering of the sensitivities of the optimization problem is a highly efficient way to ensure mesh-independency. It can also be used to very efficiently remove checkerboard patterns.

The sensitivity filter works by modifying the design sensitivity of a specified element, based on a weighted average of the element sensitivities in a fixed neighbourhood [5, 22]. It works as follows:

$$\frac{\partial \phi}{\partial \rho_e} = \frac{1}{\rho_e \cdot \sum_{i=1}^{N} \hat{H}_i} \cdot \sum_{i=1}^{N} \hat{H}_i \cdot \rho_i \cdot \frac{\partial \phi}{\partial \rho_i} \,, \tag{2.27}$$

Where $N$ is the total number of elements in the mesh and $\hat{H}_i$ the mesh independent convolution operator (weight factor) written as

$$\hat{H}_i = r_{min} - dist(e,i)\,, \quad \{i \in N | dist(e,i) \leq r_{min}\}, e = 1, \dots, N. \tag{2.28}$$

The operator $dist(e,i)$ is defined as the distance between the center of element $e$ and the center of element $i$. The convolution operator $\hat{H}_i$ is zero outside the filter area and is seen to decay with the distance from element $e$. It is worthwhile to note that the sensitivity converges to the original sensitivity when the filter radius $r_{min}$ approaches zero and that all sensitivities will be equal when $r_{min}$ approaches infinity.

The Figure 2.3 shows an example of a convolution of an image on the left using an operator $H$ that presents a similar approach to the sensitivity filtering convolution.

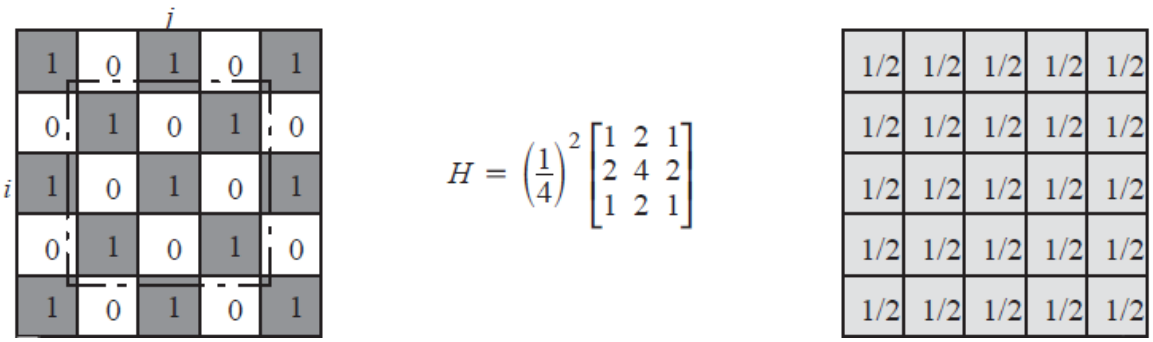


*Figure 2.3 - Convolution of input image on the left with impulse image $H$. $r_{min} = 2$ [22]*

# Chapter 3

# Microstructural Optimization

The methods of topology optimization, originally developed for structural optimization problems described in chapter 2, will be applied in this chapter to the design of materials. "*The fundamental idea is that any material is a structure if you look at it through a sufficiently strong microscope"*. Assuming a periodic material, the properties of a material can be found by the smallest repetitive unit, the base cell or representative volume element $(RVE)$. These properties can be found by a homogenization methodology or by the classical strain energy-based methodology. The homogenization translates the microscopic behaviour of a heterogeneous medium to its macroscopic behaviour, by finding the homogenized properties of its microstructure.

The Topology Optimization of a Microstructure or Material Design, consists on selecting which elements of the discretized base cell should be void or material to obtain prescribed or homogenized properties, therefore the method has also been widely called as the inverse homogenization method.

## 3.1 Linear Elasticity

Many properties of microstructured materials are direction dependent because of the arrangement of its structure. For this reason, properties, such as the elasticity and thermal expansion, cannot be expressed as scalars. Tensors are used as a tool to understand the behaviour of materials.

By Hooke's Law it is possible to relate Stress and Strain to each other, assuming a linear elastic medium [35]. In its general form, Hooke's Law reads:

$$\sigma_{ij} = C_{ijkl} \cdot \varepsilon_{kl} \,, \qquad with\ i,j,k,l = 1,2,3 \tag{3.1}$$

The fourth-rank tensor $C_{ijkl}$ is called the stiffness tensor. It holds the elastic constants of a medium. This tensor links the deformation of a medium to an applied stress. In general, Hooke's law leads to complicated relations, but simplifies remarkably, especially in the case of isotropic media. In its most general form the stiffness tensor has 81 entries. However, due to the symmetry of stress and strain the number of independent entries reduces to 36:

$$C_{ijkl} = C_{jikl} = C_{ijlk} = C_{jilk} \,, \tag{3.2}$$

Moreover, the existence of a unique strain energy potential requires that

$$C_{ijkl} = C_{klij}\,, \tag{3.3}$$

Thus, the number of independent entries reduces to 21 and can be written as a symmetric matrix

$$C_{ijkl} = \begin{bmatrix} C_{1111} & C_{1122} & C_{1133} & C_{1123} & C_{1113} & C_{1112} \\ & C_{2222} & C_{2233} & C_{2223} & C_{2213} & C_{2212} \\ & & C_{3333} & C_{3323} & C_{3313} & C_{3312} \\ & & & C_{2323} & C_{2313} & C_{2312} \\ & Sym & & & C_{1313} & C_{1312} \\ & & & & & C_{1212} \end{bmatrix}, \tag{3.4}$$

For 2-Dimensional Elasticity, it reduces to

$$C_{ijkl} = \begin{bmatrix} C_{1111} & C_{1122} & C_{1112} \\ & C_{2222} & C_{2212} \\ Sym & & C_{1212} \end{bmatrix}, \tag{3.5}$$

Which leads to

$$\begin{bmatrix} \sigma_{11} \\ \sigma_{22} \\ \sigma_{33} \\ \sigma_{23} \\ \sigma_{13} \\ \sigma_{12} \end{bmatrix} = \begin{bmatrix} C_{1111} & C_{1122} & C_{1133} & C_{1123} & C_{1113} & C_{1112} \\ & C_{2222} & C_{2233} & C_{2223} & C_{2213} & C_{2212} \\ & & C_{3333} & C_{3323} & C_{3313} & C_{3312} \\ & & & C_{2323} & C_{2313} & C_{2312} \\ & Sym & & & C_{1313} & C_{1312} \\ & & & & & C_{1212} \end{bmatrix} \cdot \begin{bmatrix} \varepsilon_{11} \\ \varepsilon_{22} \\ \varepsilon_{33} \\ \gamma_{23} \\ \gamma_{13} \\ \gamma_{12} \end{bmatrix}, \tag{3.6}$$

And for 2-D

$$\begin{bmatrix} \sigma_{11} \\ \sigma_{22} \\ \sigma_{12} \end{bmatrix} = \begin{bmatrix} C_{1111} & C_{1122} & C_{1112} \\ & C_{2222} & C_{2212} \\ Sym & & C_{1212} \end{bmatrix} \cdot \begin{bmatrix} \varepsilon_{11} \\ \varepsilon_{22} \\ \gamma_{12} \end{bmatrix}, \tag{3.7}$$

Note that $\gamma_{ij} = \varepsilon_{ij} + \varepsilon_{ji} = 2\varepsilon_{ij}$.

For simplicity, it is sometimes useful to apply the Voigt notation to express the $3\times3\times3\times3$ stiffness tensor

| $ij(kl)$ | $i(j)$ |
|---|---|
| 11 | 1 |
| 22 | 2 |
| 33 | 3 |
| 23 | 4 |
| 13 | 5 |
| 12 | 6 |

*Table 1 – 3D Voigt notation transformation*

Which simplifies the indicial form to the matrixial notation

$$\begin{bmatrix}\sigma_1\\ \sigma_2\\ \sigma_3\\ \sigma_4\\ \sigma_5\\ \sigma_6\end{bmatrix} = \begin{bmatrix} C_{11} & C_{12} & C_{13} & C_{14} & C_{15} & C_{16} \\ & C_{22} & C_{23} & C_{24} & C_{25} & C_{26} \\ & & C_{33} & C_{34} & C_{35} & C_{36} \\ & & & C_{44} & C_{45} & C_{46} \\ & Sym & & & C_{55} & C_{56} \\ & & & & & C_{66} \end{bmatrix} \cdot \begin{bmatrix}\varepsilon_1\\ \varepsilon_2\\ \varepsilon_3\\ \varepsilon_4\\ \varepsilon_5\\ \varepsilon_6\end{bmatrix}, \tag{3.8}$$

And

| $ij(kl)$ | $i(j)$ |
|---|---|
| 11 | 1 |
| 22 | 2 |
| 12 | 3 |

*Table 2 - 2D Voigt notation transformation*

Which simplifies the indicial form to the matrixial notation

$$\begin{bmatrix}\sigma_1\\ \sigma_2\\ \sigma_3\end{bmatrix} = \begin{bmatrix} C_{11} & C_{12} & C_{13} \\ & C_{22} & C_{23} \\ Sym & & C_{33} \end{bmatrix} \cdot \begin{bmatrix}\varepsilon_1\\ \varepsilon_2\\ \varepsilon_3\end{bmatrix}, \tag{3.9}$$

For anisotropic materials, all entries of the stiffness tensor are necessary, however for other materials, the stiffness tensor can be simplified.

For isotropic materials, the stiffness tensor can be reduced to

$$\begin{bmatrix}\sigma_1\\ \sigma_2\\ \sigma_3\\ \sigma_4\\ \sigma_5\\ \sigma_6\end{bmatrix} = \begin{bmatrix} C_{11} & C_{12} & C_{12} & 0 & 0 & 0 \\ C_{12} & C_{11} & C_{12} & 0 & 0 & 0 \\ C_{12} & C_{12} & C_{11} & 0 & 0 & 0 \\ 0 & 0 & 0 & C_{44} & 0 & 0 \\ 0 & 0 & 0 & 0 & C_{44} & 0 \\ 0 & 0 & 0 & 0 & 0 & C_{44} \end{bmatrix} \cdot \begin{bmatrix}\varepsilon_1\\ \varepsilon_2\\ \varepsilon_3\\ \varepsilon_4\\ \varepsilon_5\\ \varepsilon_6\end{bmatrix}, \tag{3.10}$$

And for 2-D isotropic materials

$$\begin{bmatrix}\sigma_1\\ \sigma_2\\ \sigma_3\end{bmatrix} = \begin{bmatrix} C_{11} & C_{12} & 0 \\ C_{12} & C_{11} & 0 \\ 0 & 0 & C_{33} \end{bmatrix} \cdot \begin{bmatrix}\varepsilon_1\\ \varepsilon_2\\ \varepsilon_3\end{bmatrix}, \tag{3.11}$$

Since $C_{11} = C_{22} = C_{33}$, $C_{12} = C_{13} = C_{23}$ and $C_{44} = C_{55} = C_{66}$

And for orthotropic materials

$$\begin{bmatrix}\sigma_1\\ \sigma_2\\ \sigma_3\\ \sigma_4\\ \sigma_5\\ \sigma_6\end{bmatrix} = \begin{bmatrix}C_{11} & C_{12} & C_{13} & 0 & 0 & 0\\ C_{12} & C_{22} & C_{23} & 0 & 0 & 0\\ C_{13} & C_{23} & C_{33} & 0 & 0 & 0\\ 0 & 0 & 0 & C_{44} & 0 & 0\\ 0 & 0 & 0 & 0 & C_{55} & 0\\ 0 & 0 & 0 & 0 & 0 & C_{66}\end{bmatrix} \cdot \begin{bmatrix}\varepsilon_1\\ \varepsilon_2\\ \varepsilon_3\\ \varepsilon_4\\ \varepsilon_5\\ \varepsilon_6\end{bmatrix}, \tag{3.12}$$

And 2-D orthotropic materials

$$\begin{bmatrix}\sigma_1\\ \sigma_2\\ \sigma_3\end{bmatrix} = \begin{bmatrix}C_{11} & C_{12} & 0\\ C_{12} & C_{11} & 0\\ 0 & 0 & C_{33}\end{bmatrix} \cdot \begin{bmatrix}\varepsilon_1\\ \varepsilon_2\\ \varepsilon_3\end{bmatrix}, \tag{3.13}$$

# 3.2 Periodic Boundary Conditions Homogenization method

If a structure is built from periodic materials it is often too cumbersome to model it taking every detail into consideration. Therefore, one substitutes the microstructure with some averaged properties that model the behaviour of the material on the macro scale. Within the scope of linear elasticity, the equivalent constitutive behaviour of periodically patterned microstructures can be evaluated using the homogenization method.

Considering a single cell $Y$ in $\mathbb{R}^3$

$$Y = ]0, y_1^0[\times]0, y_2^0[\times]0, y_3^0[\,, \tag{3.14}$$

Where $y_1^0, y_2^0$ and $y_3^0$ are the dimensions of the base cell in the three directions.

Assuming $u_e(x) = u(x, y), y = x/e$

A unique solution $u_e(x)$ depends on $x\ and\ y = x/e$, meaning that a quantity varies within a very small region with dimensions much smaller than those on the macroscopic level. In a neighbourhood of a macroscopic point $x$, it is assumed that there is a very large number of microscale small cells which are obtained by translation of the base cell. In other words, dependence on $y$ can be considered $Y\text{-}periodic$, for a fixed $x$ in the macroscopic level. It is also assumed that the form and composition of the base cells vary in a smooth way with the macroscopic variable $x$. This dependence of the solution on the macroscopic and microscopic levels makes it reasonable to assume $u_e(x, y)$ can be expressed as an asymptotic expansion [20, 5, 22]. Following the asymptotic expansion, the macroscale displacement field $u_e(x)$ depending on the aspect ratio $e$ between the macro and micro scales is expanded as

$$u_e(x, y) = u^0(x, y) + e \cdot u^1(x, y) + e^2 \cdot u^2(x, y) \dots\,, y = \frac{x}{e}, \tag{3.15}$$

When only the first order terms of the asymptotic expansion in are considered, the homogenized stiffness tensor $C_{ijkl}^{H}$ is given by averaging the integral over the base cell Y as

$$C_{ijkl}^{H} = \frac{1}{|Y|}\int_{Y} C_{pqrs}\left(\varepsilon_{pq}^{0(ij)} - \varepsilon_{pq}^{1(ij)}\right)\left(\varepsilon_{rs}^{0(kl)} - \varepsilon_{rs}^{1(kl)}\right)dY \ , \tag{3.16}$$

Where $\varepsilon_{pq}^{0(ij)} = \frac{1}{2}\left(\frac{\partial u_p^0}{\partial y_q} + \frac{\partial u_q^0}{\partial y_p}\right)$ and $\varepsilon_{pq}^{1(ij)} = \frac{1}{2}\left(\frac{\partial u_p^1}{\partial y_q} + \frac{\partial u_q^1}{\partial y_p}\right)$ is the $Y\text{-}periodic$ solution of

$$\int_{Y} C_{ijpq}\varepsilon_{pq}^{1(kl)}\frac{\partial v_i}{\partial y_j}dY = \int_{Y} C_{ijpq}\varepsilon_{pq}^{0(kl)}\frac{\partial v_i}{\partial y_j}dY\,, \tag{3.17}$$

Where $v$ is the $Y\text{-}periodic$ admissible displacement field, $\varepsilon_{pq}^{0(kl)}$corresponds to the three (2-D) or 6 (3-D) unit test strain fields and the displacements $u^1$ the $Y\text{-}periodic$ solution to the unit test strain fields.

In practice, the equilibrium equations are solved as a finite element problem

$$K\chi^{kl} = f^{kl}, \tag{3.18}$$

Where the displacements $\chi^{kl}$are constrained to be Y-periodic by assigning equal node numbers to opposing boundary nodes (periodic boundary conditions). The force vector is found from

$$f^{kl} = \sum_{e}\int_{Y_e} B_e^T C_{ijkl}^{mat}(\rho_e)\varepsilon^{0(kl)}dY\,, \tag{3.19}$$

And the global stiffness matrix is calculated as the usual assembly of element stiffness matrices $K = \sum_e K_e$ [36] plus periodicity considerations. In FE-notation, the effective properties may then be found as

$$\begin{aligned} C_{ijkl}^{H} &= \frac{1}{|Y|}\sum_{e}\left(\chi^{0(ij)} - \chi^{ij}\right)^T \int_{Ye} B_e^T C_{ijkl}^{mat}(\rho_e)B_e dY\left(\chi^{0(kl)} - \chi^{kl}\right) = \\ &= \frac{1}{|Y|}\sum_{e}\left(\chi^{0(ij)} - \chi^{ij}\right)^T K_e(\rho_e)\left(\chi^{0(kl)} - \chi^{kl}\right) \end{aligned}\ , \tag{3.20}$$

Where $C_{ijkl}^{mat}$ is the isotropic material constitutive matrix, $B_e$ is the finite element strain-displacement matrix [36, 5] and $\chi^{0(ij)}$ is the nodal displacement vector corresponding to the test strain field $\varepsilon^{0(ij)}$.

The sensitivity of a component with respect to the density design variable $\rho_e$ can again be found by the adjoint method resulting in the expression

$$\frac{\partial C_{ijkl}}{\partial \rho_e} = \frac{1}{|Y|}\left(\chi^{0(ij)} - \chi^{ij}\right)^T \frac{\partial K_e(\rho_e)}{\partial \rho_e}\left(\chi^{0(kl)} - \chi^{kl}\right), \tag{3.21}$$

However, to simplify the code the unit test strain fields can be applied directly on the boundaries of the base cell, which induces $\varepsilon^{A(ij)}$ which corresponds to the superimposed strain fields $(\varepsilon^{0(ij)} - \varepsilon^{1(ij)})$ [37]. By ascertaining that the periodic boundary conditions are well implemented in the FEM we simplify the expressions

$$C_{ijkl}^{H} = \frac{1}{|Y|}\int_{Y} C_{pqrs}\left(\varepsilon_{pq}^{A(ij)}\right)\left(\varepsilon_{rs}^{A(kl)}\right)dY \ , \tag{3.22}$$

And

$$C_{ijkl}^{H} = \frac{1}{|Y|}\sum_{e}\left(\chi^{A(ij)}\right)^{T} K_e(\rho_e)\left(\chi^{A(kl)}\right), \tag{3.23}$$

And the sensitivities can be expressed as

$$\frac{\partial C_{ijkl}}{\partial \rho_e} = \frac{1}{|Y|}\left(\chi^{A(ij)}\right)^{T}\frac{\partial K_e(\rho_e)}{\partial \rho_e}\left(\chi^{A(kl)}\right), \tag{3.24}$$

## 3.3 Strain Energy Method

The practical implementation of the homogenization Method and sensitivity analysis procedure are relatively complicated. To simplify the design of orthotropic periodic materials the classical theory of strain energy can be applied in the determination of the effective properties of periodically patterned microstructures and adapted to the topology optimization problem.

On the basis of symmetry of the material microstructure, we can use the strain energy method not only to compute the effective properties but also the sensitivity values of a $RVE$.

The premise of the method is that by applying displacements on the cell boundaries corresponding to unit strain fields, the energy calculated from the $FEM$ is equal to the homogenized energy of the cell. Thus, to calculate all the entries of the stiffness tensor 4 $FEM$ tests for $2D$ and 9 $FEM$ tests for 3D are needed.

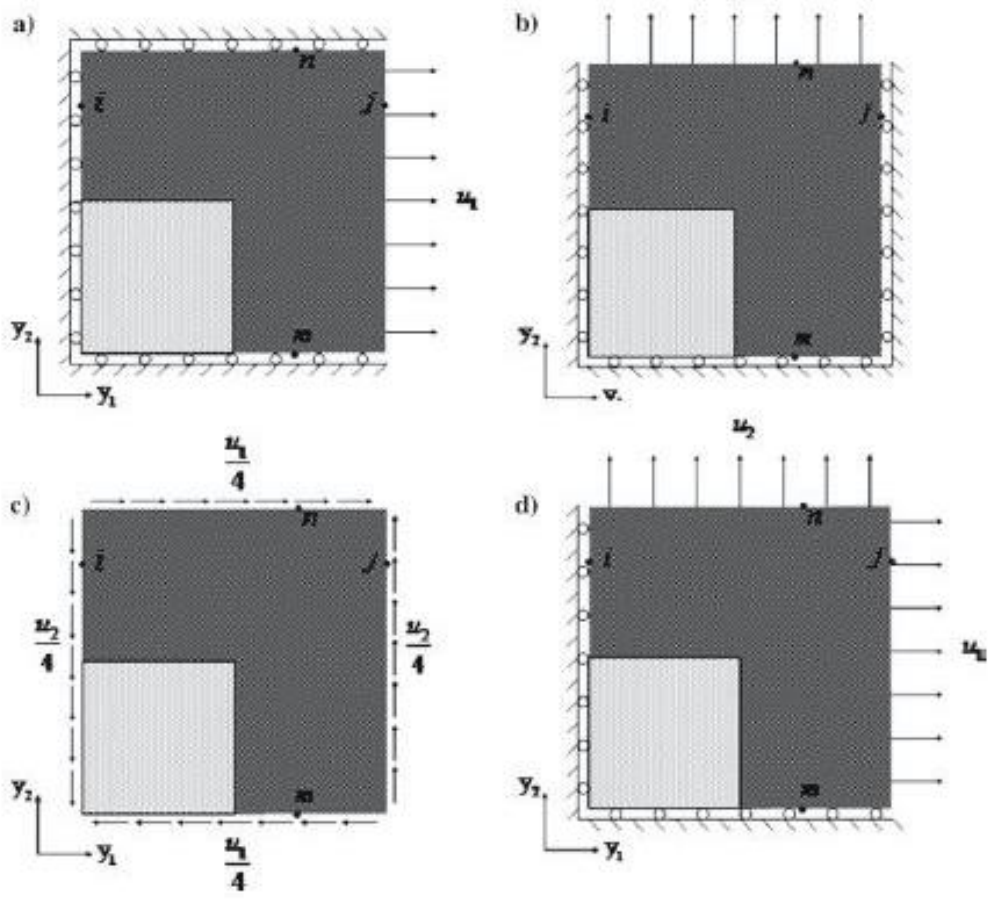


*Figure 3.1 - Boundary conditions of the unit cell. a) Load case 1. b) Load case 2. c) Load case 3. d) Load case 4. [38]*

$$\begin{aligned} C_{11}^H &= {U^1}^T \cdot K \cdot U^1, & \varepsilon^{0(1)} &= [1,0,0] \\ C_{22}^H &= {U^2}^T \cdot K \cdot U^2, & \varepsilon^{0(2)} &= [0,1,0] \\ C_{33}^H &= {U^3}^T \cdot K \cdot U^3, & \varepsilon^{0(3)} &= [0,0,1] \\ 2 \cdot C_{12}^H - C_{11}^H - C_{22}^H &= {U^4}^T \cdot K \cdot U^4, & \varepsilon^{0(4)} &= [1,1,0] \end{aligned} \tag{3.25}$$

Where $U^i$ corresponds to the displacement that apply the strain conditions on the boundaries $\varepsilon^i$, thus obtaining

$$\begin{bmatrix}\overline{\sigma_1}\\ \overline{\sigma_2}\\ \overline{\sigma_3}\end{bmatrix} = \begin{bmatrix}C_{11}^H & C_{12}^H & 0\\ C_{12}^H & C_{22}^H & 0\\ 0 & 0 & C_{33}^H\end{bmatrix} \cdot \begin{bmatrix}\overline{\varepsilon_1}\\ \overline{\varepsilon_2}\\ \overline{\varepsilon_3}\end{bmatrix}, \tag{3.26}$$

By definition, the sensitivity of the strain energy with respect to the element density variable is given by

$$\begin{aligned}\frac{\partial En^i}{\partial \rho_e} = \frac{1}{2}\cdot\frac{\partial\left({U^i}^T\cdot K\cdot U^i\right)}{\partial\rho_e} = \frac{1}{2}\cdot\left[{U^i}^T\cdot\frac{\partial K}{\partial\rho_e}\cdot U^i + 2\cdot\frac{\partial {U^i}^T}{\partial\rho_e}\cdot K\cdot U^i\right] = \\ = \frac{1}{2}\cdot\left[{U^i}^T\cdot\frac{\partial K}{\partial\rho_e}\cdot U^i + 2\cdot\frac{\partial {U^i}^T}{\partial\rho_e}\cdot F^i\right]\end{aligned}, \tag{3.27}$$

Separating the second term we have

$$\frac{\partial {U^i}^T}{\partial\rho_e}\cdot F^i = \left[\frac{\partial {U^\Gamma}^T}{\partial\rho_e}, \frac{\partial {U^\Omega}^T}{\partial\rho_e}\right]\cdot\begin{bmatrix}F^\Gamma\\ F^\Omega\end{bmatrix}, \tag{3.28}$$

Here Γ represents the boundaries and Ω the values on the inside of the cell.

By the nature of the applied conditions, the displacements on the boundaries don't vary [38, 39], and there are no forces applied inside the cell, only on the boundaries, which gives

$$\frac{\partial {U^i}^T}{\partial\rho_e}\cdot F^i = \left[0, \frac{\partial {U^\Omega}^T}{\partial\rho_e}\right]\cdot\begin{bmatrix}F^\Gamma\\ 0\end{bmatrix} = 0, \tag{3.29}$$

So

$$\frac{\partial En^i}{\partial\rho_e} = \frac{1}{2}\cdot\left[{U^i}^T\cdot\frac{\partial K}{\partial\rho_e}\cdot U^i\right], \tag{3.30}$$

The sensitivities of stiffness tensor are calculated by

$$\begin{aligned}&\frac{\partial C_{11}^H}{\partial\rho_e} = 2\cdot\frac{\partial En^1}{\partial\rho_e}, && \varepsilon^{0(1)} = [1,0,0]\\ &\frac{\partial C_{22}^H}{\partial\rho_e} = 2\cdot\frac{\partial En^2}{\partial\rho_e}, && \varepsilon^{0(2)} = [0,1,0]\\ &\frac{\partial C_{33}^H}{\partial\rho_e} = 2\cdot\frac{\partial En^3}{\partial\rho_e}, && \varepsilon^{0(3)} = [0,0,1]\\ &2\cdot\frac{\partial C_{12}^H}{\partial\rho_e} + \frac{\partial C_{11}^H}{\partial\rho_e} + \frac{\partial C_{22}^H}{\partial\rho_e} = 2\cdot\frac{\partial En^4}{\partial\rho_e}, && \varepsilon^{0(4)} = [1,1,0]\end{aligned} \tag{3.31}$$

Thus obtaining,

$$\begin{bmatrix} \frac{\partial \bar{\sigma}_1}{\partial \rho_e} \\ \frac{\partial \bar{\sigma}_2}{\partial \rho_e} \\ \frac{\partial \bar{\sigma}_3}{\partial \rho_e} \end{bmatrix} = \begin{bmatrix} \frac{\partial C_{11}^H}{\partial \rho_e} & \frac{\partial C_{12}^H}{\partial \rho_e} & 0 \\ \frac{\partial C_{12}^H}{\partial \rho_e} & \frac{\partial C_{22}^H}{\partial \rho_e} & 0 \\ 0 & 0 & \frac{\partial C_{33}^H}{\partial \rho_e} \end{bmatrix} \cdot \begin{bmatrix} \bar{\varepsilon}_1 \\ \bar{\varepsilon}_2 \\ \bar{\varepsilon}_3 \end{bmatrix}, \tag{3.32}$$

# 3.4 Problem Formulation

The objective of this work is the development of a computational model that allows the design of optimized materials with maximum stiffness while considering constraints of volume fraction and average stress of the material.

Since strain loads are used instead of stress loads, to obtain a maximum stiffness microstructure, instead of a minimization problem like in the general topology optimization, a maximization problem is formulated as

$$\begin{aligned} maximize \quad & \phi = \bar{\varepsilon}^T \cdot C_{ijkl}^H(\rho) \cdot \bar{\varepsilon}, \\ w.r.t. \quad & \rho_e, \rho = [\rho_{e=1}, \dots, \rho_{e=N}], \\ such\ that \quad & m(\rho) = \sum_{e=1}^{N} \rho_e \leq m^*, \\ & \bar{\sigma}(\rho) \leq \bar{\sigma}^*, \\ & 0 \leq \rho_e \leq 1. \end{aligned} \tag{3.33}$$

Where $\phi$ is the compliance or deformation energy, $\bar{\sigma}^*$ is the average stress constraint, and $\bar{\sigma}$ is the effective average stress.

Since it is possible to calculate all the stress components (3.26), and its sensitivities (3.32), then $\bar{\sigma}$ and $\bar{\sigma}^*$ can be any average stress criteria like Von Mises, Hydrostatic or even just one of the stress directional components.

It is also possible to constrain some of the stiffness tensor entries so that it is possible to design materials with maximum stiffness but with some prescribed properties, which is an interesting approach since it allows the design of materials with auxetic properties while also maximizing its stiffness for example. This approach is translated by

$$\begin{aligned} maximize \quad & \phi = \bar{\varepsilon}^T \cdot C_{ijkl}^H(\rho) \cdot \bar{\varepsilon}, \\ w.r.t. \quad & \rho_e, \rho = [\rho_{e=1}, \dots, \rho_{e=N}], \\ such\ that \quad & m(\rho) = \sum_{e=1}^{N} \rho_e \leq m^*, \\ & C_{ijkl}^H(\rho) \leq C_{ijkl}^{*H}(\rho), \\ & 0 < \rho_{min} \leq \rho_e \leq 1. \end{aligned} \tag{3.34}$$

Where $C_{ijkl}^{*H}(\rho)$, is the stiffness tensor parameter constraint, and $C_{ijkl}^H(\rho)$ is the effective stiffness tensor entry.

It is important to refer that, since the optimization is a maximization problem, then using the Optimality Criteria scheme, $\beta_e$ should come as

$$\beta_e = \frac{\frac{\partial \phi}{\partial \rho_e}}{\lambda \cdot \frac{\partial m(\rho)}{\partial \rho_e}}\,, \tag{3.35}$$

Since in the optimality criteria formulation, $\lambda$ is always positive.

Also, since $\bar{\varepsilon}$ are imposed values

$$\frac{\partial \phi}{\partial \rho_e} = \bar{\varepsilon}^T \cdot \frac{\partial C_{ijkl}^H(\rho)}{\partial \rho_e} \cdot \bar{\varepsilon} \tag{3.36}$$

# Chapter 4

# Computational Model Implementation

In this section, the interesting aspects of the computational model implementation are presented. Many topics of the implementation are simple code translations of aspects already described in the above chapters, which to be repeated in this chapter adds no real value. Therefore, this section will be solely focused on aspects that need $FEM$ implementations.

The computational model was written in $MATLAB$ based on the "A 99 line topology optimization code written in Matlab" [30], and of a $MATLAB\ MMA$ optimization code kindly provided by Professor Krister Svanberg. The code can be succinctly explained by the following flowchart:

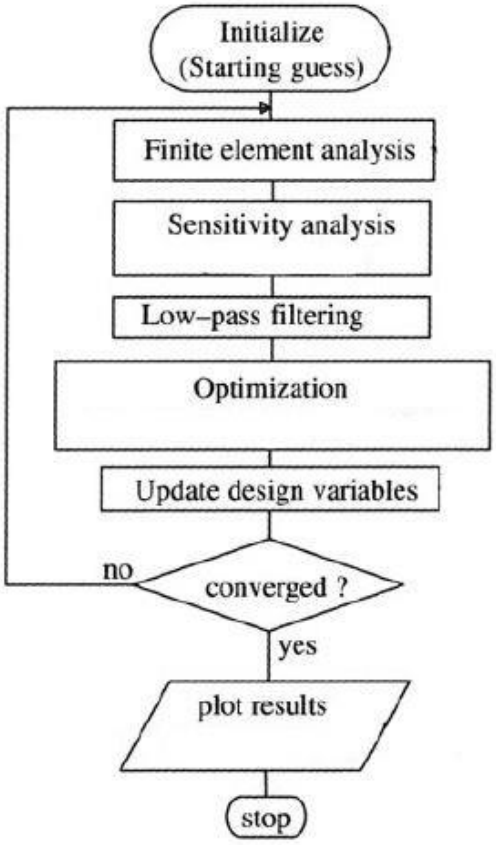


*Figure 4.1 – Flowchart of the Optimization Algorithm [5]*

# 4.1 Finite Element Method

To develop an efficient computational model with easy implementation the Bi-linear 4-node (Q4) element was selected.

By using a simpler element many implementation problems are avoided. Since the Bi-linear 4-node element can be used to create a structured mesh, it allows the simple use of the same element stiffness matrix for every element of the cell, making it implementation friendly without any wasted CPU resources. In a uniform mesh, the identification of nodes and cells is also easier, which allows a simpler coding for the mesh connectivity, boundary conditions and photographic representation of the optimization results.

By only having 4 nodes, the Q4 has an efficiency advantage against other elements such as Q8 or Q9 elements.

However, as described in chapter 2.6, the Q4 element discretizations has the problem of the appearance of artificial stiffness's in checkerboard patterns, making it the use of a sensitivity filter a necessity.

Stiffness matrix of a generic Q4 element in plane stress conditions can be written as

$$K_e = \frac{E_{mat}}{24\gamma(1-\nu^2)}\begin{bmatrix} 4\psi_3 & 3\psi_1 & 2\psi_5 & -3\psi_2 & -2\psi_3 & -3\psi_1 & -4\psi_6 & 3\psi_2 \\ & 4\psi_4 & 3\psi_2 & 4\psi_8 & -3\psi_1 & -2\psi_4 & -3\psi_2 & -2\psi_7 \\ & & 4\psi_3 & -3\psi_1 & -4\psi_6 & -3\psi_2 & -2\psi_3 & 3\psi_1 \\ & & & 4\psi_4 & 3\psi_2 & -2\psi_7 & 3\psi_1 & -2\psi_4 \\ & & & & 4\psi_3 & 3\psi_1 & 2\psi_5 & -3\psi_2 \\ & & & & & 4\psi_4 & 3\psi_2 & 4\psi_8 \\ & sym & & & & & 4\psi_3 & -3\psi_1 \\ & & & & & & & 4\psi_4 \end{bmatrix}, \tag{4.1}$$

$$\begin{aligned} \psi_1 &= (1+\nu)\gamma, \\ \psi_2 &= (1-3\nu)\gamma, \\ \psi_3 &= 2+(1-\nu)\gamma^2, \\ \psi_4 &= 2\gamma^2+(1-\nu), \\ \psi_5 &= (1-\nu)\gamma^2-4, \\ \psi_6 &= (1-\nu)\gamma^2-1, \\ \psi_7 &= 4\gamma^2-(1-\nu), \\ \psi_8 &= \gamma^2-(1-\nu). \end{aligned} \tag{4.2}$$

Where $\gamma$, is the element aspect-ratio, $\nu$ the element Poisson number and $E_{mat}$ it's Young's Modulus of the solid material.

If the elements are squares the aspect ratio used is $\gamma = 1$ then

$$K_e = \frac{E_{mat}}{24(1-\nu^2)} \begin{bmatrix} 4\psi_3 & 3\psi_1 & 2\psi_5 & -3\psi_2 & -2\psi_3 & -3\psi_1 & -4\psi_6 & 3\psi_2 \\ & 4\psi_4 & 3\psi_2 & 4\psi_8 & -3\psi_1 & -2\psi_4 & -3\psi_2 & -2\psi_7 \\ & & 4\psi_3 & -3\psi_1 & -4\psi_6 & -3\psi_2 & -2\psi_3 & 3\psi_1 \\ & & & 4\psi_4 & 3\psi_2 & -2\psi_7 & 3\psi_1 & -2\psi_4 \\ & & & & 4\psi_3 & 3\psi_1 & 2\psi_5 & -3\psi_2 \\ & & & & & 4\psi_4 & 3\psi_2 & 4\psi_8 \\ & sym & & & & & 4\psi_3 & -3\psi_1 \\ & & & & & & & 4\psi_4 \end{bmatrix}, \tag{4.3}$$

$$\begin{aligned} \psi_1 &= (1+\nu), \\ \psi_2 &= (1-3\nu), \\ \psi_3 &= (3-\nu), \\ \psi_4 &= (3-\nu), \\ \psi_5 &= -(3+\nu), \\ \psi_6 &= -\nu, \\ \psi_7 &= (3+\nu), \\ \psi_8 &= -\nu. \end{aligned} \tag{4.4}$$

# 4.2 Periodic Boundary Conditions

The displacement fields $\varepsilon^{A(ij)}$ are evaluated by considering unit strain test fields, and solving the equilibrium problem under the assumption of periodicity. The displacement field of the unit cell subjected to a given strain $\varepsilon^{0(ij)}$ can be expressed as the sum of a macroscopic displacement field and a periodic fluctuation [40]

$$\chi_i^A = \varepsilon_{ij}^0 \cdot y_j + \chi_i \,, \tag{4.5}$$

In practice, the periodic fluctuation term $\chi_i$ is unknown therefore, $(4.5)$, cannot be solved. However, by adopting a certain number of constraints between the nodes on the opposite surfaces of the cell, the periodic fluctuation terms can be eliminated [41, 42]. Considering a base cell pair of opposite boundaries

$$\begin{cases} \chi_i^{A(k+)} = \varepsilon_{ij}^0 \cdot y_j^{k+} + \chi_i \\ \chi_i^{A(k-)} = \varepsilon_{ij}^0 \cdot y_j^{k-} + \chi_i \end{cases}, \tag{4.6}$$

And

$$\chi_i^{A(k+)} - \chi_i^{A(k-)} = \varepsilon_{ij}^0 \cdot \left(y_j^{k+} - y_j^{k-}\right) = \varepsilon_{ij}^0 \cdot \Delta y_j^k, \tag{4.7}$$

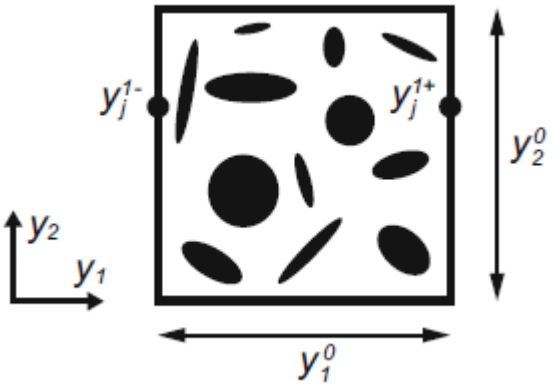


*Figure 4.2 - A 2D rectangular base cell model [43]*

For any given regular quadrilateral base cell $\Delta y_j^k$ is constant, thus with a specified $\varepsilon_{ij}^0$, the right side becomes a constant

$$\chi_i^{A(k+)} - \chi_i^{A(k-)} = w_i^k, \tag{4.8}$$

This form of boundary conditions can be directly imposed by direct substitution in the finite elements model, by constraining the corresponding pairs of nodal displacements and eliminating the redundant unknowns [44].

In finite element notation, the periodic boundary constraints can be exemplified by the following equations.

$$\begin{bmatrix} K_{11} & K_{12} & K_{13} & K_{14} \\ K_{21} & K_{22} & K_{23} & K_{24} \\ K_{31} & K_{32} & K_{33} & K_{34} \\ K_{41} & K_{42} & K_{43} & K_{44} \end{bmatrix} \cdot \begin{bmatrix} U_1 \\ U_2 \\ U_3 \\ U_4 \end{bmatrix} = \begin{bmatrix} F_1 \\ F_2 \\ F_3 \\ F_4 \end{bmatrix}, \tag{4.9}$$

Where $U_1$ are the prescribed displacement values corresponding to $\varepsilon_{ij}^0 \cdot \Delta y_j^k$ in each of the four cell vertices, $U_2$ are the unknown displacement values corresponding to the interior nodes and $U_4 = U_3 + W$, where $W = \varepsilon_{ij}^0 \cdot \Delta y_j^k$. $F_1$ is an unknow force vector, $F_2 = 0$, and $F_3 + F_4 = 0$.

The equilibrium equation can therefore be reduced to

$$\begin{bmatrix} K_{22} & K_{23} + K_{24} \\ sym & K_{33} + K_{34} + K_{43} + K_{44} \end{bmatrix} \cdot \begin{bmatrix} U_2 \\ U_3 \end{bmatrix} = -\begin{bmatrix} K_{21} \\ K_{31} + K_{41} \end{bmatrix} \cdot U_1 - \begin{bmatrix} K_{24} \\ K_{34} + K_{44} \end{bmatrix} \cdot W. \tag{4.10}$$

And therefore, the equation can be solved.

## 4.3 Strain Energy Boundary Conditions

Contrary to the periodic Boundary Conditions, the implementation of strain energy conditions is a rather simple approach, since only simple Dirichlet Boundary Conditions were needed.

In finite element notation, it can be exemplified by the following equations.

$$\begin{bmatrix} K_{11} & K_{12} \\ K_{21} & K_{22} \end{bmatrix} \cdot \begin{bmatrix} U_1 \\ U_2 \end{bmatrix} = \begin{bmatrix} F_1 \\ F_2 \end{bmatrix}, \tag{4.11}$$

In this finite element problem $U_1$ are the boundary displacements and $U_2$ are the unknown displacement values corresponding to the interior nodes.

Knowing that $F_2 = 0$, the by Dirichlet the solution comes as

$$[U_2] = -[K_{21}] \cdot [U_1], \tag{4.12}$$

# Chapter 5

# Results and Discussion

In this section, examples are presented to compare and discuss the efficiency of the proposed methods and to verify the capabilities of the computational model.

Firstly, simpler problems will be presented to better understand the influence of the user inputs in the computational model over the obtained results, as a better understanding of the input effects, allows for better choices for the more complex problems. Testing and using the computational model will enable the user to gain a certain "sensibility" over the inputs to consistently and effortlessly obtain the desired microstructures.

Secondly, examples of compliance optimizations with Stiffness Tensor Parameter's constraints will be presented. This methodology can present some interesting results, by combining Maximum Stiffness Optimizations with prescribed material properties.

And Lastly, some results for microstructure optimizations with Average Stress constraints will be presented.

## 5.1 Bulk Modulus and Shear Modulus

One important aspect to mention is that when the objective of the optimization is the maximization of the Bulk Modulus $(\kappa)$, the strain field used for the test is $\bar{\varepsilon} = [1,1,0]$. This means that the compliance is

$$\phi = C_{11} + C_{12} + C_{21} + C_{22} = C_{11} + 2 \cdot C_{12} + C_{22}, \tag{5.1}$$

To achieve an appropriate solution to the Bulk Modulus Maximization problem, the initial guesses need to have rotational symmetry, like Figure 5.17 and Figure 5.39. This means that by rotating the cell in $90°$ the result is the same cell. In this way, $C_{11} = C_{22}$ in the initial guess and since the weight of both parameters is the same in this optimization, then $C_{11}$ will always be equal to $C_{22}$ across all iterations.

This translates into

$$\phi = 2 \cdot C_{11} + 2 \cdot C_{12}, \tag{5.2}$$

Since

$$\kappa = \frac{C_{11} + C_{12}}{2}, \tag{5.3}$$

Then in the tests that follow

$$\phi = 4 \cdot \kappa, \tag{5.4}$$

Maximizing the compliance of the strain field $\bar{\varepsilon} = [1,1,0]$, can be said to be equivalent to maximize the bulk modulus.

In the same way to maximize the Shear Modulus the strain field used is $\bar{\varepsilon} = [0,0,1]$. The compliance becomes

$$\phi = C_{33}, \tag{5.5}$$

Since

$$C_{33} = G, \tag{5.6}$$

Then the compliance is equivalent to the Shear Modulus Maximization.

$$\phi = G. \tag{5.7}$$

## 5.2 Validation of the Computational Model

The validation of the optimization was divided in two steps. In the first step, the Finite Element Analysis was validated by determining the material constitutive matrix for homogeneous materials and comparing the results with the expected analytical ones.

So, for a material with $E_{mat} = 1$, and $v = 0.3$, the analytical constitutive matrix, in plane stress conditions is

$$C_{ij} = \begin{bmatrix} \frac{E_{mat}}{1-v^2} & \frac{v \cdot E_{mat}}{1-v^2} & 0 \\ \frac{v \cdot E_{mat}}{1-v^2} & \frac{E_{mat}}{1-v^2} & 0 \\ 0 & 0 & \frac{(1-v) \cdot E_{mat}}{2 \cdot (1-v^2)} \end{bmatrix} = \begin{bmatrix} 1{,}0989 & 0{,}3297 & 0 \\ 0{,}3297 & 1{,}0989 & 0 \\ 0 & 0 & 0{,}3846 \end{bmatrix}$$

And the obtained FEM results for both homogenization methods are

$$C_{ij} = \begin{bmatrix} 1{,}0989 & 0{,}3297 & 0 \\ 0{,}3297 & 1{,}0989 & 0 \\ 0 & 0 & 0{,}3846 \end{bmatrix}$$

As can be seen the obtained results are equal to the expected solution so the FEM are working as intended.

The second step of the validation is to compare some of the obtained optimization results, with results from previous works.

For example, the results from Figure 5.1 can be compared to Figure 5.2, the results from Figure 5.3 can be compared to Figure 5.4 and the mechanism that gives the auxetic properties for the results in Figure 5.5 is comparable to Figure 5.6.

Note that there is a translation of the designs in Figure 5.1 to Figure 5.2 and from Figure 5.3 to Figure 5.4, but since the materials are periodic the obtained results are equivalent.

The similarity in the obtained results demonstrates that the optimization is correctly implemented.

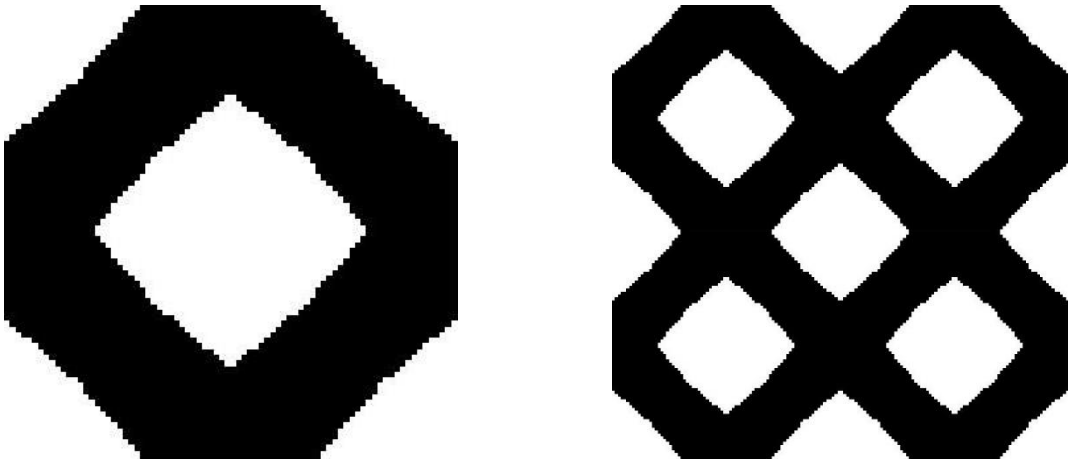

*Figure 5.1 - Material with Maximum Shear Modulus obtained using Homogenization Approach, $r = 2$, $m = 0.6$, $\nu = 0.3$, $p = 8$, $mv = 0.1$, $N = 6400$, OC, SIMP*

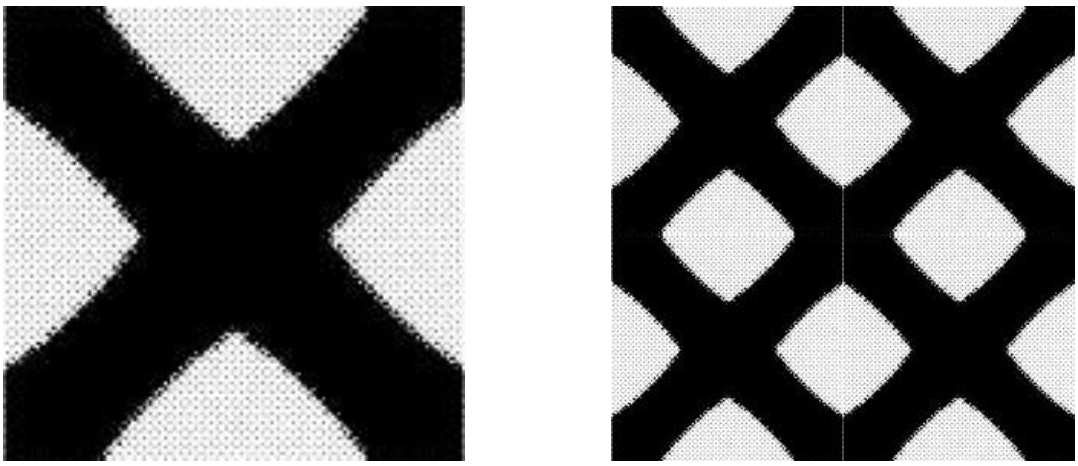

*Figure 5.2 - Material with Maximum Shear Modulus from Neves et al. [21]*

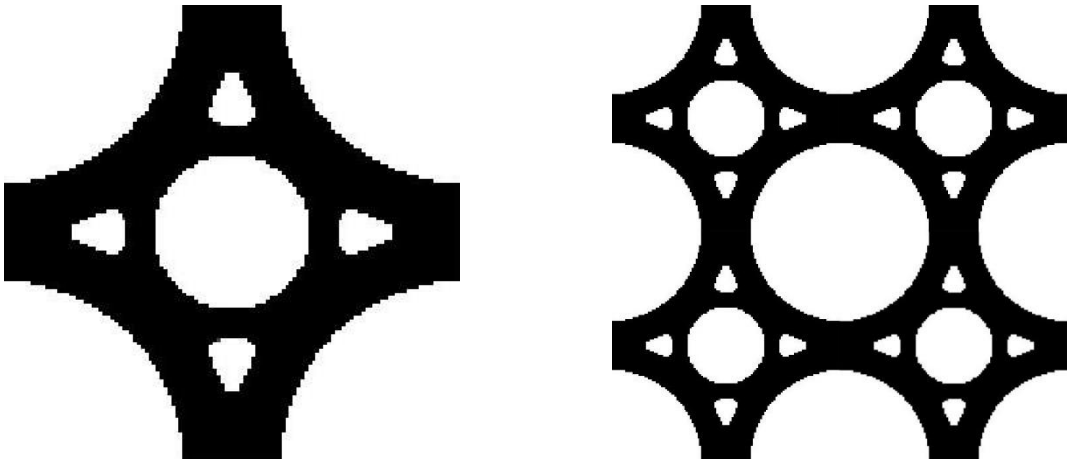

*Figure 5.3 – Material with Maximum Bulk Modulus obtained using Homogenization Approach, $\phi = 0.5626$, $r = 3$, $m = 0.4$, $\nu = 0.3$, $p = 8$, $mv = 0.1$, $N = 14400$, OC, SIMP*

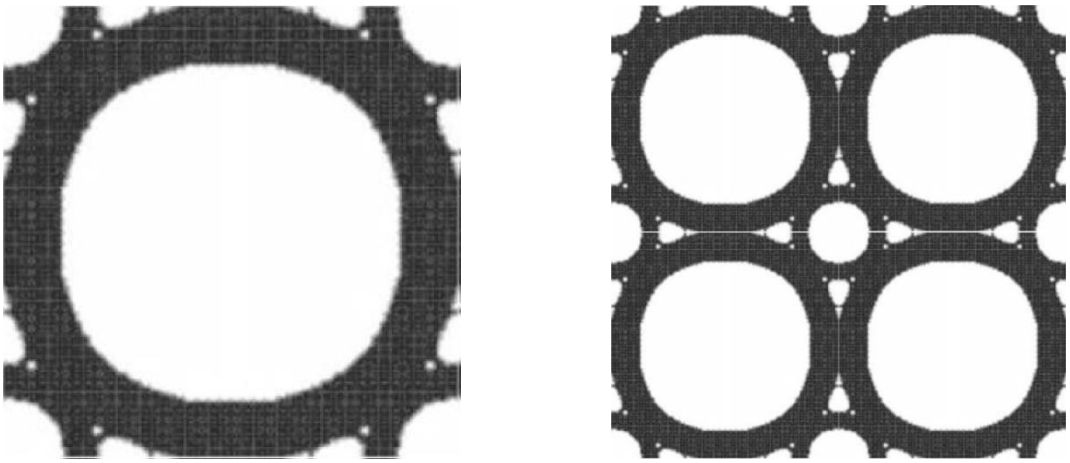

*Figure 5.4 – Material with Maximum Bulk Modulus from Amstutz et al. [45]*

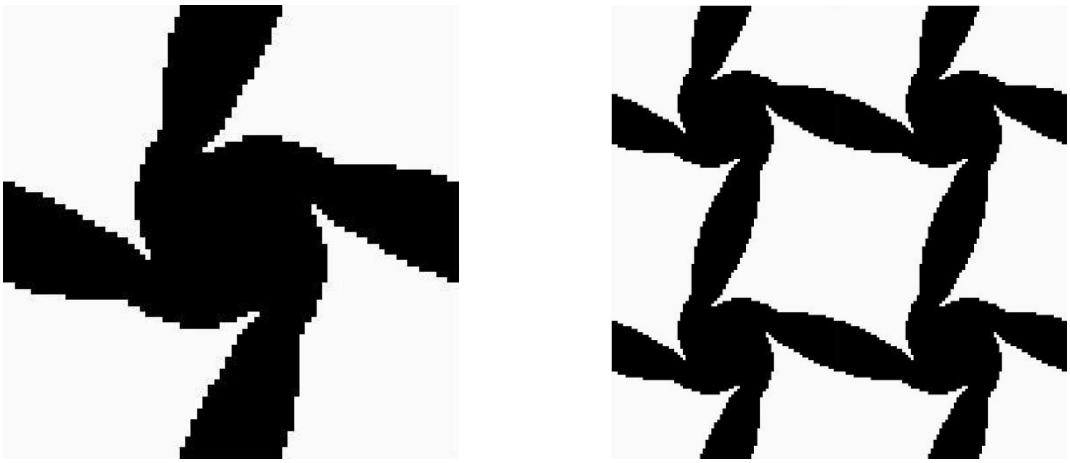

*Figure 5.5 – Material with Negative Poisson obtained using Homogenization Approach, $r = 2$, $m = 0.4$, $v = 0.3$, $p = 8$, $mv = 0.1$, $N = 6400$, MMA, SIMP*

*Figure 5.6 - – Material with Negative Poisson from Wang et al. [46]*

## 5.3 Optimization Evolution

It is important to understand how the program solves the optimization problem so in this chapter it is shown the evolution of the design every 5 iterations in Figure 5.7, starting at iteration 0, and its respective compliance evolution in Figure 5.8, for a Maximum Bulk Modulus Optimization.

In Figure 5.8 is interesting to see that the solution starts converging very slowly in the first few iterations, but after finding the right direction it has a fast convergence, then stagnating after iteration 20. Even though, the compliance has stagnated after iteration we can see in Figure 5.7, the designs between iteration 20 and 35 present some differences.

The slight growth of the compliance after iteration 35 corresponds to turning off the filtering, culminating in the final design in iteration 45.

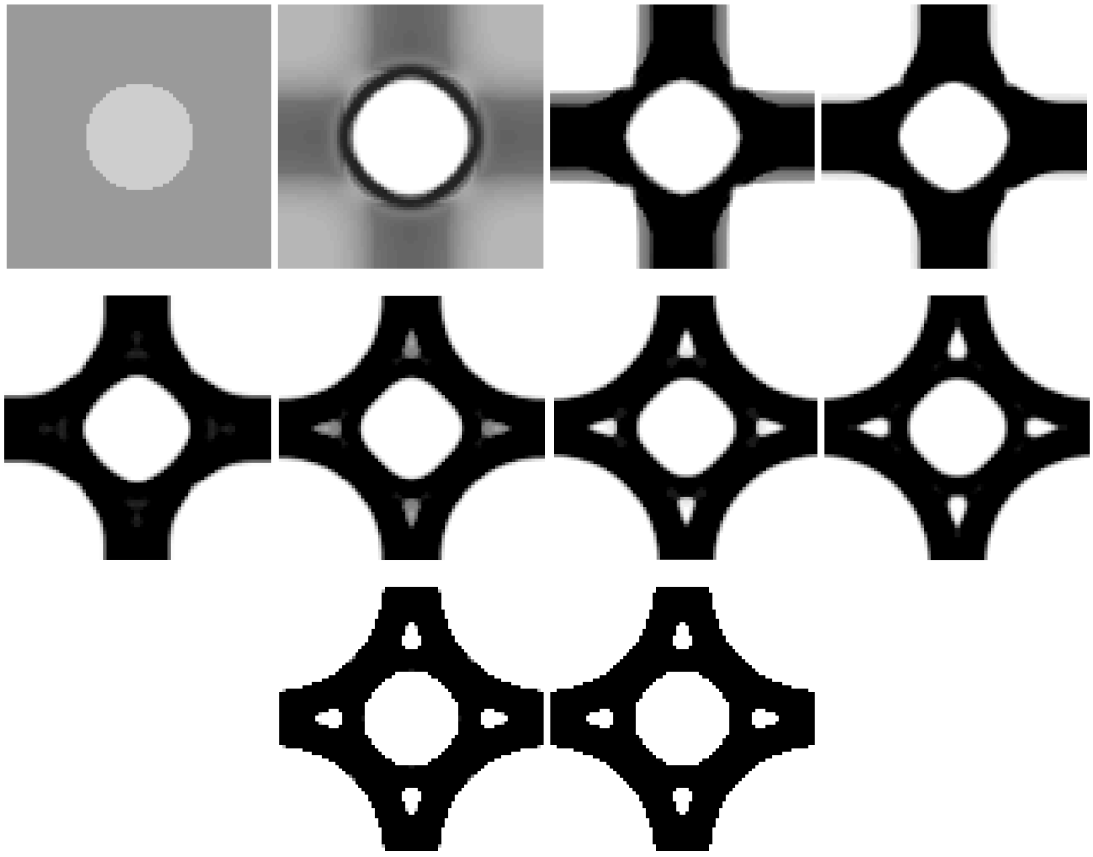

*Figure 5.7 – Evolution of the design optimization for a Material with Maximum Bulk Modulus obtained using Homogenization Approach, $E_{min} = 10^{-3} \cdot E_{mat}$, $r = 2$, $m = 0.4$, $\nu = 0.3$, $p = 8$, $mv = 0.1$, $N = 6400$, OC, SIMP*

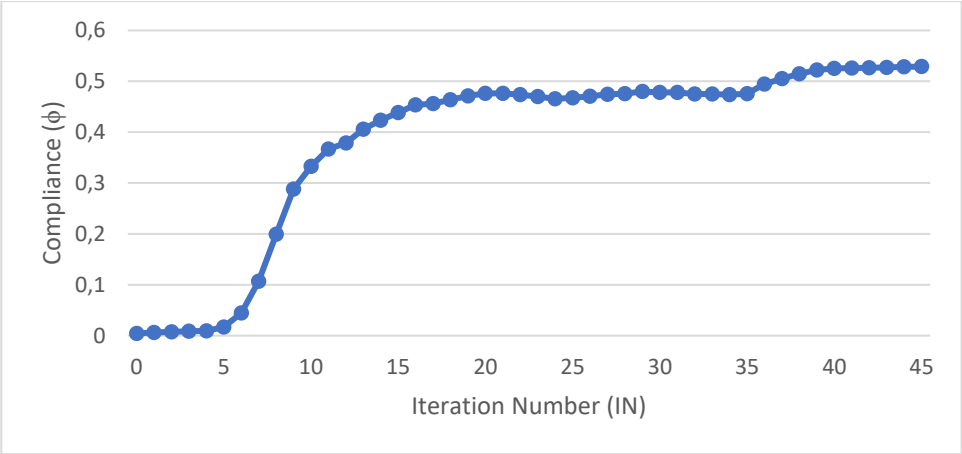


*Figure 5.8 – Graph of the evolution of the compliance with the iteration number, for a Material with Maximum Bulk Modulus*

## 5.4 Simplified Homogenization vs Strain Energy Results

As discussed in 0, to obtain the effective properties and sensitivity of the microstructures, both the simplified Homogenization approach and Strain Energy Approach can be used. It is interesting to see if there is a significant difference in the designs obtained through each method. Three different strain fields are used for each approach.

Comparing Figure 5.9 to Figure 5.10, Figure 5.11 to Figure 5.12 and Figure 5.13 to Figure 5.14, using the same inputs between both approaches, it can be verified that both the Homogenization and Strain Energy produce similar designs. Even though there is some difference in the obtained compliances, it is very negligible.

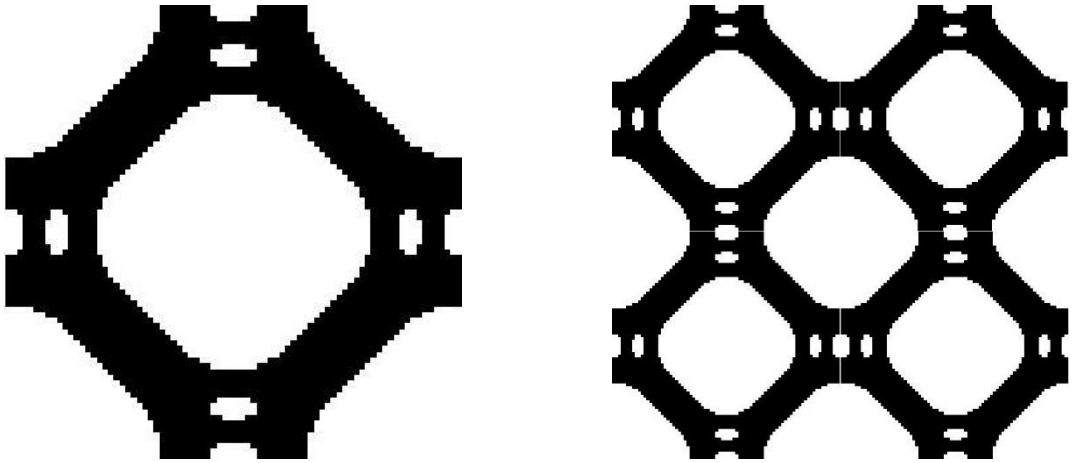

*Figure 5.9– Material with Maximum Bulk Modulus obtained using Homogenization Approach, $\phi = 0.5626$, $r = 2$, $m = 0.4$, $\nu = 0.3$, $p = 8$, $mv = 0.05$, $N = 6400$, OC, SIMP*

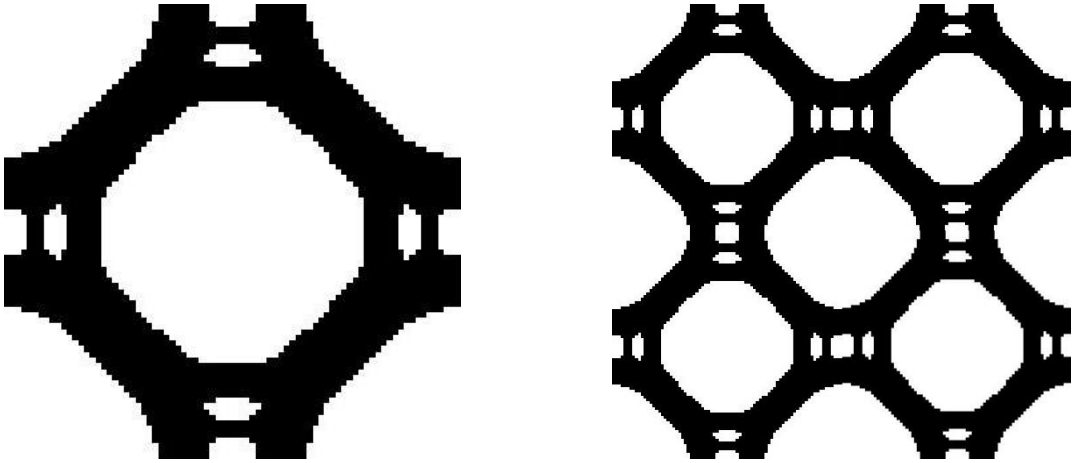

*Figure 5.10 – Material with Maximum Bulk Modulus obtained using Strain Energy Approach, $\phi = 0.5595$, $r = 2$, $m = 0.4$, $\nu = 0.3$, $p = 8$, $mv = 0.05$, $N = 6400$, OC, SIMP*

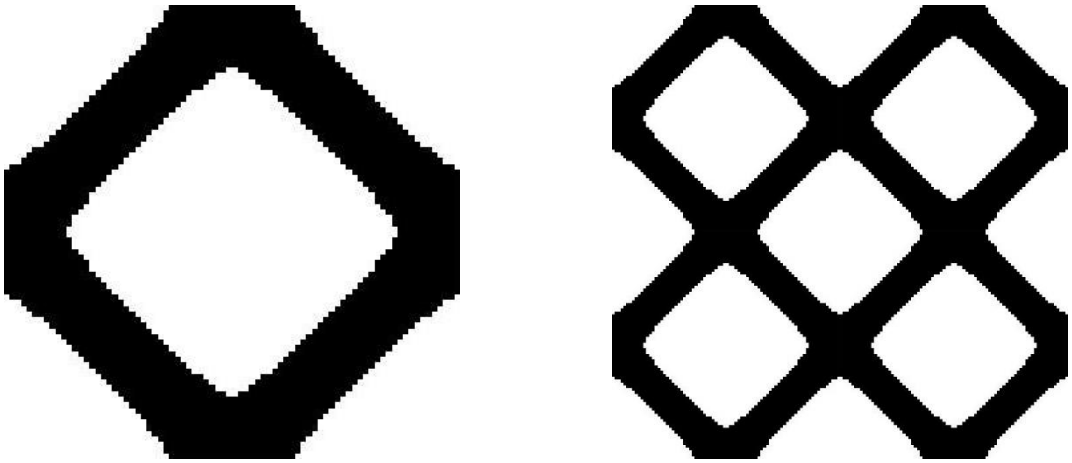

*Figure 5.11 - Material with Maximum Shear Modulus obtained using Homogenization Approach, $\phi = 0.1113$, $r = 2$, $m = 0.4$, $\nu = 0.3$, $p = 8$, $mv = 0.05$, $N = 6400$, OC, SIMP*

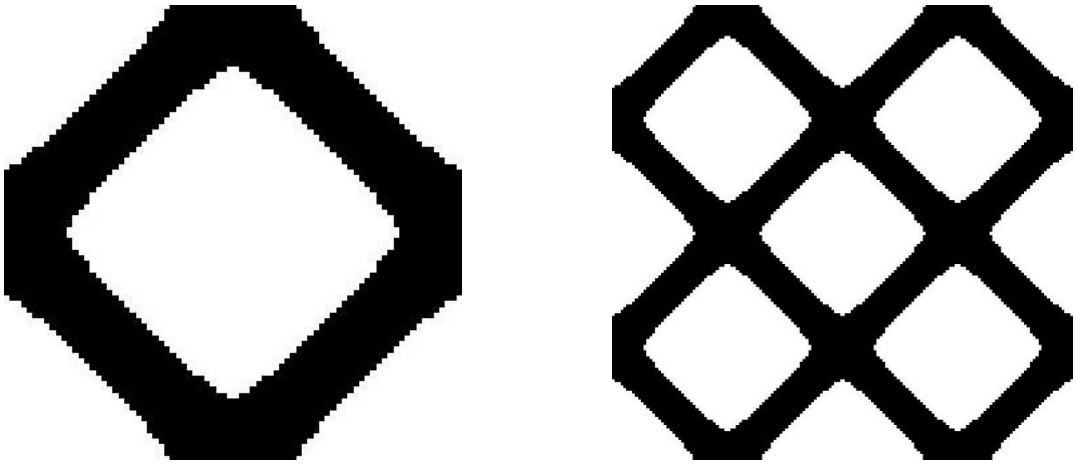

*Figure 5.12 - Material with Maximum Shear Modulus obtained using Strain Energy Approach, $\phi = 0.1113$, $r = 2$, $m = 0.4$, $\nu = 0.3$, $p = 8$, $mv = 0.05$, $N = 6400$, OC, SIMP*

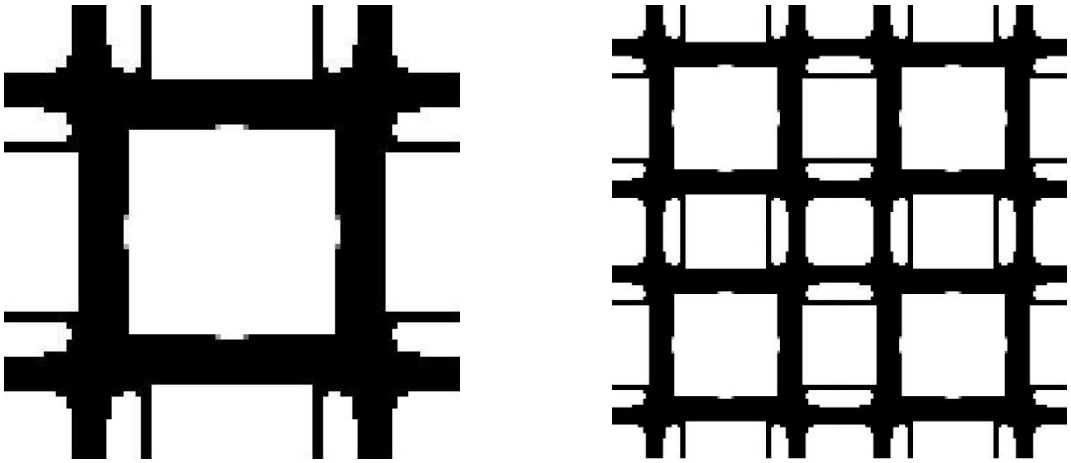

*Figure 5.13 – Material with Maximum Compliance for $45°$ Pure Shear Strain, corresponding to the strain field $\bar{\varepsilon} = [1, -1, 0]$, obtained using Homogenization Approach, $\phi = 0.4420$, $r = 2$, $m = 0.4$, $\nu = 0.3$, $p = 8$, $mv = 0.05$, $N = 6400$, OC, SIMP*

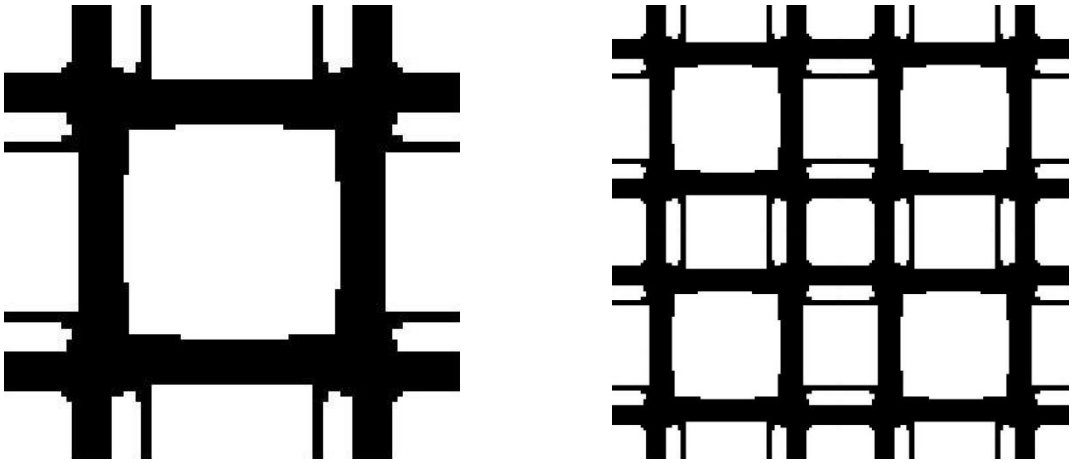

*Figure 5.14 - Material with Maximum Compliance for* $45°$ *Pure Shear Strain, corresponding to the strain field* $\bar{\varepsilon} = [1, -1, 0]$*, obtained using Strain Energy Approach,* $\phi = 0.4431$*,* $r = 2$*,* $m = 0.4$*,* $\nu = 0.3$*,* $p = 8$*,* $mv = 0.05$*,* $N = 6400$*, OC, SIMP*

Even though the obtained results are very similar, the biggest difference between both approaches is the ability of simplified homogenization to correctly evaluate non-symmetric microstructures, since the strain energy approach can be said to be an upper bound evaluation of material properties.

Since the results are identical, and given the additional flexibility of the homogenization approach, it will be the preferred method in following examples.

## 5.5 Move limit influence

The move limit is the maximum limit an element density can change in the optimization process, which corresponds to the maximum difference an element density can have in two sequential iterations.

The move limit is an interesting parameter of the optimization problems. A too big move limit will hinder the optimization's stability. On the other side of the spectrum, a too small move limit will prevent the optimization convergence.

Some sensibility is needed in the way this parameter is used. As can be seen below through the comparison of the examples from Figure 5.9 to Figure 5.15 and the examples from Figure 5.13 to Figure 5.16, a small change in the move limit parameter can have an effect on the final results.

Usually the move limit is within the values $0{,}05 \leq \Delta\rho_e \leq 0{,}2$.

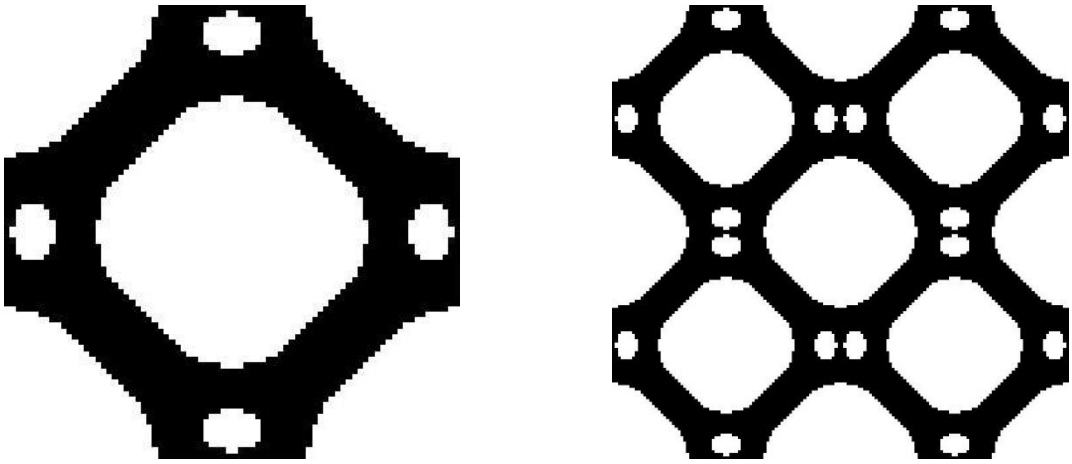

*Figure 5.15 – Material with Maximum Bulk Modulus obtained using Homogenization Approach, $\phi = 0.5592$, $r = 2$, $m = 0.4$, $\nu = 0.3$, $p = 8$, $mv = 0.1$, $N = 6400$, OC, SIMP*

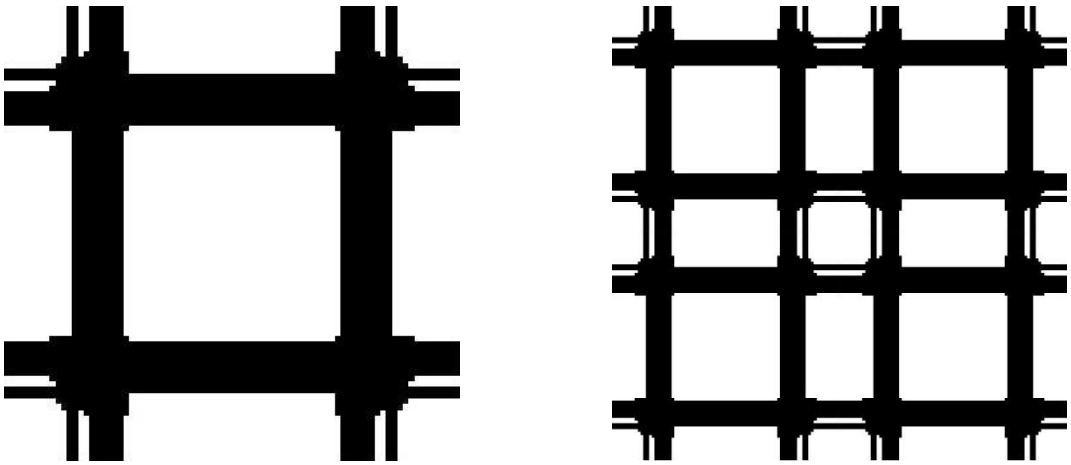

*Figure 5.16 – Material with Maximum Compliance for $45°$ Pure Shear Strain, corresponding to the strain field $\bar{\varepsilon} = [1, -1, 0]$, obtained using Homogenization Approach, $\phi = 0.4464$, $r = 2$, $m = 0.4$, $\nu = 0.3$, $p = 8$, $mv = 0.1$, $N = 6400$, OC, SIMP*

## 5.6 Initial design Influence

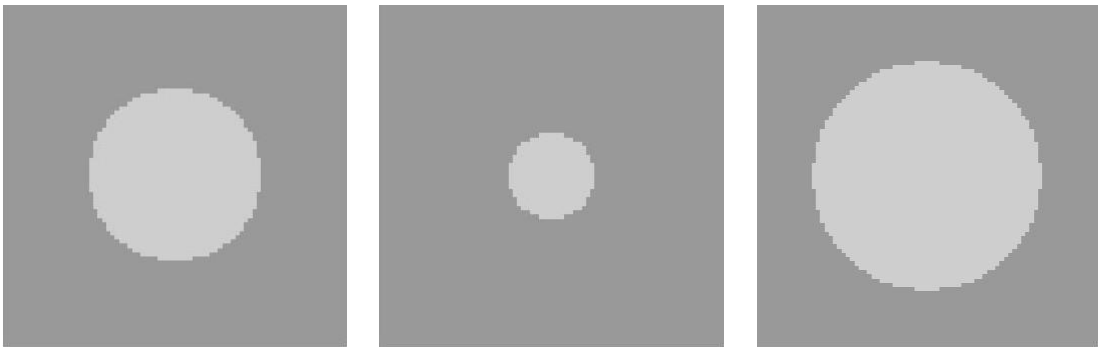

*Figure 5.17 – Three different initial designs, $N = 6400$, $m = 0.4$*

In structural design, the initial guess usually consists of a uniformly distributed density field to avoid local minimum designs [30]. However, this cannot be employed for material designs because the applied boundary conditions would result in a uniformly distributed sensitivity field, thus making the variable update impossible [23, 47, 48]. The initial guesses influence in the results are very significant, leading to converged designs in different local maximums or minimums.

Some initial designs are presented in Figure 5.17 where a circular region with softer material is introduced in the center of the material [45]. The difference between the final designs when using the 3 different initial guesses can be seen by comparing the examples from Figure 5.15 to Figure 5.18 and Figure 5.19 for Bulk Modulus Maximization, and the examples from Figure 5.11 to Figure 5.20 for Shear Modulus Maximization.

There are many initial designs that can be used, however it is important to take in consideration the speed of convergence of the solution, and the circular initial designs presents a rather fast convergence speed, thanks to the easier to detect sensitivity differences in the circular border, while at the same time leading the solution to a certain local maximum, because of the initial iterations. It is also important to note that if the non-symmetric results are the objective, the initial guesses also need to be non-symmetric.

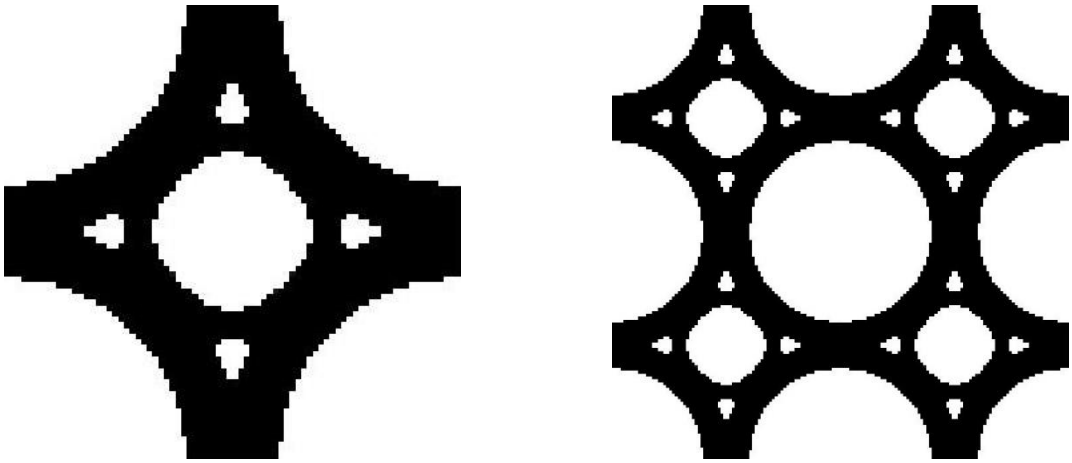

*Figure 5.18 – Material with Maximum Bulk Modulus obtained using Homogenization Approach, $\phi = 0.5593$, $r = 2$, $m = 0.4$, $\nu = 0.3$, $p = 8$, $mv = 0.1$, $N = 6400$, OC, SIMP*

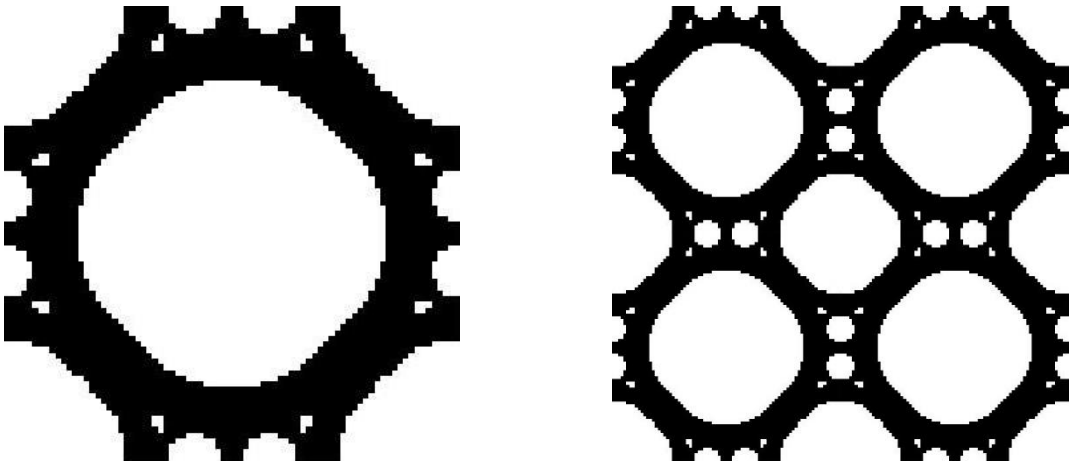

*Figure 5.19 - Material with Maximum Bulk Modulus obtained using Homogenization Approach, $\phi = 0.5568$, $r = 2$, $m = 0.4$, $\nu = 0.3$, $p = 8$, $mv = 0.1$, $N = 6400$, OC, SIMP*

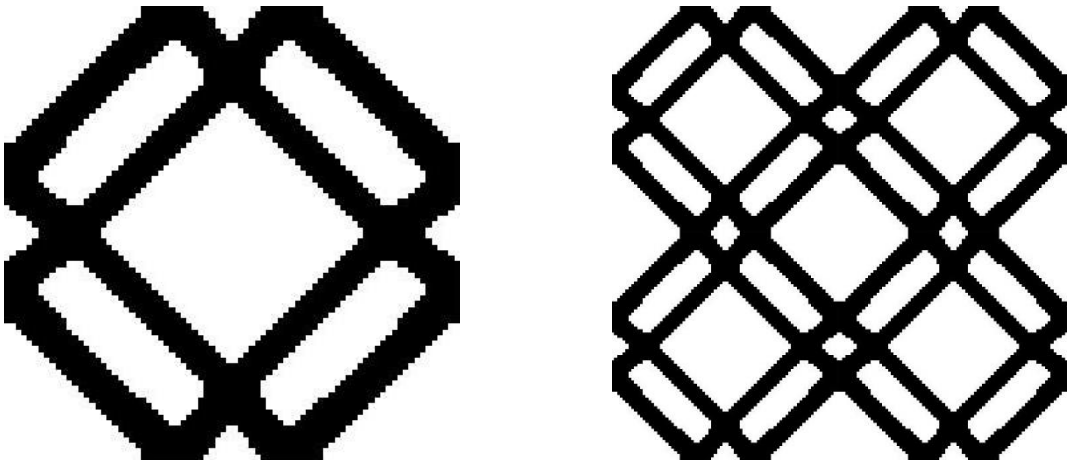

*Figure 5.20 – Material with Maximum Shear Modulus obtained using Homogenization Approach, $\phi = 0.1101$, $r = 2$, $m = 0.4$, $\nu = 0.3$, $p = 8$, $mv = 0.1$, $N = 6400$, OC, SIMP*

## 5.7 Volume fraction influence

The Volume fraction is the amount of material that is available to the optimization design.

For stiffness optimizations, a bigger volume fraction is surely translated in a bigger compliance. The stiffest material design possible is without a doubt a completely solid material $RVE$. However, even though the expected results of a variation in the amount of available material is a proportionate variation in the structure thickness, sometimes the optimization results, specially for smaller volume fractions, present different microstructures than the expected ones.

The lack of material, in smaller volume fraction solutions, can interfere with the convergence speed in the initial iterations, which can lead the solution to different local maximums. A too small volume fraction can also make the optimization impossible to solve.

Comparing Figure 5.18 to Figure 5.21 and Figure 5.22 and Figure 5.11 to Figure 5.23 can exemplify this problem, specially Figure 5.21.

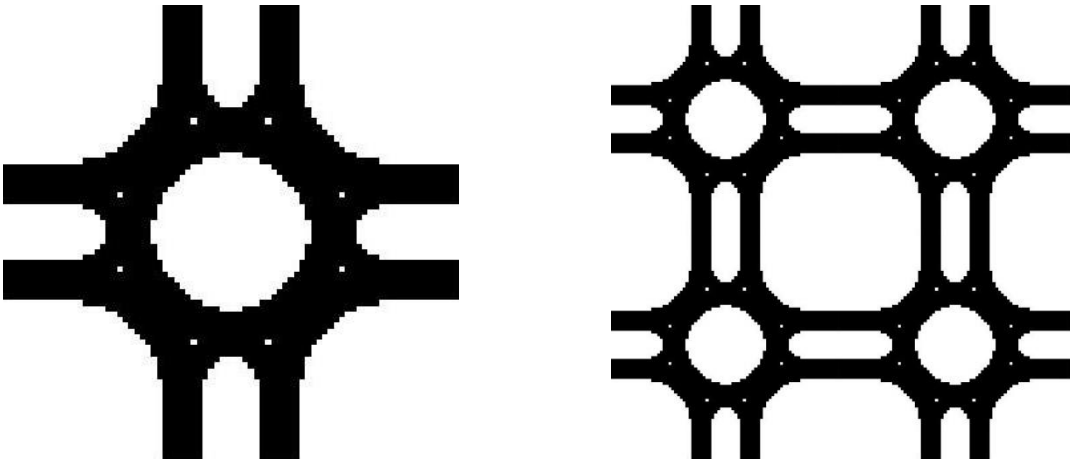

*Figure 5.21 – Material with Maximum Bulk Modulus obtained using Homogenization Approach, $\phi = 0.4877$, $r = 2$, $m = 0.3$, $\nu = 0.3$, $p = 8$, $mv = 0.1$, $N = 6400$, OC, SIMP*

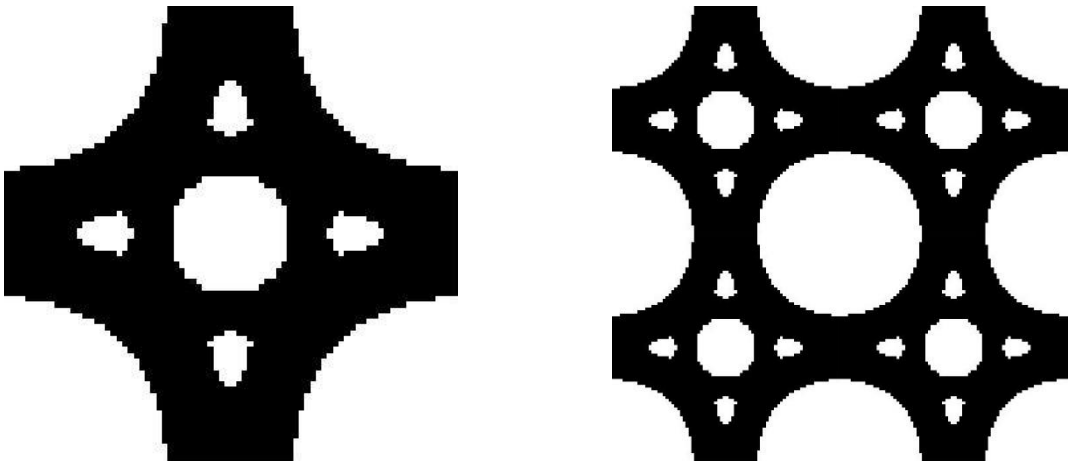

*Figure 5.22 - Material with Maximum Bulk Modulus obtained using Homogenization Approach, $\phi = 0.7551$, $r = 2$, $m = 0.5$, $\nu = 0.3$, $p = 8$, $mv = 0.1$, $N = 6400$, OC, SIMP*

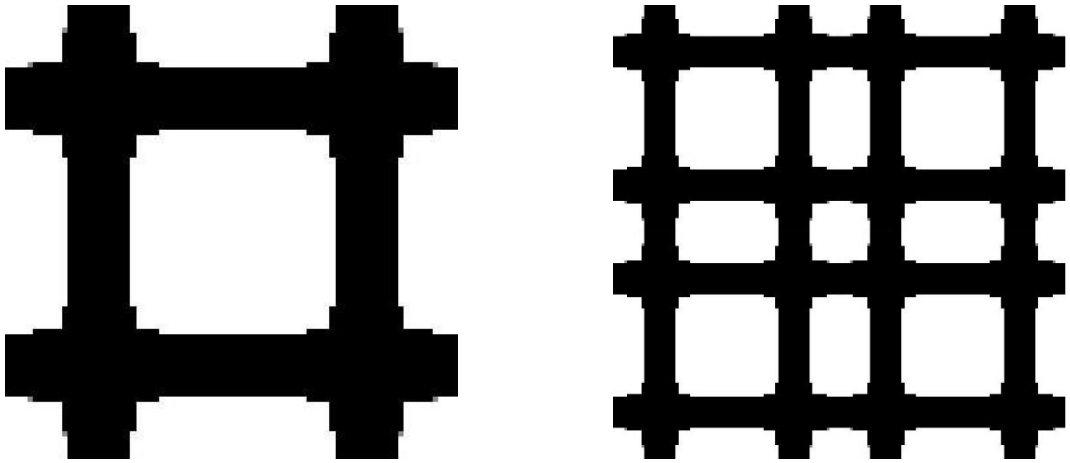

*Figure 5.23 – Material with Maximum Compliance for $45°$ Pure Shear Strain, corresponding to the strain field $\bar{\varepsilon} = [1, -1, 0]$, obtained using Homogenization Approach, $\phi = 0.5640$, $r = 2$, $m = 0.5$, $\nu = 0.3$, $p = 8$, $mv = 0.05$, $N = 6400$, OC, SIMP*

# 5.8 Mesh-dependency

Mesh-dependency is the relation of the acquired results with the mesh discretization. For some problems, it is important that the solution design doesn't change with the variation of the number of elements in the mesh.

Considering this problem, to maintain independent solutions from the mesh refinement, a well-chosen sensitivity filtering radius is necessary. A proportionate filter radius variation should be applied with the mesh refinement variation. When this rule is followed the results between two different meshes should be similar designs.

It is however expected a slight compliance increase with the mesh refinement increase thanks to the additional smoothness of the $FEM$ mesh.

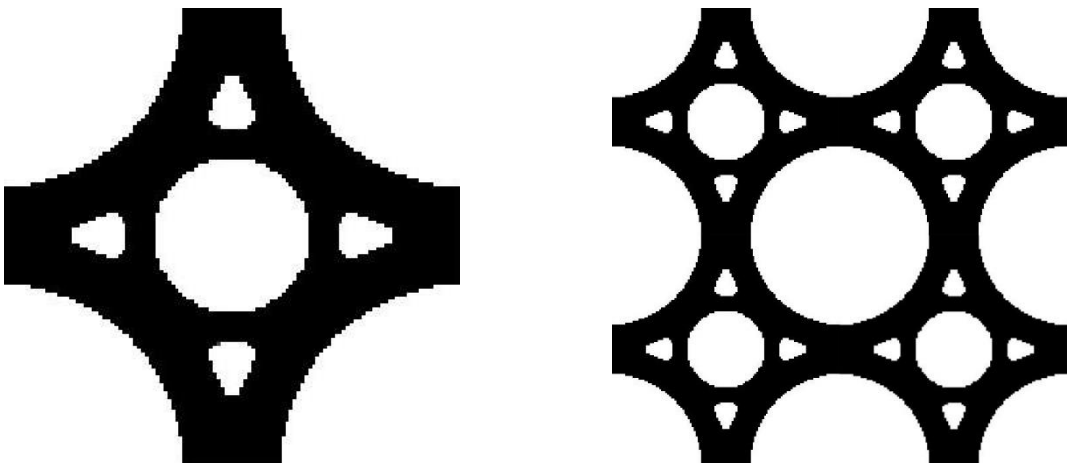

*Figure 5.24 – Material with Maximum Bulk Modulus obtained using Homogenization Approach, $\phi = 0.5626$, $r = 3$, $m = 0.4$, $\nu = 0.3$, $p = 8$, $mv = 0.1$, $N = 14400$, OC, SIMP*

## 5.9 Penalization influence

The penalization choice is very important for the overall performance of the optimization.

A too small penalization will produce convergence problems, since the intermediate densities are not sufficiently penalized, while a too big penalization will converge the solution to non-optimum designs, because the lighter elements contribution to the overall stiffness will be too small. An intermediate penalization, $6 \leq p \leq 9$, will produce better results with faster convergence times. However, depending on the initial guess, a higher penalization may sometimes be necessary to force a solution initial convergence.

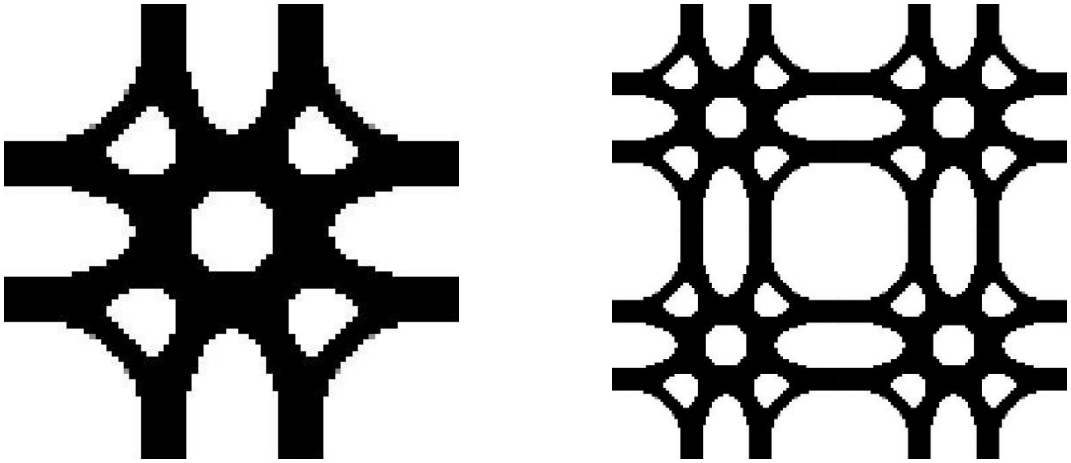

*Figure 5.25 – Material with Maximum Bulk Modulus obtained using Homogenization Approach, $\phi = 0.5585$, $r = 2$, $m = 0.4$, $\nu = 0.3$, $p = 4$, $mv = 0.1$, $N = 6400$, OC, SIMP*

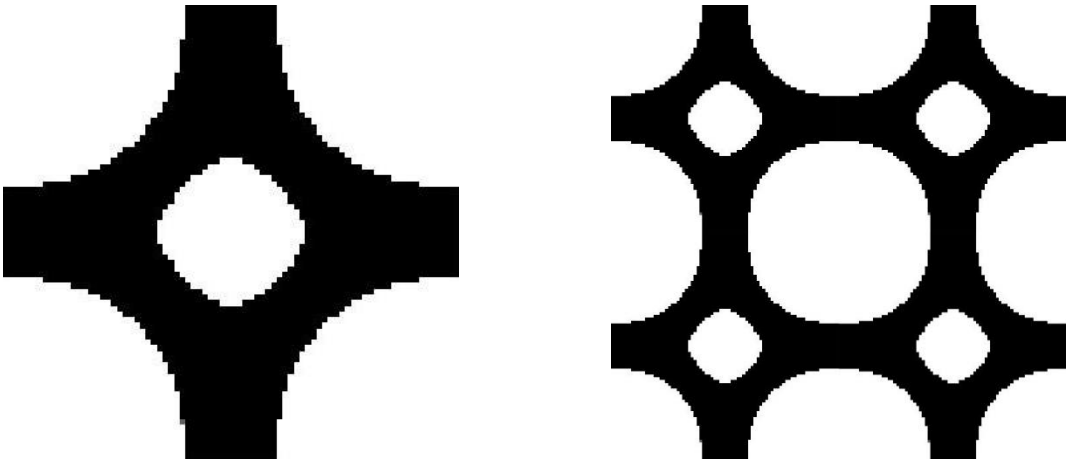

*Figure 5.26 – Material with Maximum Bulk Modulus obtained using Homogenization Approach, $\phi = 0.5624$, $r = 2$, $m = 0.4$, $\nu = 0.3$, $p = 12$, $mv = 0.1$, $N = 6400$, OC, SIMP*

## 5.10 Poisson number influence

When doing an optimization test, the properties of the material that is pretended to be emulated, should always be taken in account. As can be seen by Figure 5.27, Figure 5.28 and Figure 5.29, different solid material Poisson Numbers can affect the optimum microstructure final design.

As expected, for a Bulk Modulus maximization, the compliance increases with the increase of the solid material Poisson Number value.

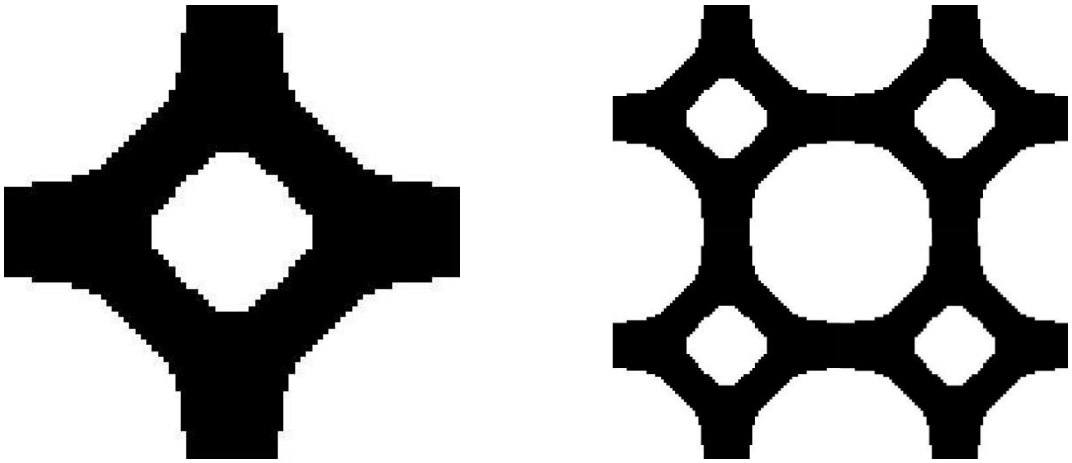

*Figure 5.27 – Material with Maximum Bulk Modulus obtained using Homogenization Approach, $\phi = 0.5262$, $r = 2$, $m = 0.4$, $\nu = 0.1$, $p = 8$, $mv = 0.1$, $N = 6400$, OC, SIMP*

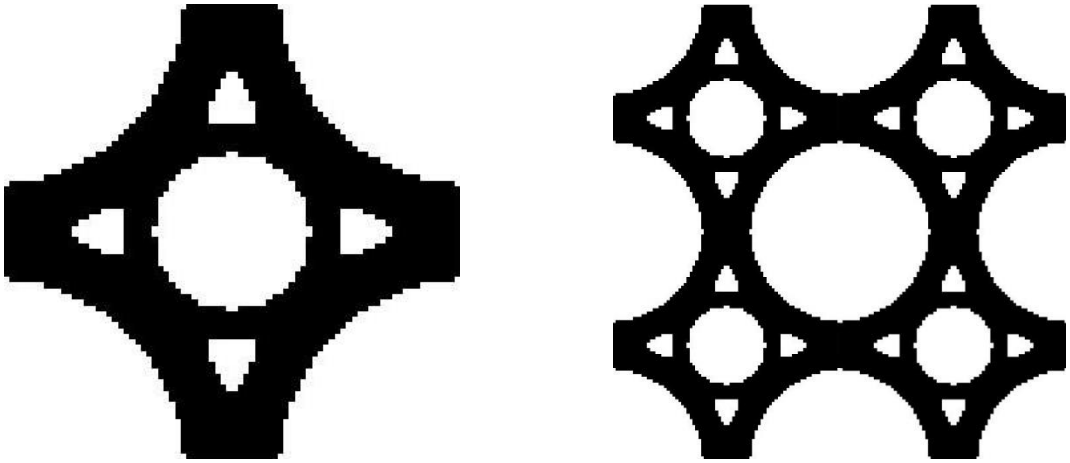

*Figure 5.28 - Material with Maximum Bulk Modulus obtained using Homogenization Approach, $\phi = 0.6040$, $r = 2$, $m = 0.4$, $\nu = 0.5$, $p = 8$, $mv = 0.1$, $N = 6400$, OC, SIMP*

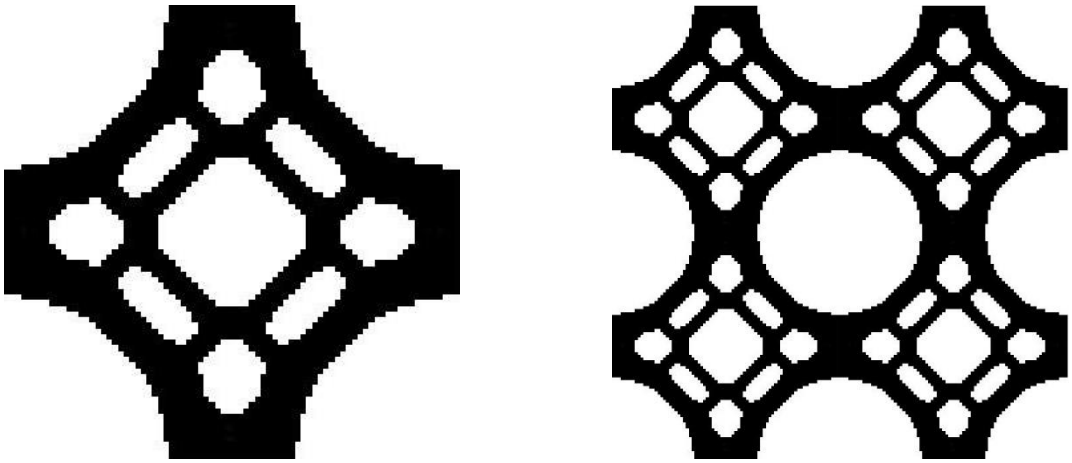

*Figure 5.29 - Material with Maximum Bulk Modulus obtained using Homogenization Approach, $\phi = 0.7495$, $r = 2$, $m = 0.4$, $\nu = 0.8$, $p = 8$, $mv = 0.1$, $N = 6400$, OC, SIMP*

# 5.11Method of Moving Asymptotes

As can be seen by comparing Figure 5.18 to Figure 5.30 the results obtained through the two different optimizations are very similar. Even though $SIMP$ approach is slightly faster for non-constrained (except volume) optimizations, the differences in optimization speed is negligible.

Even though in this example the compliance obtained is slightly bigger using the Optimality Criteria, this is not always the case. Sometimes, the method of Moving Asymptotes presents better results. These differences can be explained by errors relative to $FEM$ method and by the convergence speed of both methods, especially when the sensitivity filtering is removed.

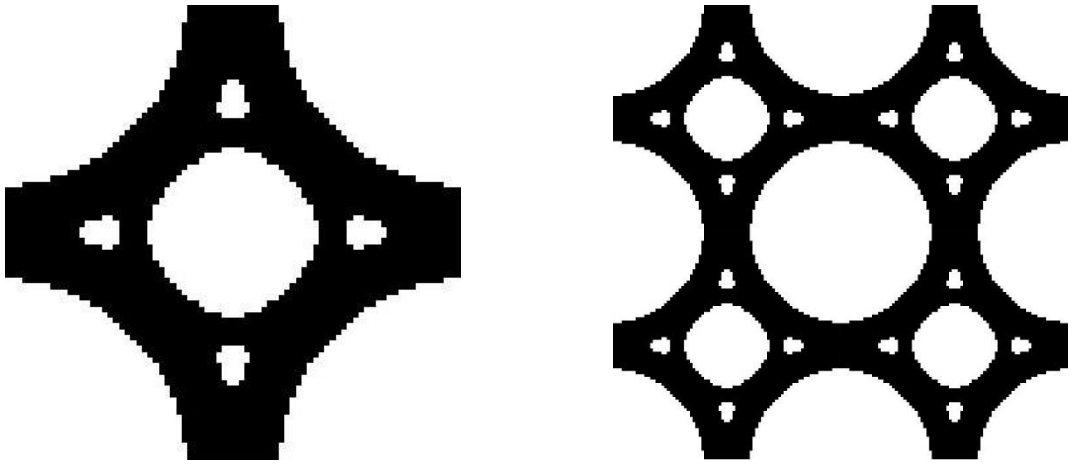

*Figure 5.30 - Material with Maximum Bulk Modulus obtained using Homogenization Approach, $\phi = 0.5555$, $r = 2$, $m = 0.4$, $\nu = 0.3$, $p = 8$, $mv = 0.1$, $N = 6400$, MMA, SIMP*

# 5.12$SIMP$ vs $RAMP$ interpolation and $E_{min}$ influence

There were some difficulties implementing the $RAMP$ approach. Even though the interpolation scheme would occasionally converge, often the results were not satisfactory. For example, when using smaller $Volume\ fractions\ (m)$, the program would not converge, no matter how big the $penalization\ (q)$ used was.

It was later discovered that the $RAMP$ interpolation convergence was very dependent on the $E_{min}$ used. For $E_{min} \leq {}^{E_{mat}}/_{100}$ the solution would many times reach a homogeneous grey state. Since the $RAMP$ approach was first introduced to tackle multi material optimization problems, then the appearance of this problem is not unthinkable.

$E_{min}$'s influence over the solution was not so predominant in $SIMP$, however, it was also discovered that for the solutions to converge, the smaller the $E_{min}$, the bigger the $penalization\ (p)$ needed.

On one side using smaller $E_{min}$ leads to less errors in mathematical model since theoretically, $E_{min}$ should be equal to 0. On the other, using smaller $E_{min}$ leads to big penalizations that negatively influence the final designs, since the darker elements become too predominant.

It was also noticed that when using a bigger $E_{min}$, the solution would find a stable convergence direction on the early iterations which led to faster solutions.

Figure 5.31, Figure 5.32, Figure 5.33 and Figure 5.34 were some tests, to see how the solution was affected with the variation of $E_{min}$.

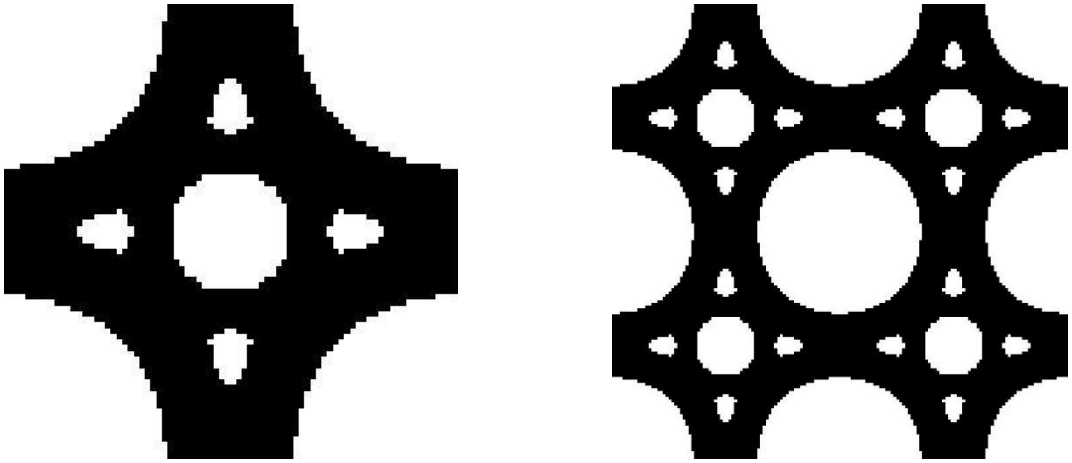

*Figure 5.31 - Material with Maximum Bulk Modulus obtained using Homogenization Approach, $\phi = 0.7551$, $E_{min} = E_{mat} * 10^{-2}$, $r = 2$, $m = 0.5$, $\nu = 0.3$, $p = 8$, $mv = 0.1$, $N = 6400$, OC, SIMP*

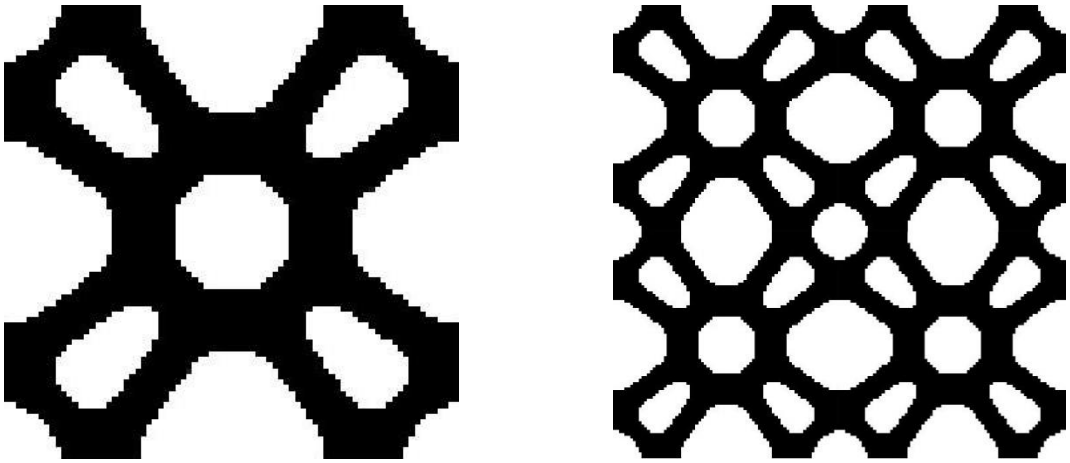

*Figure 5.32 - Material with Maximum Bulk Modulus obtained using Homogenization Approach, $\phi = 0.7195$, $E_{min} = E_{mat} * 10^{-3}$, $r = 2$, $m = 0.5$, $\nu = 0.3$, $p = 8$, $mv = 0.1$, $N = 6400$, OC, SIMP*

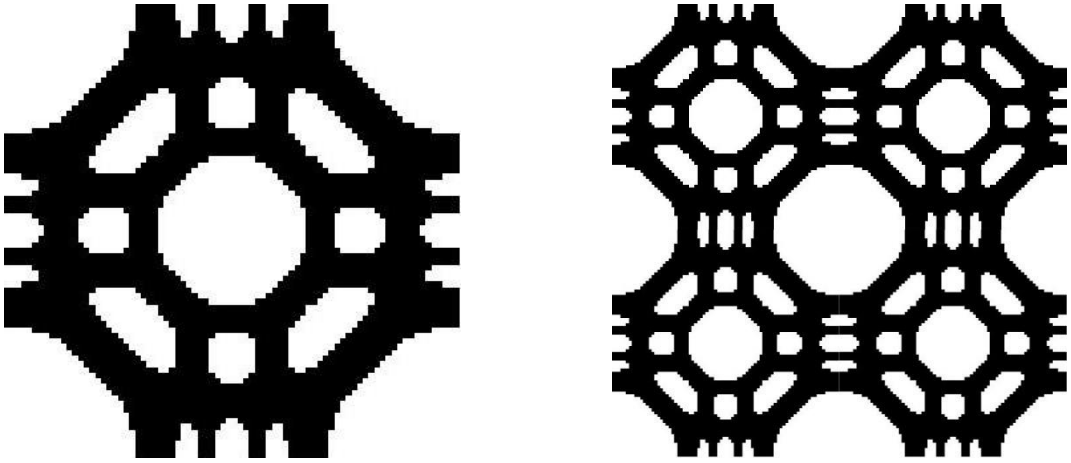

*Figure 5.33 - Material with Maximum Bulk Modulus obtained using Homogenization Approach, $\phi = 0.7219$, $E_{min} = E_{mat} * 10^{-4}$, $r = 2$, $m = 0.5$, $\nu = 0.3$, $p = 8$, $mv = 0.1$, $N = 6400$, OC, SIMP*

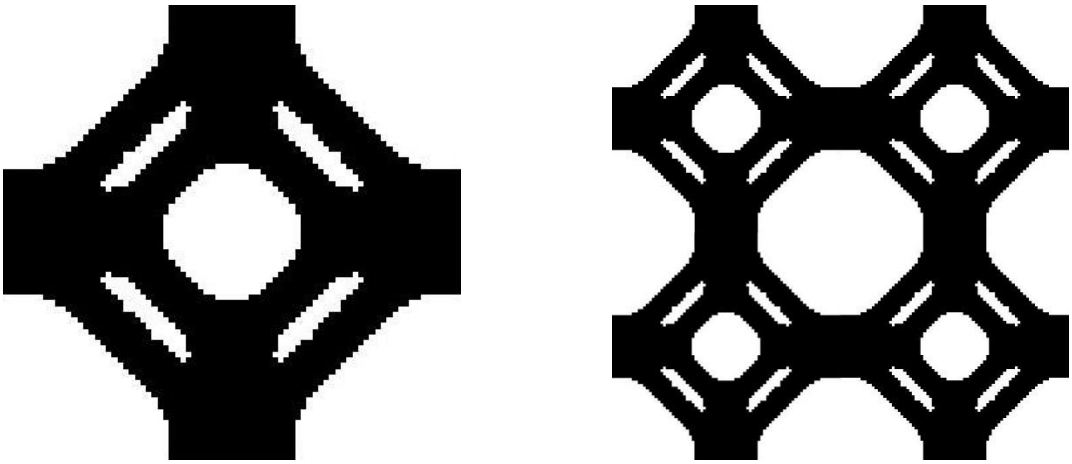

*Figure 5.34 - Material with Maximum Bulk Modulus obtained using Homogenization Approach, $\phi = 0.7211$, $E_{min} = E_{mat} * 10^{-5}$, $r = 2$, $m = 0.5$, $\nu = 0.3$, $p = 10$, $mv = 0.1$, $N = 6400$, OC, SIMP*

A bigger stiffness is expected for the results that use higher values of $E_{min}$, so in order to correctly evaluate the influence of $E_{min}$ in the results a new evaluation of the material properties of the solutions using the same $E_{min}$ should be executed.

So, evaluating all the results with $E_{min} = 1 * 10^{-6} * E_{mat}$ for the void elements, the compliances would respectively be for Figure 5.31 $\phi = 0.7226$, Figure 5.32 $\phi = 0.7162$, Figure 5.33 $\phi = 0.7216$ and Figure 5.34 $\phi = 0.7210$, leading to the conclusion that using a bigger $E_{min}$ doesn't negatively affect the solution, it just leads the solution to different local maximums. Using a smaller $E_{min}$ will however evaluate more correctly the void elements, lessening the errors related to this parameter.

Since using bigger $E_{min}$ doesn't negatively affect the solutions obtained, then we can use $RAMP$ approach for material design optimizations with one material. However, when comparing this approach to $SIMP$ the conclusion is that $SIMP$ interpolation is more stable. Even when using higher $E_{min}$ values, it is necessary to use higher values of $penalization\ (q)$ for smaller $volume\ fractions\ (m)$, otherwise the solution won't converge, as can be seen in Figure 5.36 which needed a $q = 40$ to converge while in Figure 5.35, $q = 12$.

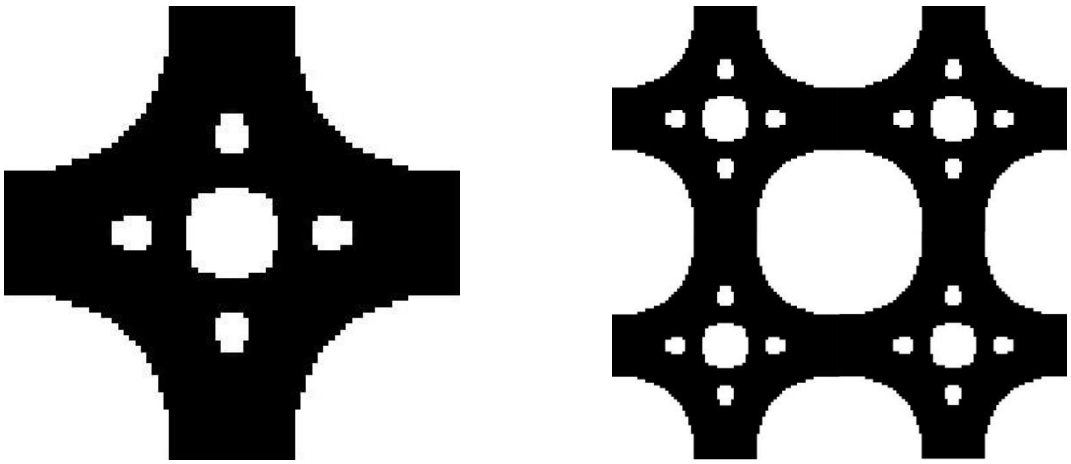

*Figure 5.35 - Material with Maximum Bulk Modulus obtained using Homogenization Approach, $\phi = 0.7596$, $E_{min} = E_{mat} * 10^{-2}$, $r = 2$, $m = 0.5$, $v = 0.3$, $q = 12$, $mv = 0.1$, $N = 6400$, OC, RAMP*

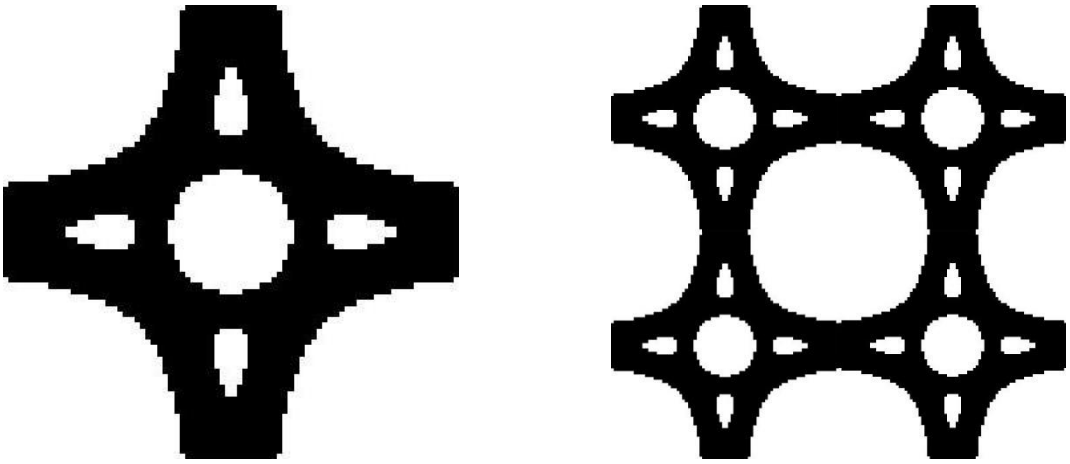

*Figure 5.36 - Material with Maximum Bulk Modulus obtained using Homogenization Approach, $\phi = 0.5567$, $E_{min} = E_0 * 10^{-2}$, $r = 2$, $vm = 0.4$, $v = 0.3$, $q = 40$, $mv = 0.1$, $N = 6400$, OC, RAMP*

Modifying $E_{min}$ also allows the design of multi material composite microstructures. For example, using $E_{min} = 0.3 \cdot E_{mat}$ corresponds to the design of a 2-phase microstructure, in which the softer material corresponds to a material with $30\%$ Young's Modulus value, in relation to the harder material.

Using both $SIMP$ and $RAMP$ interpolations, the results obtained are presented.

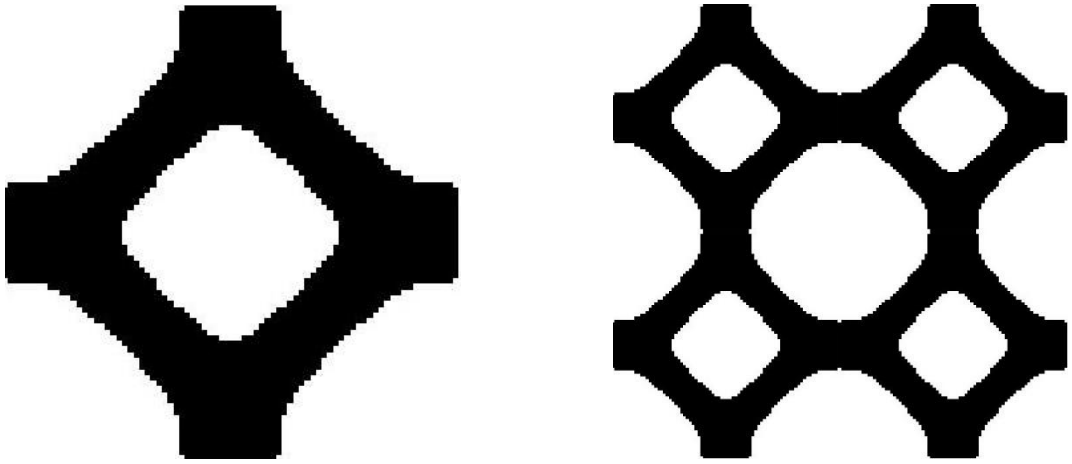

*Figure 5.37 – 2-Phase Material with Maximum Bulk Modulus obtained using Homogenization Approach, $\phi = 1.3897$, $E_{min} = 0.3 \cdot E_{mat}$, $r = 2$, $m = 0.5$, $\nu = 0.3$, $p = 3$, $mv = 0.1$, $N = 6400$, OC, SIMP*

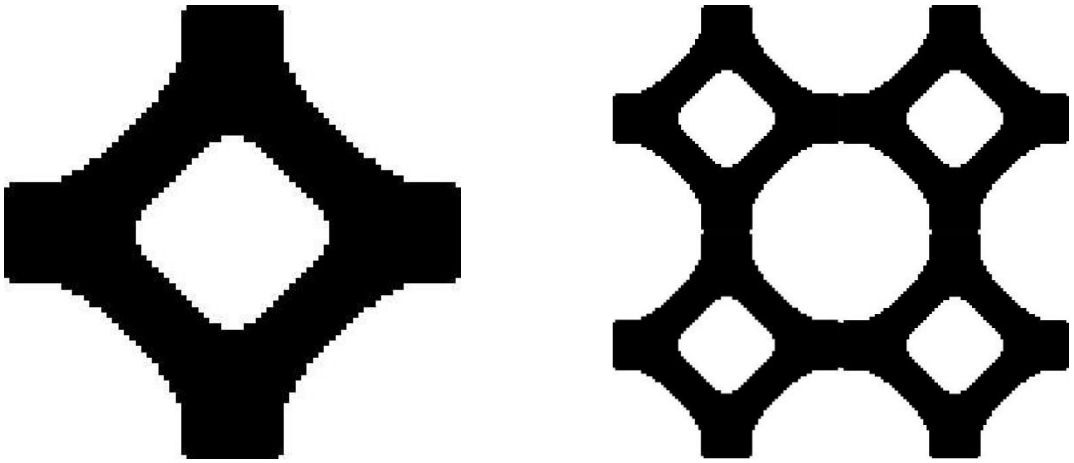

*Figure 5.38 – 2-Phase Material with Maximum Bulk Modulus obtained using Homogenization Approach, $\phi = 1.3900$, $E_{min} = 0.3 \cdot E_{mat}$, $r = 2$, $mv = 0.5$, $\nu = 0.3$, $q = 3$, $mv = 0.1$, $N = 6400$, OC, RAMP*

## 5.13 Maximize Stiffness with Material Properties Constraints

An interesting problem can be formulated by considering maximum stiffness optimizations with certain material properties constraints.

Taking full use of the capabilities of the $MMA$ algorithm, the computational model can produce some interesting designs.

However, some understanding of the mathematical sensitivity problem and of the $MMA$ algorithm behaviour is necessary to produce the expected results.

Firstly, it is important to remember that the constraints in the $MMA$ method are always inequalities. For some cases, it is useful to apply two inequality constraints for the same parameter to appropriately converge the solution. An example would be $0.37 \leq m(\rho) \leq 0.4$.

Secondly, the $MMA$ method priority is to make sure every constraint is satisfied. Only after, will the $MMA$ start optimizing the objective function. Also, filtering the constraint sensitivities can perturb the well-functioning of the optimizer since the constraint parameters are very sensitive. Errors introduced by filtering operations can easily make the optimizer violate the given constraints. On the other side, the lack of filtering will introduce some smoothing problems in the solutions. This problem appears because the $SIMP$ interpolation has the tendency to get “stuck” in 0-1 designs in which experimental evidence has shown that the use of filtering tends to attenuate this behaviour. So, to get the best results, the user should use the filtering until a point where the constraint is close to active and only then should the optimization continue without filtering in the constraints. The objective function filtering should continue to be used until the solution has reached a converged state.

Lastly, for specific constraints, the sensitivities cannot be evaluated in a very homogeneous initial guess. For example, negative Poisson constraints would be impossible to implement in the first initial guess of Figure 5.39 because in a very homogenous micro-structure, every added density in a random element would increase the overall structure Poisson number making it impossible for the program to start converging. However, using the slightly converged design on the right initial guess of Figure 5.39, the constraints can be applied and the solution will converge.

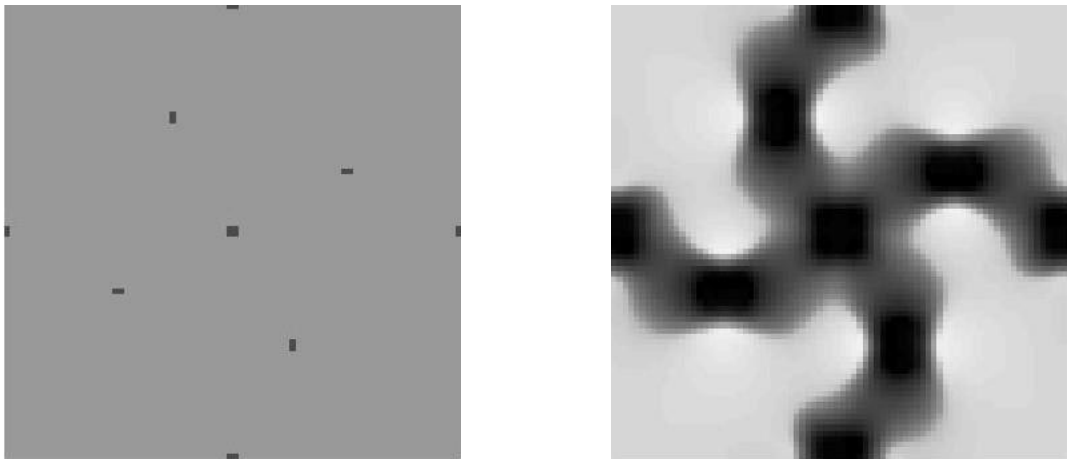

*Figure 5.39 – Non-Symmetric Initial Design on the left, Slightly Converged Non-Symmetric Initial Design on the right*

Considering the above explanation, it was implemented a Bulk Modulus Maximization problem with $C_{12}$ constraints. By constraining $C_{12}$, the Poisson number of the microstructure is artificially constrained. If $C_{12} \leq 0$, then it follows that $\nu \leq 0$, which translates into the design of auxetic materials. The design problem becomes a problem of maximum stiffness materials with auxetic properties.

To attenuate the smoothness problems introduced by the lack of filtering, two different initial guesses were used. For the designs depicted in Figure 5.42, Figure 5.44 and Figure 5.46 the initial design used was the Slightly Converged initial design from Figure 5.39. For the designs depicted in Figure 5.43, Figure 5.45 and Figure 5.47 the initial design was the converged solution to the $C_{12}$ minimization problem depicted in Figure 5.41.

By comparison we can see that the solutions that used the converged solution of the $C_{12}$ minimization problem as the initial guess tend to have higher compliances. However, it is necessary to notice that using Figure 5.41 as a starting point for the solution is a very rigid initial guess, which means that the following results will be very similar in design to the initial design.

One other important thing to notice is that, in all the 6 solutions, the constraint is active. This is an expected result. After all, $\phi = 2 \cdot C_{11} + 2 \cdot C_{12}$, as was explained in chapter 5. Then by constraining $C_{12}$ to values below the obtained in the non-constrained optimization in Figure 5.40, we are imposing a constraint that has an opposite gradient in relation to $\phi$, since the compliance is directionally proportional to $C_{12}$.

It's also important to mention that the results using the non-symmetric initial guess resulted in materials with non-symmetric designs.

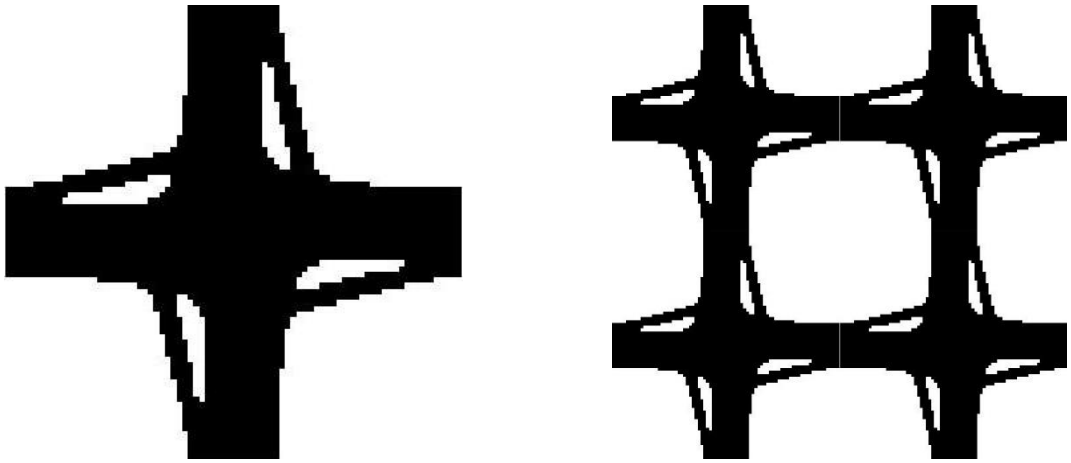

*Figure 5.40 - Material with Maximum Bulk Modulus obtained using Homogenization Approach, $\phi = 0.5495$, $r = 2$, $m = 0.4$, $\nu = 0.3$, $p = 8$, $mv = 0.1$, $N = 6400$, MMA, SIMP*

$$C_{ij} = \begin{bmatrix} 0.2445 & 0.0302 & -0.0025 \\ 0.0302 & 0.2445 & 0.0025 \\ -0.0025 & 0.0025 & 0.0188 \end{bmatrix}$$

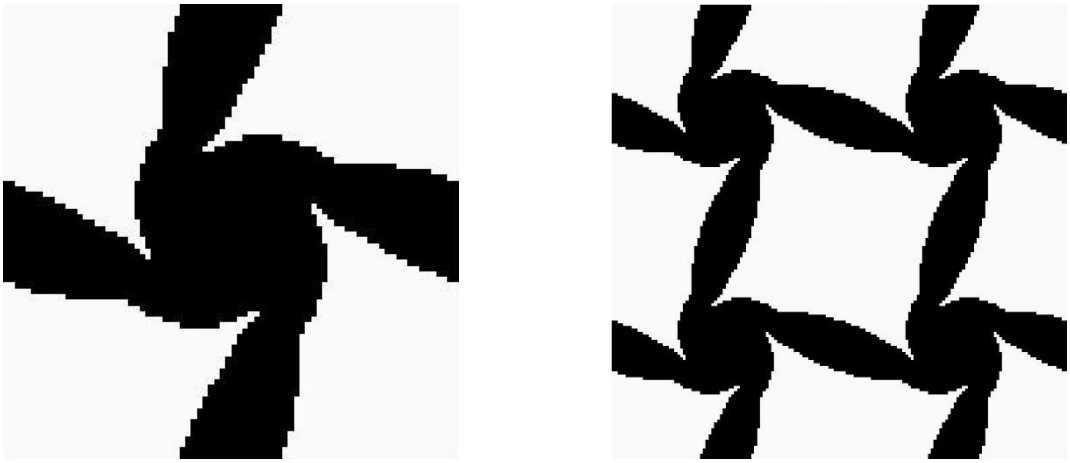

*Figure 5.41 – Material with Minimum $C_{12}$, obtained using Homogenization Approach, $C_{12} = -0.0355$, $r = 2$, $m = 0.4$, $\nu = 0.3$, $p = 8$, $mv = 0.1$, $N = 6400$, MMA, SIMP*

$$C_{ij} = \begin{bmatrix} 0.1043 & -0.0355 & 0.0201 \\ -0.0355 & 0.1043 & -0.0201 \\ 0.0201 & -0.0201 & 0.0150 \end{bmatrix}$$

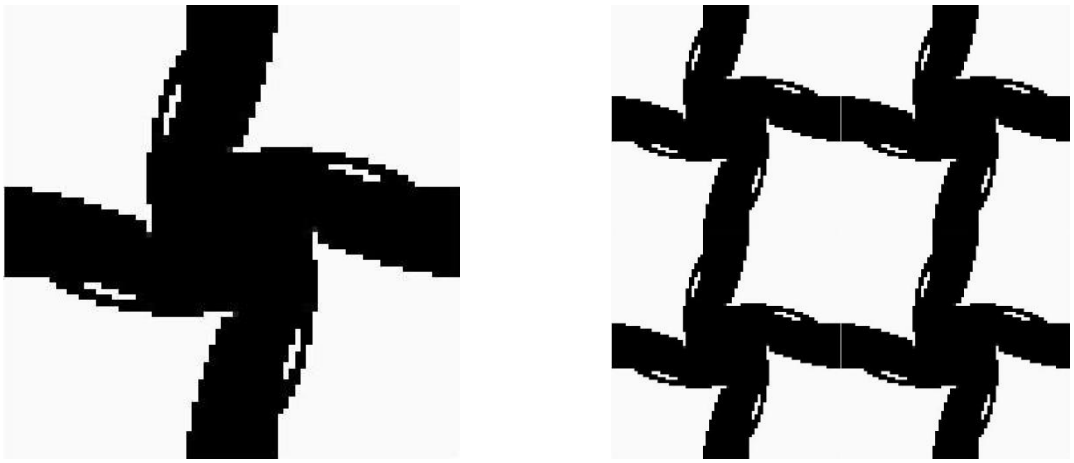

*Figure 5.42 - Material with Maximum Bulk Modulus and $C_{12} \leq -0{,}02$, obtained using Homogenization Approach, $\phi = 0.2689$, $C_{12} = -0{,}0200$ $r = 2$, $m = 0.4$, $\nu = 0.3$, $p = 8$, $mv = 0.1$, $N = 6400$, MMA, SIMP*

$$C_{ij} = \begin{bmatrix} 0.1544 & -0.0200 & 0.0169 \\ -0.0200 & 0.1544 & -0.0169 \\ 0.0169 & -0.0169 & 0.0143 \end{bmatrix}$$

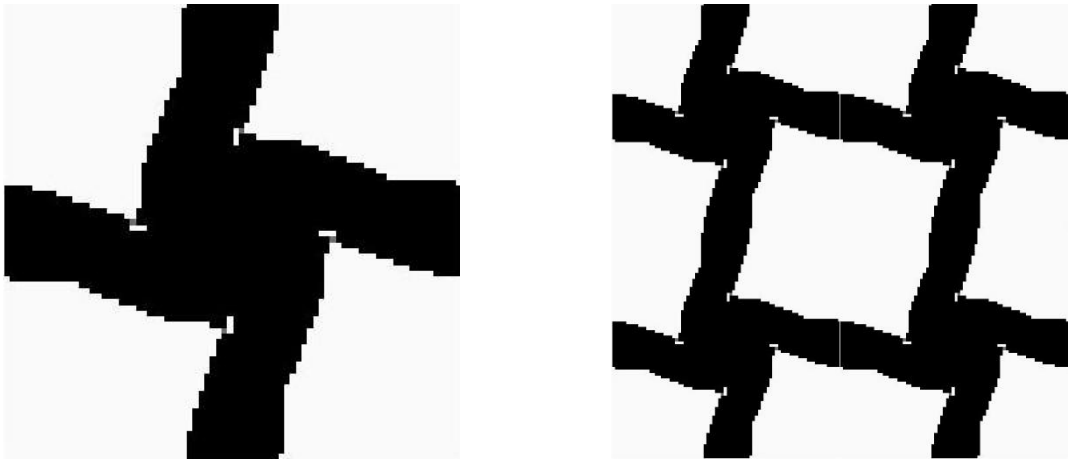

*Figure 5.43 - Material with Maximum Bulk Modulus and $C_{12} \leq -0{,}02$, obtained using Homogenization Approach, $\phi = 0.2749$, , $C_{12} = -0{,}0200$, $r = 2$, $m = 0.4$, $\nu = 0.3$, $p = 8$, $mv = 0.1$, $N = 6400$, MMA, SIMP*

$$C_{ij} = \begin{bmatrix} 0.1574 & -0.0200 & 0.0180 \\ -0.0200 & 0.1574 & -0.0180 \\ 0.0180 & -0.0180 & 0.0152 \end{bmatrix}$$

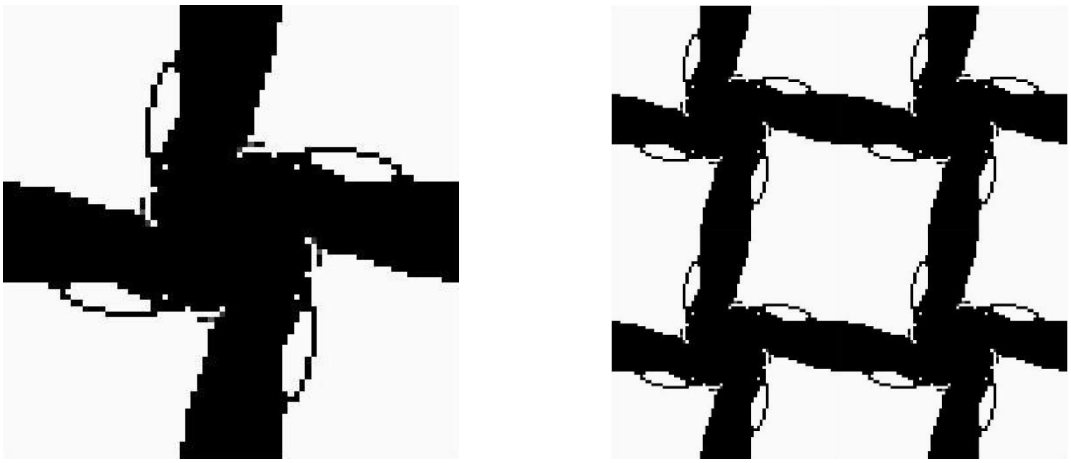

*Figure 5.44 - Material with Maximum Bulk Modulus and $C_{12} \leq -0{,}01$, obtained using Homogenization Approach, $\phi = 0.3252$, $C_{12} = -0{,}0100$, $r = 2$, $m = 0.4$, $\nu = 0.3$, $p = 8$, $mv = 0.1$, $N = 6400$, MMA, SIMP*

$$C_{ij} = \begin{bmatrix} 0.1726 & -0.0100 & 0.0134 \\ -0.0100 & 0.1726 & -0.0134 \\ 0.0134 & -0.0134 & 0.0131 \end{bmatrix}$$

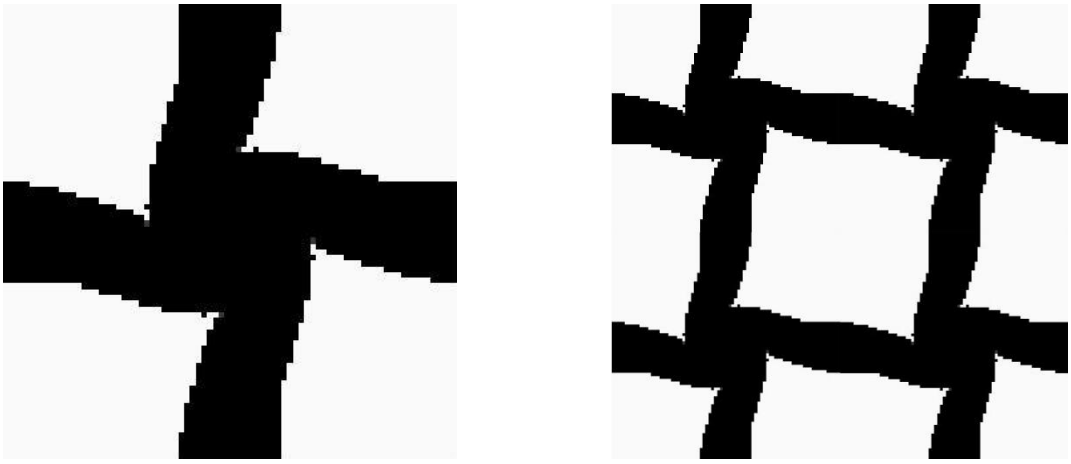

*Figure 5.45 - Material with Maximum Bulk Modulus and $C_{12} \leq -0{,}01$, obtained using Homogenization Approach, $\phi = 0.3364$, $C_{12} = -0{,}0100$, $r = 2$, $m = 0.4$, $\nu = 0.3$, $p = 8$, $mv = 0.1$, $N = 6400$, MMA, SIMP*

$$C_{ij} = \begin{bmatrix} 0.1782 & -0.0100 & 0.0144 \\ -0.0100 & 0.1782 & -0.0144 \\ 0.0144 & -0.0144 & 0.0135 \end{bmatrix}$$

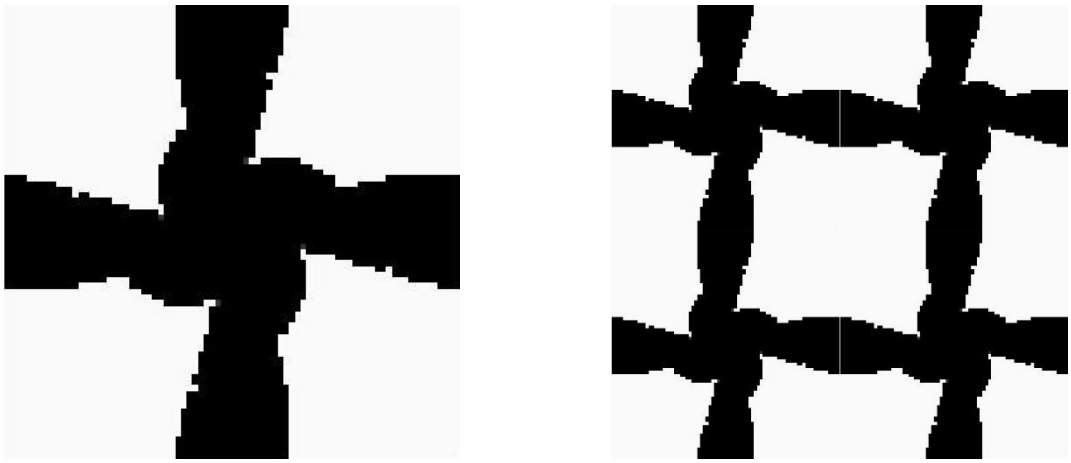

*Figure 5.46 - Material with Maximum Bulk Modulus and $C_{12} \leq 0{,}00$, obtained using Homogenization Approach, $\phi = 0.3688$, $C_{12} = 0{,}0000, r = 2$, $m = 0.4$, $\nu = 0.3$, $p = 8$, $mv = 0.1$, $N = 6400$, MMA, SIMP*

$$C_{ij} = \begin{bmatrix} 0.1844 & 0.0000 & 0.0096 \\ 0.0000 & 0.1844 & -0.0096 \\ 0.0096 & -0.0096 & 0.0111 \end{bmatrix}$$

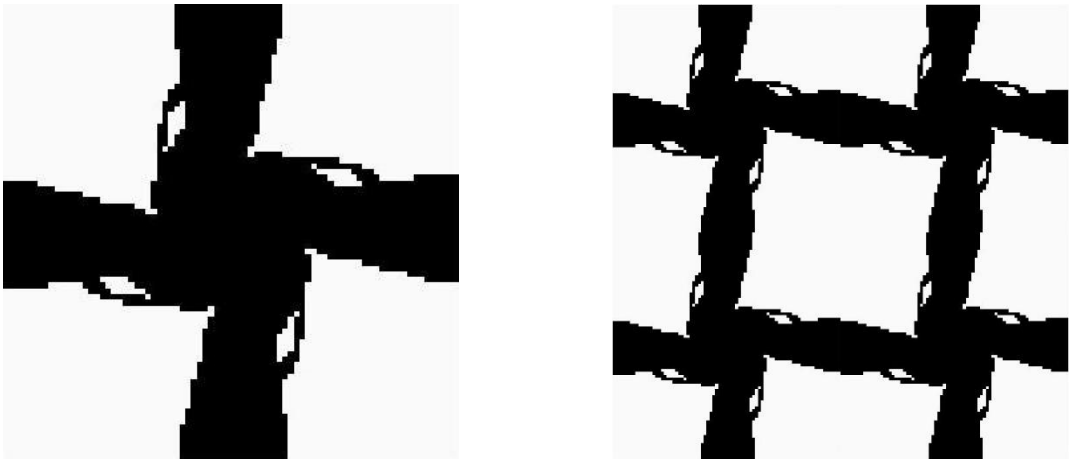

*Figure 5.47 - Material with Maximum Bulk Modulus and $C_{12} \leq 0{,}00$, obtained using Homogenization Approach, $\phi = 0.3844$, $C_{12} = 0{,}0000$, $r = 2$, $mv = 0.4$, $\nu = 0.3$, $p = 8$, $mv = 0.1$, $N = 6400$, MMA, SIMP*

$$C_{ij} = \begin{bmatrix} 0.1922 & 0.0000 & 0.0115 \\ 0.0000 & 0.1922 & -0.0115 \\ 0.0115 & -0.0115 & 0.0111 \end{bmatrix}$$

Following the same methodology, the program was tested for other examples of Bulk Modulus Maximization problem with $C_{12}$ constraints. However, this time the objective was constraining $C_{12}$ to be higher than the value obtained with the simple Bulk Modulus Maximization of Figure 5.40.

Firstly, a maximization of the $C_{12}$ was executed in Figure 5.48. After, two identical tests were performed for Bulk Modulus Maximization problem with $C_{12}$ constraints. For Figure 5.49 the initial guess used was the microstructure presented in Figure 5.39, and for Figure 5.50 the starting point was the solution to the non-constrained maximization problem depicted in Figure 5.48.

Contrary to the anterior results, this time the best compliance was obtained in solution that used the less rigid initial guess, the reason being that the results still managed to be very smooth without any checkerboard problem for the first solution, which translated a less rigid initial guess into an added liberty of the optimization to find the best local maximum.

It is also interesting to notice that even though the constraint used was $C_{12} \geq 0{,}07$, this constrain was satisfied without being active and that the compliance from Figure 5.40 was overtaken by the constrained results, which leads to the conclusion that the added constraint led the solution to an even better local maximum than before, which means that even without the constraint, a different initial guess could possibly achieve the same results.

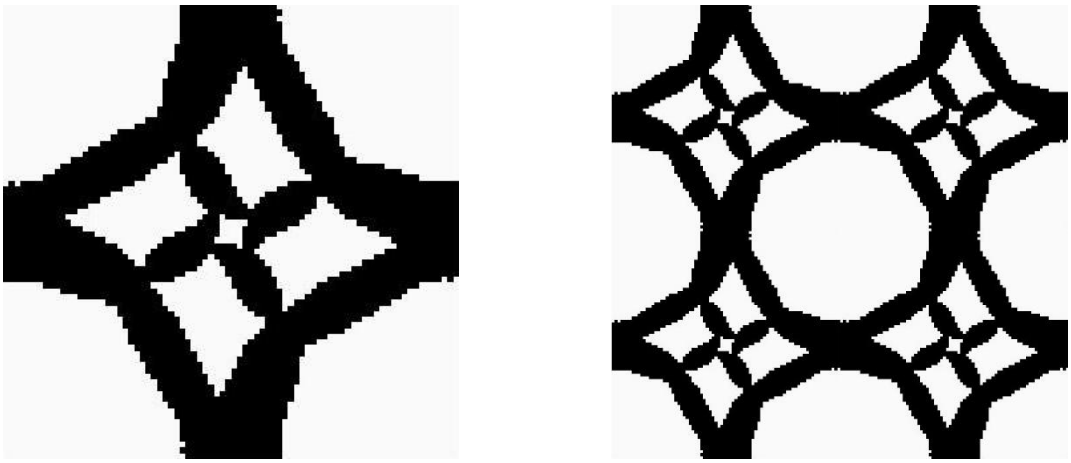

*Figure 5.48 - Material with Maximum $C_{12}$, obtained using Homogenization Approach, $\phi = 0.0980$, $r = 2$, $m = 0.4$, $\nu = 0.3$, $p = 8$, $mv = 0.1$, $N = 6400$, MMA, SIMP*

$$C_{ij} = \begin{bmatrix} 0.1421 & 0.0980 & 0.0002 \\ 0.0980 & 0.1421 & -0.0002 \\ 0.0002 & -0.0002 & 0.0391 \end{bmatrix}$$

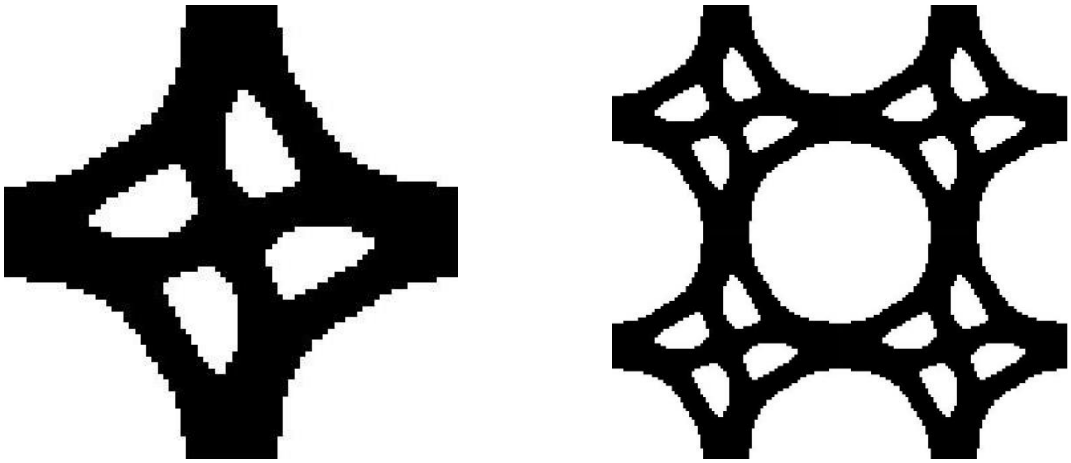

*Figure 5.49 - Material with Maximum Bulk Modulus and $C_{12} \geq 0{,}07$, obtained using Homogenization Approach, $\phi = 0.5521$, $C_{12} = 0{,}0775$, $r = 2$, $m = 0.4$, $\nu = 0.3$, $p = 8$, $mv = 0.1$, $N = 6400$, MMA, SIMP*

$$C_{ij} = \begin{bmatrix} 0.1986 & 0.0775 & 0.0022 \\ 0.0775 & 0.1986 & -0.0022 \\ 0.0022 & -0.0022 & 0.0360 \end{bmatrix}$$

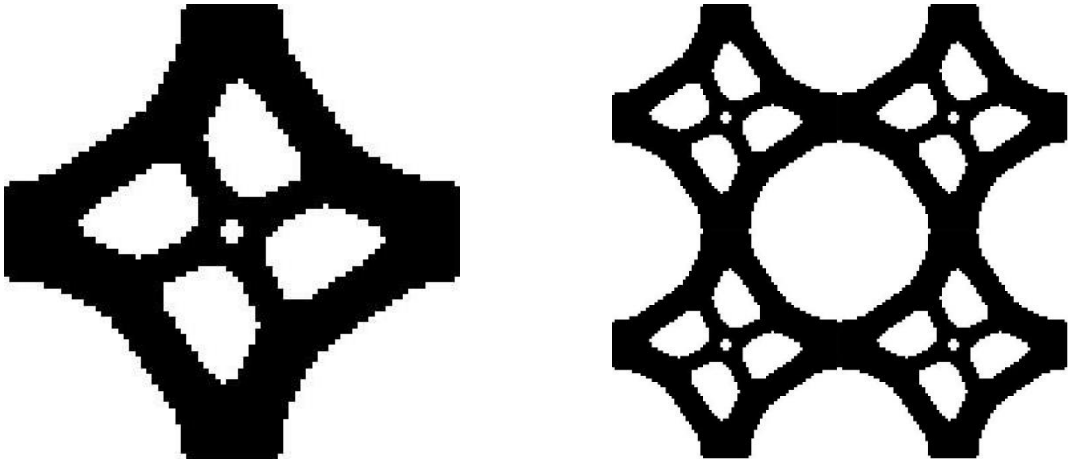

*Figure 5.50 - Material with Maximum Bulk Modulus and $C_{12} \geq 0{,}07$, obtained using Homogenization Approach, $\phi = 0.5496$, $C_{12} = 0{,}0988$, $r = 2$, $m = 0.4$, $\nu = 0.3$, $p = 8$, $mv = 0.1$, $N = 6400$, MMA, SIMP*

$$C_{ij} = \begin{bmatrix} 0.1760 & 0.0988 & 0.0022 \\ 0.0988 & 0.1760 & -0.0022 \\ 0.0022 & -0.0022 & 0.0482 \end{bmatrix}$$

There are many examples that are possible to study with this methodology. In the next case, it is presented a problem of Compliance Maximization for a stress field $\bar{\varepsilon} = [1,0,0]$, which is equal to a problem of $C_{11}$ maximization, with constraints on the $C_{22}$ parameter. In other words, the objective is the design of a material with maximum stiffness in the horizontal direction, while still maintaining a minimum value of stiffness in the vertical one.

In this case a symmetric initial guess was used, specifically, the initial guess with soft material in a circular region represented in Figure 5.17.

As can be seen, the microstructure presents a high stiffness in the horizontal direction, since most of the material is distributed parallel to the horizontal axis.

It is important to understand that even though the constraint is not active in this solution, it only happened after deactivating the sensitivity filter of the objective function. This is related to the $SIMP$ interpolation problem of getting “stuck” in 0-1 designs.

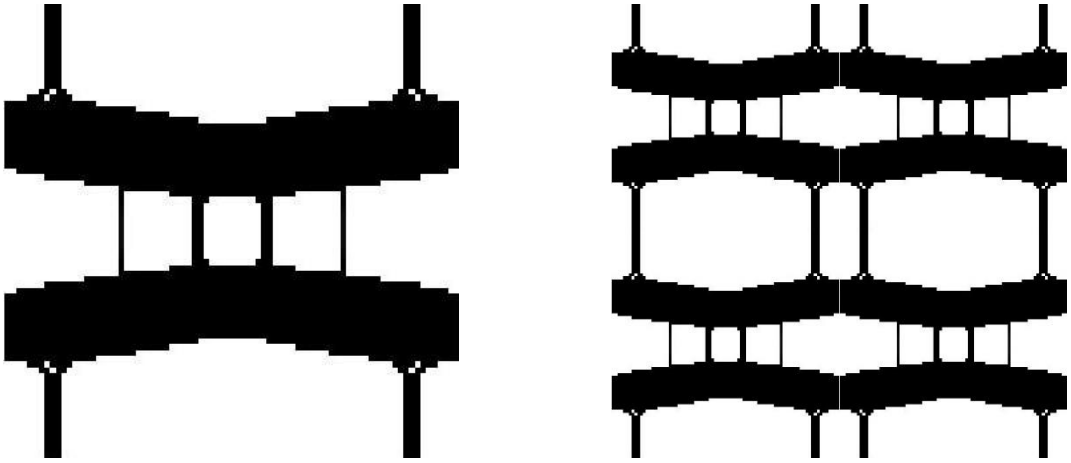

*Figure 5.51 - Material with Maximum $C_{11}$ and $C_{22} \geq 0{,}07$, obtained using Homogenization Approach, $\phi = 0.3337$, $r = 2$, $m = 0.4$, $\nu = 0.3$, $p = 8$, $mv = 0.1$, $N = 6400$, MMA, SIMP*

$$C_{ij} = \begin{bmatrix} 0.3337 & 0.0389 & 0 \\ 0.0389 & 0.0703 & 0 \\ 0 & 0 & 0.0087 \end{bmatrix}$$

## 5.14 Maximize Stiffness with Stress Criteria Constraints

One of the principal objectives of this work was to develop a computational model that could Maximize the stiffness of a microstructure, given specific average stress criteria constraints.

These constraints can be introduced in the average Von Mises Stress criteria ($\bar{\sigma}_{VM}^2$) [1] or in the average Hydrostatic Stress ($\bar{\sigma}_H$).

In plane stress,

$$\bar{\sigma}_{VM}^2 = \bar{\sigma}_1^2 + \bar{\sigma}_2^2 - \bar{\sigma}_1 \cdot \bar{\sigma}_2 + 3 \cdot \bar{\sigma}_3^2, \tag{5.8}$$

$$\bar{\sigma}_H = \bar{\sigma}_1 + \bar{\sigma}_2, \tag{5.9}$$

And the stiffness is calculated by the compliance

$$\phi = \bar{\sigma}_1 \cdot \bar{\varepsilon}_1 + \bar{\sigma}_2 \cdot \bar{\varepsilon}_2 + \bar{\sigma}_3 \cdot \bar{\varepsilon}_3, \tag{5.10}$$

For a strain field $\bar{\varepsilon} = [1,1,0]$, 3 different tests are presented. In Figure 5.52 a maximization of the average Von Mises Stress is executed. In Figure 5.53 a material with maximum average Hydrostatic Stress is presented. And in Figure 5.54, a maximum stiffness optimization of the material structure is shown.

Comparing those 3 results, we notice that all the designs and the obtained average stresses and compliances are identical. This implies that the solutions evolved identically.

Looking at the sensitivities of the equations

$$\frac{\partial \bar{\sigma}_{VM}^2}{\partial \rho_e} = 2 \cdot \bar{\sigma}_1 \cdot \frac{\partial \bar{\sigma}_1}{\partial \rho_e} + 2 \cdot \bar{\sigma}_2 \cdot \frac{\partial \bar{\sigma}_2}{\partial \rho_e} - \bar{\sigma}_2 \cdot \frac{\partial \bar{\sigma}_1}{\partial \rho_e} - \bar{\sigma}_1 \cdot \frac{\partial \bar{\sigma}_2}{\partial \rho_e} + 6 \cdot \bar{\sigma}_3^2 \cdot \frac{\partial \bar{\sigma}_1}{\partial \rho_e}, \tag{5.11}$$

$$\frac{\partial \bar{\sigma}_H}{\partial \rho_e} = \frac{\partial \bar{\sigma}_1}{\partial \rho_e} + \frac{\partial \bar{\sigma}_2}{\partial \rho_e}, \tag{5.12}$$

$$\frac{\partial \phi}{\partial \rho_e} = \frac{\partial \bar{\sigma}_1}{\partial \rho_e} \cdot \bar{\varepsilon}_1 + \frac{\partial \bar{\sigma}_2}{\partial \rho_e} \cdot \bar{\varepsilon}_2 + \frac{\partial \bar{\sigma}_3}{\partial \rho_e} \cdot \bar{\varepsilon}_3, \tag{5.13}$$

For a strain field $\bar{\varepsilon} = [1,1,0]$,

[1] To simplify the Von Mises stress equations and sensitivity analysis, in this work Von Mises stress is evaluated by its square result $\sigma_{VM}^2$

$$\frac{\partial \phi}{\partial \rho_e} = \frac{\partial \bar{\sigma}_1}{\partial \rho_e} + \frac{\partial \bar{\sigma}_2}{\partial \rho_e}, \tag{5.14}$$

However, as discussed in chapter 0, when $\bar{\varepsilon} = [1,1,0]$, and the material has rotational symmetry then $C_{11} = C_{22}$, which leads to $\bar{\sigma}_1 = \bar{\sigma}_2$ and $\frac{\partial \bar{\sigma}_1}{\partial \rho_e} = \frac{\partial \bar{\sigma}_2}{\partial \rho_e}$. Also, when rotational symmetry exists $C_{13} = -C_{23}$, and therefore when $\bar{\varepsilon} = [1,1,0]$

$$\bar{\sigma}_3 = C_{13} + C_{23} + 0 \cdot C_{33} = 0, \tag{5.15}$$

This means that

$$\frac{\partial \bar{\sigma}_{VM}^2}{\partial \rho_e} = 2 \cdot \bar{\sigma}_1 \cdot \frac{\partial \bar{\sigma}_1}{\partial \rho_e}, \tag{5.16}$$

$$\frac{\partial \bar{\sigma}_H}{\partial \rho_e} = 2 \cdot \frac{\partial \bar{\sigma}_1}{\partial \rho_e}, \tag{5.17}$$

$$\frac{\partial \phi}{\partial \rho_e} = 2 \cdot \frac{\partial \bar{\sigma}_1}{\partial \rho_e} \tag{5.18}$$

So, the explanation for the identical designs is that the sensitivities of the optimization were parallel. In other words, the behaviour of the stiffness is equivalent to the average stress criterias.

This deduction opens an ill posed design problem.

After all, trying to maximize the solution stiffness while imposing parallel constraints, would make the convergence of the solution impossible.

For a strain field $\bar{\varepsilon} = [1,1,0]$,

$$\frac{\frac{\partial \phi}{\partial \rho_e}}{\frac{\partial \bar{\sigma}_{VM}^2}{\partial \rho_e}} = constant, \qquad \forall\, e \in [1, N] \tag{5.19}$$

Imposing this type of constraints would be equivalent to a maximum stiffness optimization with constraints on the maximum stiffness itself, which is not a well posed problem.

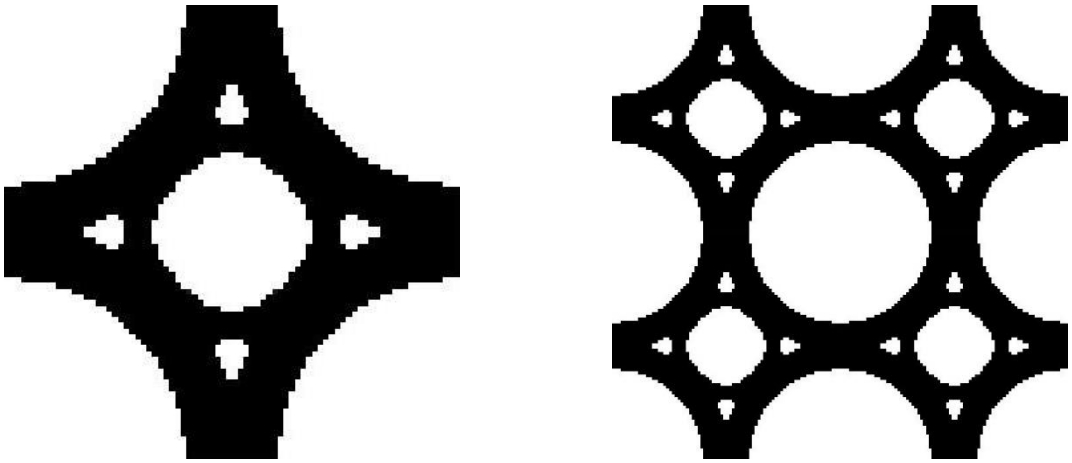

*Figure 5.52 - Material with Maximum $\bar{\sigma}_{VM}^2$ for $\bar{\varepsilon} = [1,1,0]$, obtained using Homogenization Approach, $\phi = 0.5593$, $\bar{\sigma}_{VM}^2 = 0.0782$, $\bar{\sigma}_H = 0.5593$, $r = 2$, $m = 0.4$, $\nu = 0.3$, $p = 8$, $mv = 0.1$, $N = 6400$, Optimality Criteria, SIMP*

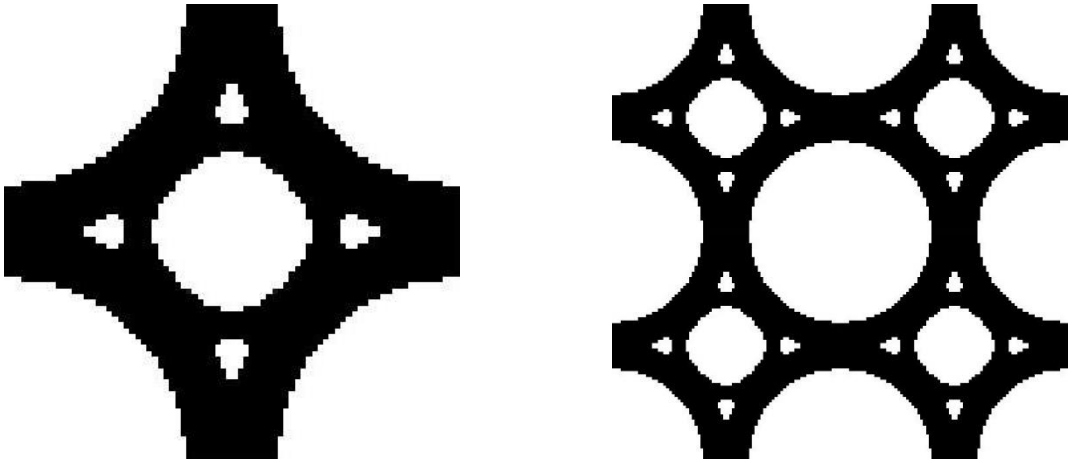

*Figure 5.53 - Material with Maximum $\bar{\sigma}_H$ for $\bar{\varepsilon} = [1,1,0]$, obtained using Homogenization Approach,$\phi = 0.5593$, $\bar{\sigma}_{VM}^2 = 0.0782$, $\bar{\sigma}_H = 0.5593$, $r = 2$, $m = 0.4$, $\nu = 0.3$, $p = 8$, $mv = 0.1$, $N = 6400$, OC, SIMP*

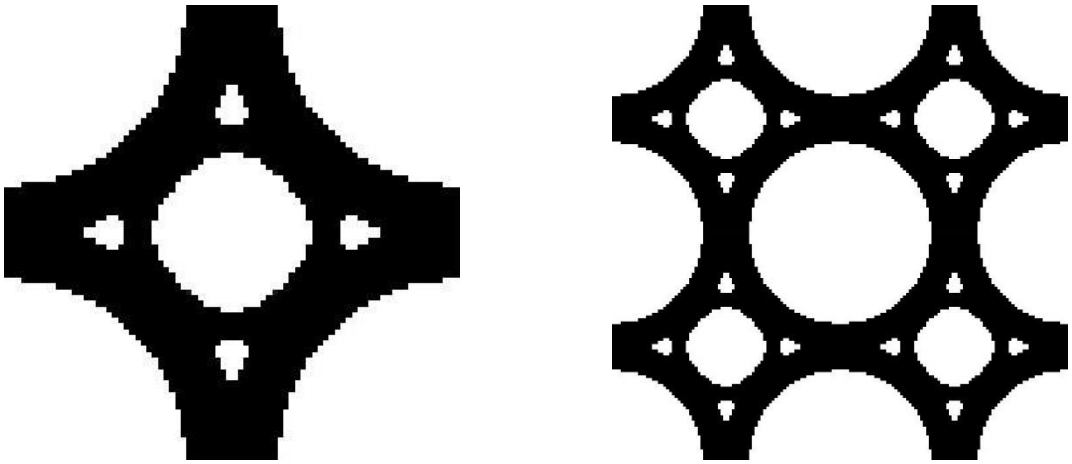

*Figure 5.54 - Material with Maximum $\phi$ for $\bar{\varepsilon} = [1,1,0]$, obtained using Homogenization Approach, $\phi = 0.5593$, $\bar{\sigma}_{VM}^2 = 0.0782$, $\bar{\sigma}_H = 0.5593$, $r = 2$, $m = 0.4$, $\nu = 0.3$, $p = 8$, $mv = 0.1$, $N = 6400$, OC, SIMP*

Imposing a different strain field, $\bar{\varepsilon} = [1,1.2,0]$, the maximum stiffness optimization problem with average Von Mises stress constraints was tackled.

As we can see in Figure 5.55 and Figure 5.56, this time the non-constrained maximization problems evolved to very different designs.

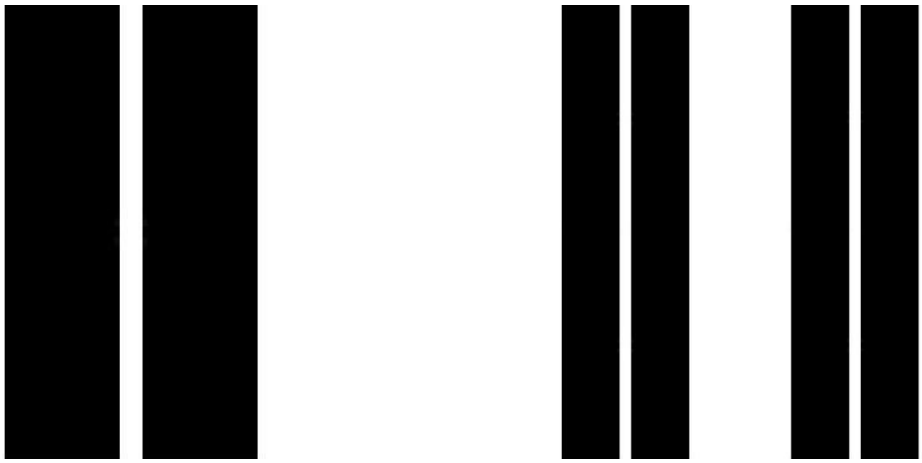

*Figure 5.55 - Material with Maximum $\bar{\sigma}_{VM}^2$ for $\bar{\varepsilon} = [1,1.2,0]$, obtained using Homogenization Approach, $\phi = 0.7243$, $\bar{\sigma}_{VM}^2 = 0.3596$,, $r = 2$, $m = 0.5$, $\nu = 0.3$, $p = 6$, $mv = 0.1$, $N = 6400$, OC, SIMP*

.

*Figure 5.56 - Material with Maximum $\phi$ for $\bar{\varepsilon} = [1,1.2,0]$, obtained using Homogenization Approach,$\phi = 0.8942$, $\bar{\sigma}_{VM}^2 = 0.1762$, $r = 2$, $m = 0.5$, $\nu = 0.3$, $p = 6$, $mv = 0.1$, $N = 6400$, OC, SIMP*

Since the ill posed parallel problem is not present, it becomes possible to solve this problem. Two different tests will be executed.

In one of the tests, a constraint on the maximum average Von Mises stress will be introduced. In other words, the objective is to limit the maximum average Von Mises stress, while at the same time maximizing the microstructure stiffness.

Since the maximum average Von Mises stress optimization evolved in to a distribution of material only on the vertical direction, an interesting problem would be to try maxing the material stiffness while

constraining the average Von Mises stress to be bigger than the obtained value in the maximum stiffness optimization, while at the same time not big enough to evolve in the vertical direction only.

The results are shown in Figure 5.57 and Figure 5.58.

In Figure 5.58, the constraint appears not to be active. However, it is important to notice that this happened after the filter was turned off. When the sensitivity filter was taken off the solution converged to the closest local maximum which increased the stiffness in a direction that also increased the average Von Mises stress, which is expected.

In Figure 5.57 the material with Maximum Stiffness and constrained Maximum Average Von Mises Stress is shown. However, this result is not an optimal material design. As it is seen, grey patches start to appear in the final design. The more rigid the constraints are, the greyer the solutions become. This is easily explained because of the intermediate density penalizations. The smallest possible average stress criteria values, happen for the homogeneous grey material, and it is to that state that the solutions start to converge when these constraints are implemented. This is a limitation of the computational model.

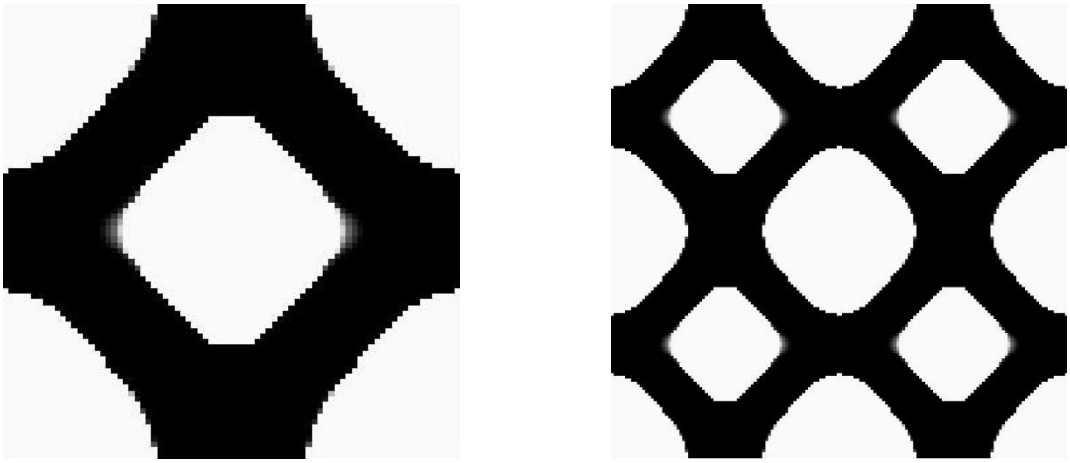

*Figure 5.57 - Material with Maximum $\phi$ for $\bar{\varepsilon} = [1,1.2,0]$ and $\bar{\sigma}_{VM}^2 \leq 0.14$, obtained using Homogenization Approach, $\phi = 0.8243$, $\bar{\sigma}_{VM}^2 = 0.1400$, $r = 2$, $m = 0.5$, $\nu = 0.3$, $p = 6$, $mv = 0.1$, $N = 6400$, MMA, SIMP*

*Figure 5.58 - Material with Maximum $\phi$ for $\bar{\varepsilon} = [1,1.2,0]$ and $\bar{\sigma}_{VM}^2 \geq 0.2$, obtained using Homogenization Approach, $\phi = 0.8769$, $\bar{\sigma}_{VM}^2 = 0.2120$, $r = 2$, $m = 0.5$, $\nu = 0.3$, $p = 6$, $mv = 0.1$, $N = 6400$, MMA, SIMP*

Some other stress fields were tested to verify if there was any other example that could be tested with Hydrostatic Stress constraints, however as we can see in Figure 5.59 and Figure 5.60, and Figure 5.61 and Figure 5.62, even though the results change slightly in design, the Hydrostatic Stress constraint remains too similar between the pair of solutions. It can be said that both the compliance and hydrostatic stress are very plane parameters. This means that, a small change in the designs, has little difference in these parameters values, making this problem very difficult to implement.

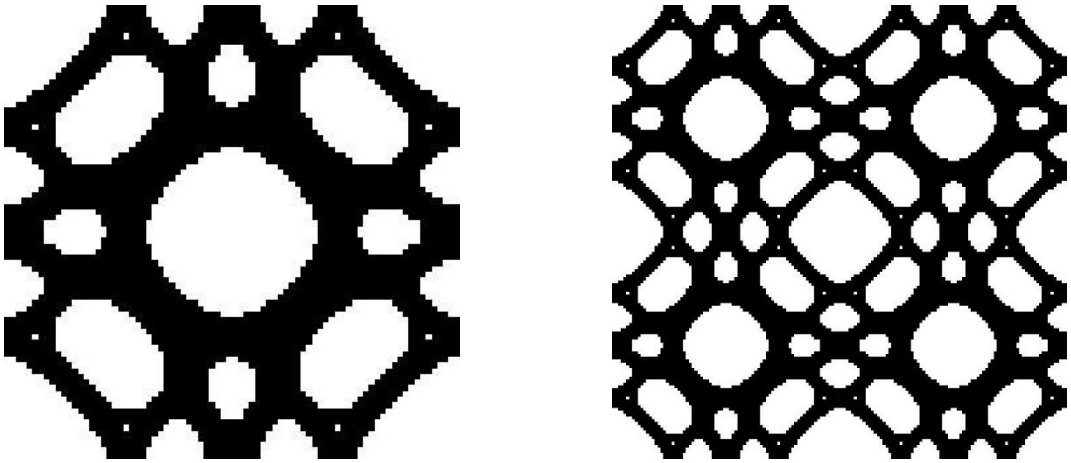

*Figure 5.59 - Material with Maximum $\phi$ for $\bar{\varepsilon} = [1,1,1]$, obtained using Homogenization Approach, $\phi = 0.8191$, $\bar{\sigma}_H = 0.7178$, $r = 2$, $m = 0.5$, $\nu = 0.3$, $p = 6$, $mv = 0.1$, $N = 6400$, MMA, SIMP*

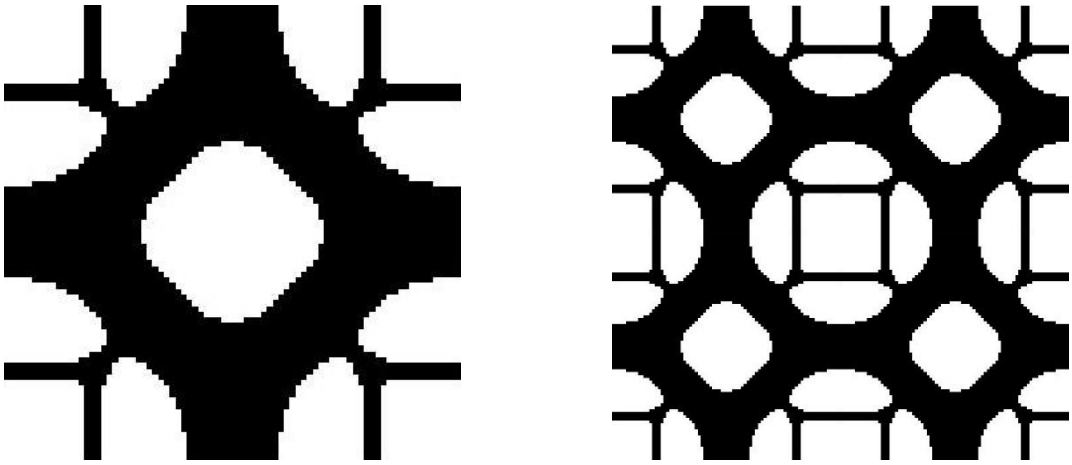

*Figure 5.60 - Material with Maximum $\bar{\sigma}_H$ for $\bar{\varepsilon} = [1,1,1]$, obtained using Homogenization Approach, $\phi = 0.7597$, $\bar{\sigma}_H = 0.7234$, $r = 2$, $m = 0.5$, $\nu = 0.3$, $p = 6$, $mv = 0.05$, $N = 6400$, MMA, SIMP*

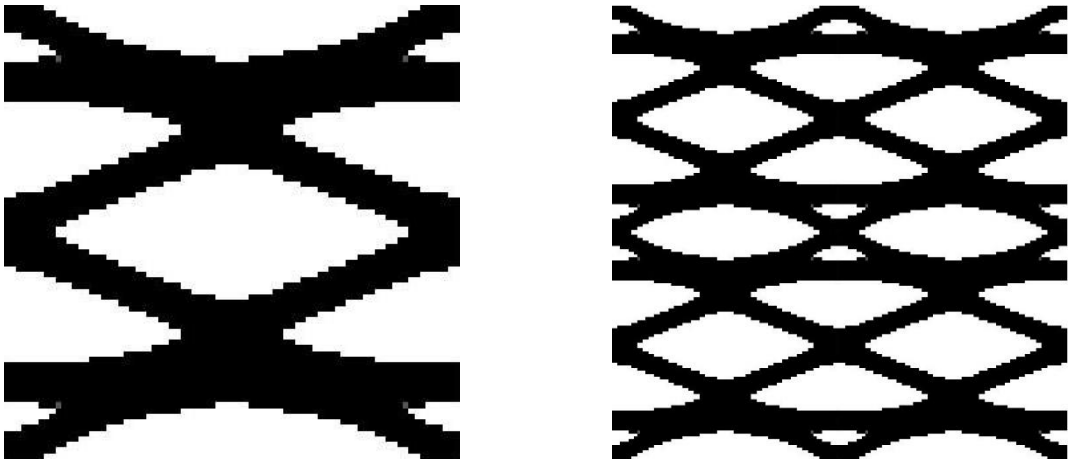

*Figure 5.61 - Material with Maximum $\phi$ $\bar{\varepsilon} = [1,0,1]$, obtained using Homogenization Approach, $\phi = 0.5051$, $\bar{\sigma}_H = 0.4907$, $r = 2$, $m = 0.5$, $\nu = 0.3$, $p = 6$, $mv = 0.1$, $N = 6400$, MMA, SIMP*

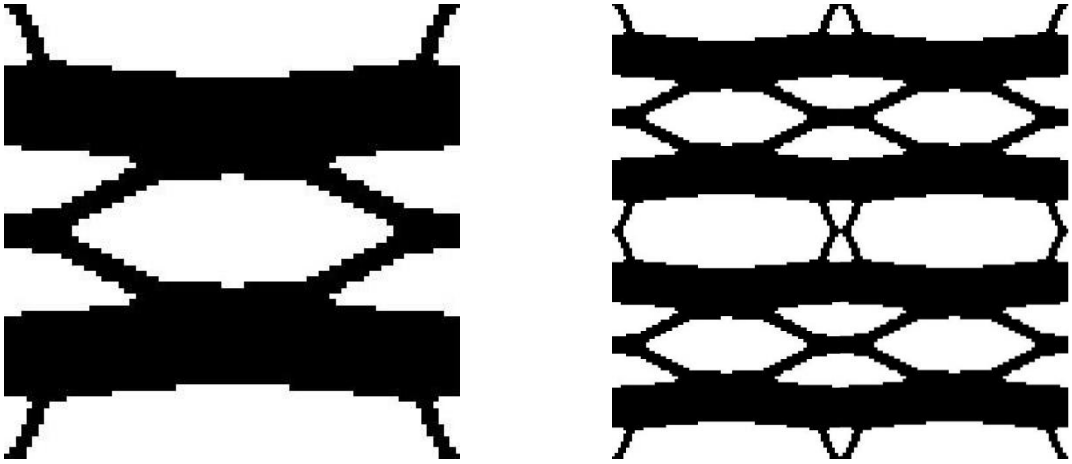

*Figure 5.62 – Material with Maximum $\bar{\sigma}_H$ for $\bar{\varepsilon} = [1,0,1]$, obtained using Homogenization Approach, $\phi = 0.4726$, $\bar{\sigma}_H = 0.4910$, $r = 2$, $m = 0.5$, $\nu = 0.3$, $p = 6$, $mv = 0.05$, $N = 6400$, MMA, SIMP*

# 5.15Minimize/Maximize Material properties with Stress Constraints

Stress constraints were difficult to implement in compliance maximization problems. However, when the optimization objective is not to find the stiffest designable material, then, the overall problems of the above chapter become non-existent.

In this chapter, it will be understood that it is possible to maximize or minimize material properties parameters while at same time introducing average stress criteria constraints. Evidently, the stress constraints are very similar to material stiffness constraints. After all, $\bar{\varepsilon}$ is an introduced term, and $\phi = \bar{\sigma} \cdot \bar{\varepsilon}$.

If the constraints are of the minimum allowed value type, then the problem is the design of a material with minimized/maximized properties that still maintains a certain degree of stiffness.

On the other hand, if the constraints are of the maximum allowed value type, then the problem is the design of a material with minimized/maximized properties that cannot have more than a certain degree of stiffness. However, whenever this type of constraint is used in stress criteria constraints the program will start converging to the grey zone. This was already explained as a problem of the intermediate density penalizations. The smallest possible average stress criteria value, happens for the homogeneous grey material, and it is to that state that the solution starts to converge when such constraints are introduced. If the stress constraint is however only a directional stress parameter then this problem doesn't exist as can be seen in Figure 5.66.

In Figure 5.64 and Figure 5.65 a problem of $C_{12}$ minimization with $\sigma_{VM}^2$ constraint is tackled. As can be seen, the higher the constraint, the stiffer the material and the bigger $C_{12}$ becomes. The constraints are active as expected.

In Figure 5.66 a problem of $C_{12}$ minimization with $\sigma_2$ constraint is presented. The constraint is also active. This constrain reduced the $C_{12}$ Value and the stiffness of the microstructure in vertical and horizontal direction compared to the solution in Figure 5.63. It was however expected an increase in the horizontal stiffness and a decrease in the vertical one.

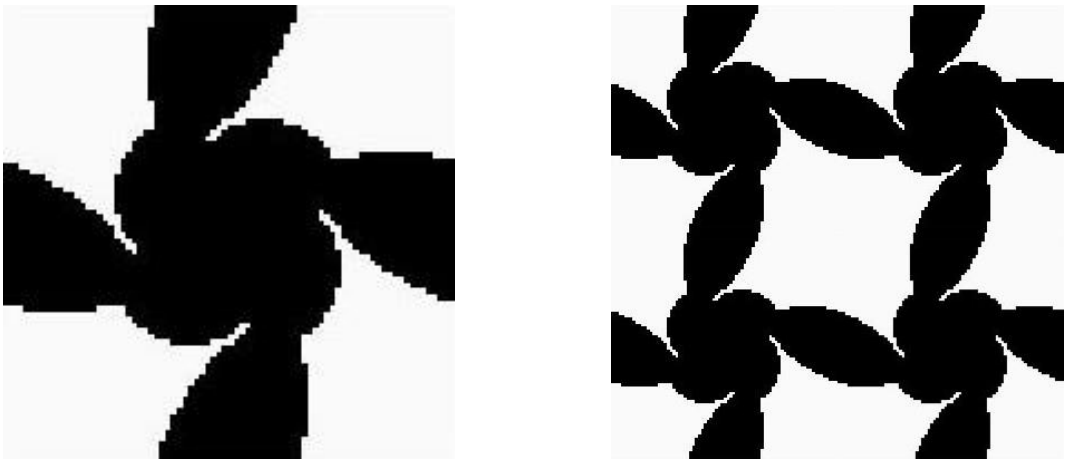

*Figure 5.63 - Material with Minimum $C_{12}$ obtained using Homogenization Approach for $\bar{\varepsilon} = [1,1,0]$, $\phi = 0.0988$, $\sigma_{VM}^2 = 0.0024$, $\sigma_H = 0.0988$, $C_{12} = -0.0535$, $r = 2$, $m = 0.5$, $\nu = 0.3$, $p = 6$, $mv = 0.1$, $N = 6400$, MMA, SIMP*

$$C_{ij} = \begin{bmatrix} 0.1029 & -0.0535 & 0.0265 \\ -0.0535 & 0.1029 & -0.0265 \\ 0.0265 & -0.0265 & 0.0132 \end{bmatrix}$$

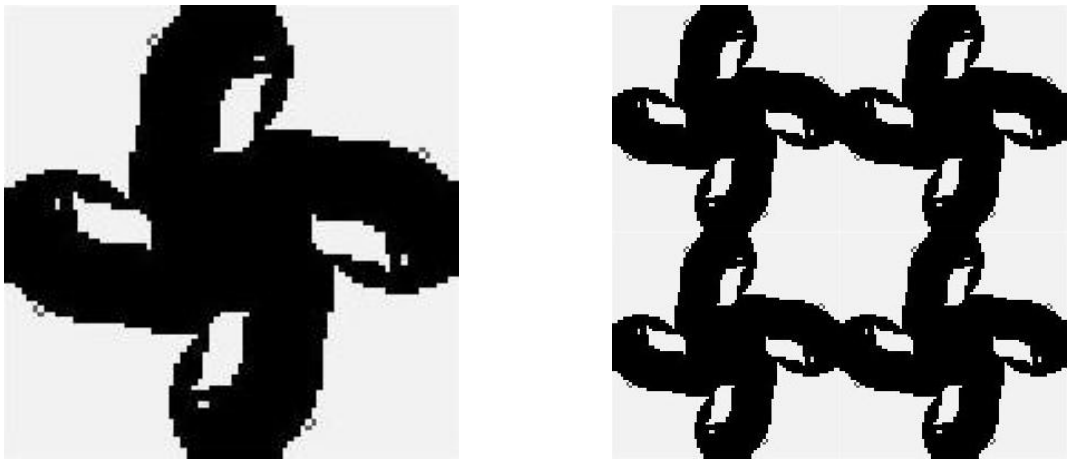

*Figure 5.64 - Material with Minimum $C_{12}$ and $\sigma_{VM}^2 \geq 0.2$ for $\bar{\varepsilon} = [1,1,0]$, obtained using Homogenization Approach, $\phi = 0.2828$, $\sigma_{VM}^2 = 0.0200$, $\sigma_H = 0.2828$, $C_{12} = -0.0250$, $r = 2$ ,$m = 0.5$, $\nu = 0.3$, $p = 6$, $mv = 0.1$, $N = 6400$, MMA, SIMP*

$$C_{ij} = \begin{bmatrix} 0.1662 & -0.0250 & 0.0210 \\ -0.0250 & 0.1662 & -0.0210 \\ 0.0210 & -0.0210 & 0.0131 \end{bmatrix}$$

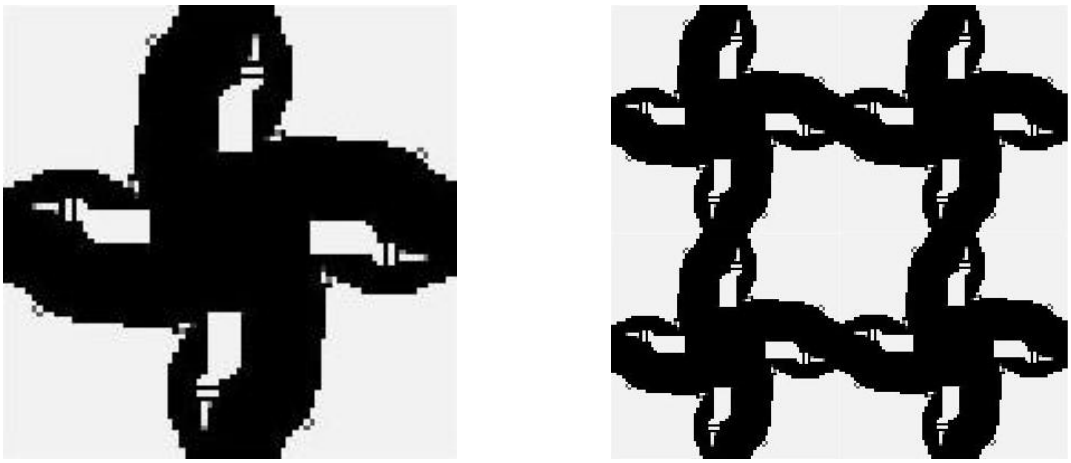

*Figure 5.65 - Material with Minimum $C_{12}$ and $\sigma_{VM}^2 \geq 0.3$ for $\bar{\varepsilon} = [1,1,0]$, obtained using Homogenization Approach, $\phi = 0.3465$, $\sigma_{VM}^2 = 0.0300$, $\sigma_H = 0.3465, C_{12} = -0.0142$, $r = 2$, $m = 0.5$, $\nu = 0.3$, $p = 6$, $mv = 0.1$, $N = 6400$, MMA, SIMP*

$$C_{ij} = \begin{bmatrix} 0.1874 & -0.0142 & 0.0178 \\ -0.0142 & 0.1874 & -0.0178 \\ 0.0178 & -0.0178 & 0.0130 \end{bmatrix}$$

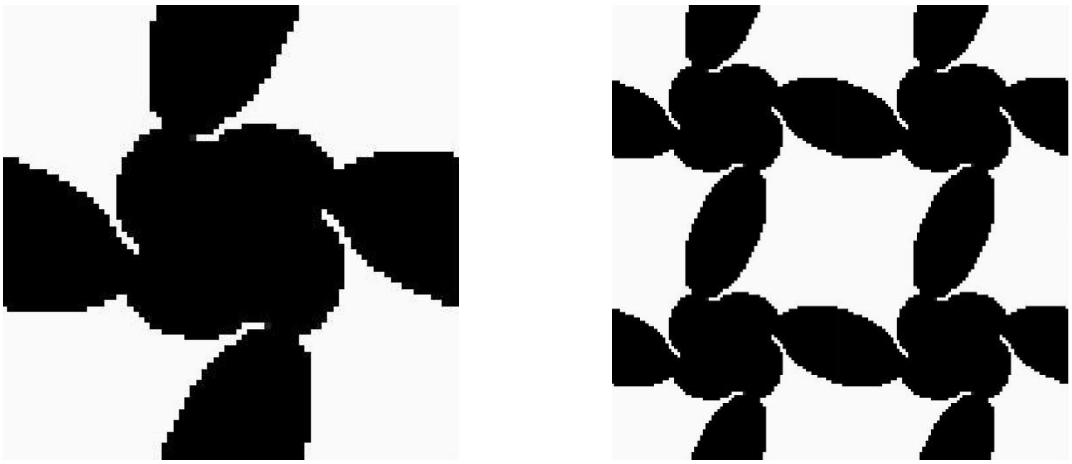

*Figure 5.66 - Material with Minimum $C_{12}$ and $\sigma_y \leq 0.02$ for $\bar{\varepsilon} = [1,1,0]$, obtained using Homogenization Approach, $\phi = 0.0683$, $\sigma_{VM}^2 = 0.0018$, $C_{12} - 0.0526$, $\sigma_y = 0.02$, $r = 2$, $m = 0.5$, $\nu = 0.3$, $p = 6$, $mv = 0.1$, $N = 6400$, MMA, SIMP*

$$C_{ij} = \begin{bmatrix} 0.1009 & -0.0526 & 0.0247 \\ -0.0526 & 0.0726 & -0.0226 \\ 0.0247 & -0.0226 & 0.0130 \end{bmatrix}$$

# 5.16Maximize Stiffness with single Directional Stress Constraints

In this chapter, materials with maximum stiffness and average directional Stress Constraints will be presented. Contrary to chapter 0, this type of optimization doesn't present the ill posed problems of parallel sensitivities. Having directional stress instead of stress criteria constraints, in a sense, adds some freedom to the optimizer.

Three different problems were tested.

The first problem consisted in an optimization of the material stiffness for an applied strain, $\bar{\varepsilon} = [1,0,0]$, while constraining the $\bar{\sigma}_2$ stress. This signifies that, by stretching the material in the horizontal direction, the vertical direction is tensioned or compressed depending on the $\sigma_2$ constraint. If the constraint is $\bar{\sigma}_2 \leq \bar{\sigma}_2^* \leq 0$, then the vertical direction is under compression, which means the designed material is auxetic. Figure 5.67 is an example of a material with high horizontal stiffness and auxetic properties.

On the other hand, if the constraint is $\bar{\sigma}_2 \geq \bar{\sigma}_2^* \geq 0$, then the vertical direction is under tension. In Figure 5.68 and Figure 5.69, we can see the results of this optimization, for $\bar{\sigma}_2 \geq 0.1$. In Figure 5.68 the initial guess was not symmetric which resulted in an non-symmetric and peculiar microstructure. In Figure 5.69 the initial guess was symmetric. Comparing both results to each other, it appears that Figure 5.68 has a slightly higher stiffness. However, the complexity of the microstructure is very high. Manufacturing such kind of cell would be extremely hard.

On Figure 5.70 a second problem was introduced. Instead of constraining $\bar{\sigma}_2$ to a scalar value, the objective is constraining $\bar{\sigma}_2$ in relation to $\bar{\sigma}_1$. The constraint applied was $\bar{\sigma}_2 \leq \bar{\sigma}_1/2$ . With this constraint, it can be said that both $\bar{\sigma}_1$ and $\bar{\sigma}_2$ are constrained. Since the strain applied is $\bar{\varepsilon} = [1,1,0]$, then $\phi = \bar{\sigma}_2 + \bar{\sigma}_1$. If the constraint is active, then the compliance could be calculated by $\phi = 3 \cdot \bar{\sigma}_2$ or $\phi = {}^{3}/_{2} \cdot \bar{\sigma}_1$. The program produced a very good result. There were some concerns that the constraint would be too rigid, however the computational model was successful in solving this problem.

The third problem is also an optimization of stiffness with $\bar{\sigma}_2$ stress constraints like in the first problem. However, the applied strain is $\bar{\varepsilon} = [1,1,0]$. This mean that the objective is the maximization of stiffness, $\phi = \bar{\sigma}_2 + \bar{\sigma}_1$, but with an imposed constraint on the vertical tension. Figure 5.71 represents the results from this kind of problem. The constraint applied was $\sigma_2 \leq 0.2262$, so that the results obtained could be compared to the results of Figure 5.70 where $\sigma_2 = 0.2262$.

As can be seen, Figure 5.71 is very similar to Figure 5.70. However even though the constraints are active, the results were not completely equal. The solution from Figure 5.70 is slightly stiffer than the solution in Figure 5.71, which is an interesting result because it was expected that the most rigid constraint would produce slightly worse results.

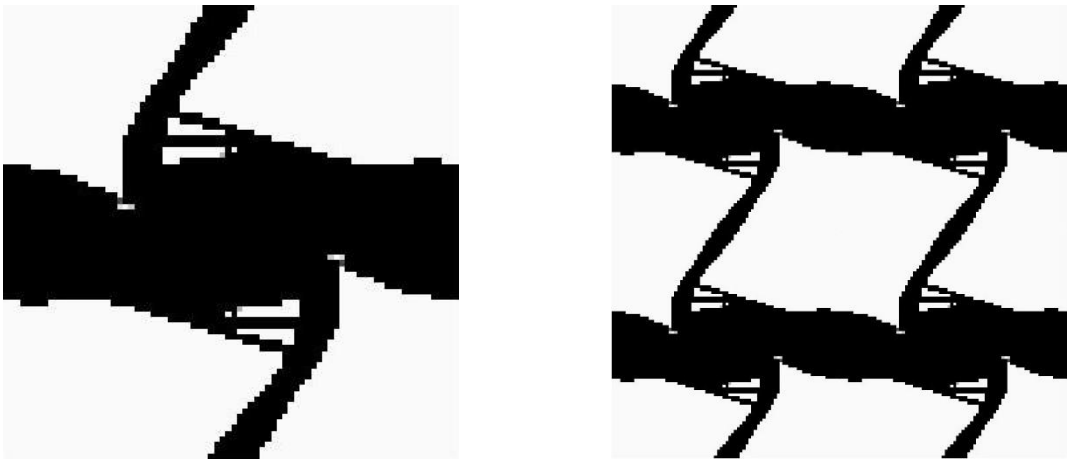

*Figure 5.67 - Material with Maximum $C_{11}$ and $\sigma_2 \leq -0.02$ for $\bar{\varepsilon} = [1,0,0]$, obtained using Homogenization Approach, $C_{11} = 0.2311, \sigma_2 = -0.0200$, $r = 2$, $m = 0.5$, $\nu = 0.3$, $p = 6$, $mv = 0.1$, $N = 6400$, MMA, SIMP*

$$C_{ij} = \begin{bmatrix} 0.2311 & -0.0200 & 0.0155 \\ -0.0200 & 0.0281 & -0.0166 \\ 0.0155 & -0.0166 & 0.0126 \end{bmatrix}$$

*Figure 5.68 - Material with Maximum $C_{11}$ and $\sigma_2 \geq 0.1$ for $\bar{\varepsilon} = [1,0,0]$, obtained using Homogenization Approach, $C_{11} = 0.3606, \sigma_2 = 0.1049$, $r = 2$, $m = 0.5$, $\nu = 0.3$, $p = 6$, $mv = 0.1$, $N = 6400$, MMA, SIMP*

$$C_{ij} = \begin{bmatrix} 0.3606 & 0.1049 & -0.0071 \\ 0.1049 & 0.0736 & 0.0054 \\ -0.0071 & 0.0054 & 0.0580 \end{bmatrix}$$

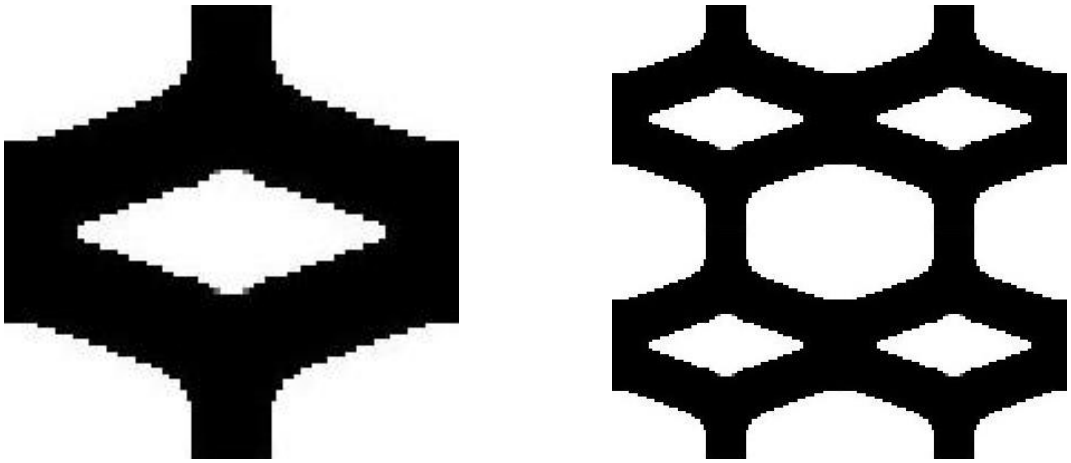

*Figure 5.69 - Material with Maximum $C_{11}$ and $\sigma_2 \geq 0.1$ for $\bar{\varepsilon} = [1,0,0]$, obtained using Homogenization Approach, $C_{11} = 0.3582, \sigma_2 = 0.1000$, $r = 2$, $m = 0.5$, $\nu = 0.3$, $p = 6$, $mv = 0.1$, $N = 6400$, MMA, SIMP*

$$C_{ij} = \begin{bmatrix} 0.3582 & 0.1000 & 0 \\ 0.1000 & 0.0989 & 0 \\ 0 & 0 & 0.3725 \end{bmatrix}$$

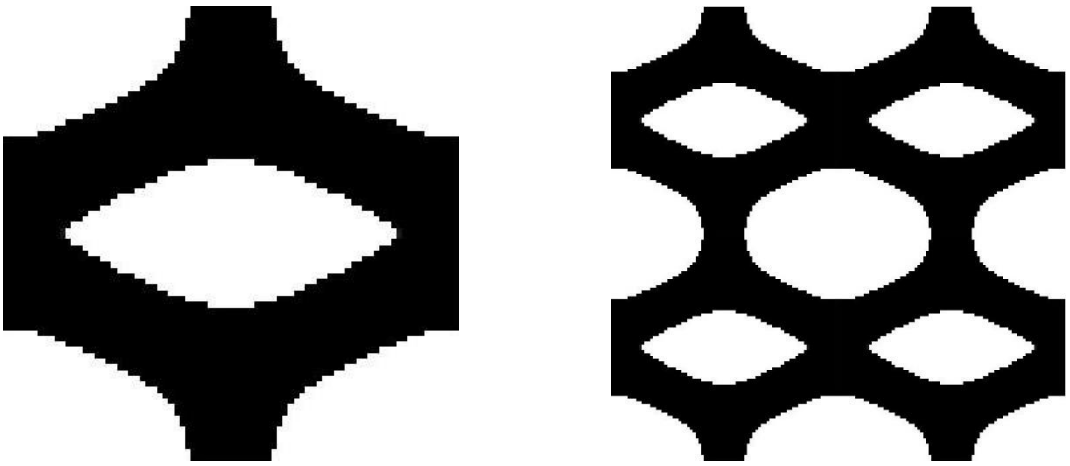

*Figure 5.70 - Material with Maximum $\phi$ for $\bar{\varepsilon} = [1,1,0]$ and $\sigma_2 \leq {}^{\sigma_1}/_2$, obtained using Homogenization Approach, $\phi = 0.6785, \sigma_2 = 0.2262$, $\sigma_1 = 0{,}4524$, $r = 2$, $m = 0.5$, $\nu = 0.3$, $p = 8$, $mv = 0.1$, $N = 6400$, MMA, SIMP*

$$C_{ij} = \begin{bmatrix} 0.3377 & 0.1147 & 0 \\ 0.1147 & 0.1115 & 0 \\ 0 & 0 & 0.0641 \end{bmatrix}$$

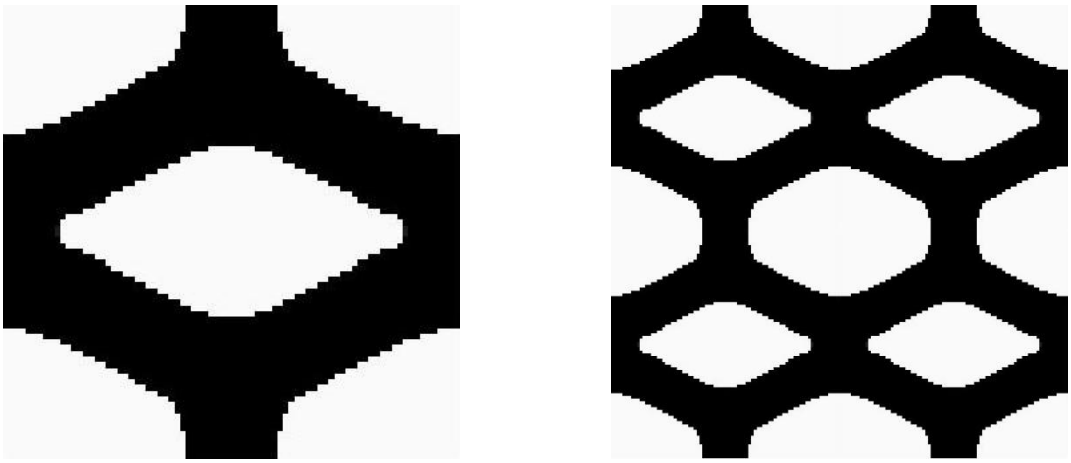

*Figure 5.71 - Material with Maximum $\phi$ for $\bar{\varepsilon} = [1,1,0]$ and $\sigma_2 \leq 0.2262$, obtained using Homogenization Approach, $\phi = 0.6643, \sigma_2 = 0.2262$, $r = 2$, $m = 0.5$, $\nu = 0.3$, $p = 8$, $m\nu = 0.1$, $N = 6400$, MMA, SIMP*

$$C_{ij} = \begin{bmatrix} 0.3197 & 0.1147 & 0 \\ 0.1184 & 0.1078 & 0 \\ 0 & 0 & 0.0674 \end{bmatrix}$$

# Chapter 6

# Conclusion

Even though Topology optimization in material design problems has been a big subject of discussion and investigation over the last 3 decades, there are still many problems and important innovations that need to be deepened. Many papers on material design already touched on subjects such as design of materials with prescribed properties or materials with extreme properties such as a higher stiffness.

The essence of this work was however, the combination of this subjects into a single design problem. A different approach, that may very well have a real interest in future investigations and or real-life applications

.

## 6.1 Summary

In this work, topology optimization ideas were studied and applied to material design problems. Structural Optimization, Homogenization theories and Finite Element practices were combined to produce a computational model that allowed for a wide array of design problems to be solved.

After discussing the general theory behind the methodology, the program was put to the test, firstly by solving non-constrained general problems, to verify the programs reliability and response to user programmable inputs. This first exercise was necessary step to understand which inputs should be introduced in the more complex constrained problems.

The advantages and successes of this work can be summarized:

- Creation of a very intuitive program with satisfactory performance;
- Varied problem-solving capabilities that can be adapted, for a wide range of strain fields and constraints at user's choice;
- Easy modification of the actual code for potential future research.

Although the many good points of the computational model, there also exist some flaws that need to be discussed:

- Some smoothness problems were detected in some constrained optimizations. This problems stem from the necessity of using constraints without filtering, since they are so sensitive that small errors introduced by the filtering would impair the optimization's solution;
- Stiffness Optimization problems with Average Stress Criteria's Constraints were hard to implement, since these optimizations were sometimes not a well posed problem depending on the imposed average strain fields;

- The intermediate density penalization, causes the convergence of the model to the grey zone, whenever the constraint is a limit on a maximum average stress criteria. Since intermediate densities are penalized then the least stiff material will occur for a homogeneous grey state. Since the average stress Criteria's behaviour is very similar to the stiffness, then the solution will start converging to that state.

To reduce the smoothness problems two approaches were used. Firstly, was to use a constraint filtering of sensitivities in the early iterations of the convergence and taking it away when the solution required an additional stability to converge. Secondly, using a previous converged solution as an initial guess to the constrained problem, also gave a smoothness improvement, although, at the expense of additional rigidity of the final results design.

## 6.2 Future Work

As described in Chapter 2, a decision was made to implement the computational model with $Q4$ Finite Elements. This decision was made on an early planning stage of the work. However, during later stages the smoothness problem was discovered. Although, using $Q4$ elements has given very satisfactory results, the introduction of $Q8$ or Q9 elements will probably give some attenuation of this problem, since the artificial stiffness given by checkerboard patterns in $Q4$ elements would not exist. However, this would mean a complete overhaul of the Finite Element implementation since every aspect, including Element Stiffness Matrix, connectivities and Boundary Conditions would need to be adapted to the new reality.

It would also be of major interest the implementation of the actual methodology in a $3D$ setting, and to compare the results between the $2D$ and $3D$ implementation.

# Bibliography


[1] A. G. M. Mitchell, “LVIII. The limits of economy of material in frame-structures.,” *The London, Edinburgh, and Dublin Philosophical Magazine and Journal of Science,* vol. 8, no. 47, pp. 589-597, 1904.

[2] M. P. Bendsøe and N. Kikuchi, “Generating optimal topologies in structural design using a homogenization method.,” *Computer methods in applied mechanics and engineering,* vol. 71, no. 2, pp. 197-224, 1988.

[3] M. P. Bendsøe, “Optimal shape design as a material distribution problem.,” *Structural and multidisciplinary optimization,* vol. 1(4), pp. 193-202, 1989.

[4] G. I. Rozvany, M. Zhou and T. Birker, “Generalized shape optimization without homogenization,” *Structural and Multidisciplinary Optimization,* vol. 4(3), pp. 250-252, 1992.

[5] M. P. Bendsøe and O. Sigmund, Topology Optimization, Theory Methods and Aplications, Berlin: Springer, 2003.

[6] L. Krog, A. Tucker, M. Kemp and R. Boyd, “Topology optimization of aircraft wing box ribs,” *10th AIAA/ISSMO multidisciplinary analysis and optimization conference,* pp. 1-11, 2004.

[7] H. A. Eschenauer and N. Olhoff, “Topology optimization of continuum structures: a review.,” *Applied Mechanics Reviews,* vol. 54(4), pp. 331-390, 2001.

[8] K. A. James, J. S. Hansen and J. R. R. A. Martins, “Structural topology optimization for multiple load cases using a dynamic aggregation technique.,” *Engineering Optimization,* vol. 41(12), pp. 1103-1118, 2009.

[9] A. R. Diaz and M. P. Bendsøe, “Shape optimization of structures for multiple loading conditions using a homogenization method,” *Structural and Multidisciplinary Optimization,* vol. 4(1), pp. 17-22, 1992.

[10] A. R. Díaz and N. Kikuchi, “Solutions to shape and topology eigenvalue optimization,” *International Journal for Numerical Methods in Engineering,* vol. 35(7), pp. 1487-1502, 1992.

[11] J. Du and N. Olhoff, “Topological design of freely vibrating continuum structures for,” *Structural and Multidisciplinary Optimization,* vol. 34(2), pp. 91-110, 2007.

[12] T. E. Bruns and D. A. Tortorelli, “Topology optimization of non-linear elastic structures and compliant mechanisms.,” *Computer Methods in Applied Mechanics and Engineering,* vol. 190(26), pp. 3443-3459, 2001.

[13] M. Frecker , N. Kikuchi and S. Kota, “Topology optimization of compliant mechanisms with multiple outputs.,” *Structural and Multidisciplinary Optimization,* vol. 17(4), pp. 269-278, 1999.

[14] J. S. Jensen and O. Sigmund, “Topology optimization of photonic crystal structures: a high-bandwidth low-loss t-junction waveguide.,” *JOSA B,* vol. 22(6), pp. 1191-1198, 2005.

[15] G. D. Cheng and X. Guo, “ε-relaxed approach in structural topology optimization.,” *Structural and Multidisciplinary Optimization,* vol. 13(4), pp. 258-266, 1997.

[16] P. Duysinx and O. Sigmund, “New developments in handling stress constraints in optimal material distribution.,” in *Proc of the 7th AIAA/USAF/NASAISSMO Symp on Multidisciplinary Analysis and Optimization*, St. Louis, Montana, U.S.A., 1998.

[17] J. T. Pereira, E. A. Fancello and C. S. Barcellos, “Topology optimization of continuum structures with material failure constraints.,” *Structural and Multidisciplinary Optimization,* vol. 26(1), pp. 50-66, 2004.

[18] M. Bruggi and P. Venini, “A mixed FEM approach to stress-constrained topology,” *International Journal for Numerical Methods in Engineering,* vol. 73(12), pp. 1693-1714, 2008.

[19] J. París, F. Navarrina, I. Colominas and M. Casteleiro, “Topology optimization of continuum structures with local and global stress constraints,” *Structural and Multidisciplinary Optimization,* vol. 39(4), pp. 419-437, 2009.

[20] J. M. Guedes and N. Kikuchi, “Preprocessing and postprocessing for materials based on the homogenization method with adaptive finite element methods.,” *Computer methods in applied mechanics and engineering,* vol. 83(2), pp. 143-198, 1990.

[21] M. M. Neves, H. C. Rodrigues and J. M. Guedes, “Optimal design of periodic linear elastic microstructures,” *Computers and Structures,* vol. 76, pp. 421-429, 2000.

[22] O. Sigmund, “Design of Material Structures Using Topology Optimization,” *PHD Thesis Technical University of Denmark,* 1994.

[23] O. Sigmund and S. Torquato, “Design of materials with extreme thermal expansion using a three-phase topology optimization method,” *Journal of the Mechanics and Physics of Solids,* vol. 45(6), pp. 1037-1067, 1997.

[24] O. Sigmund, “Materials with prescribed constitutive parameters: An inverse homogenization problem,” *International Journal of Solids and Structures,* vol. 31(17), pp. 2313-2329, 1994.

[25] O. Sigmund, “Tailoring materials with prescribed elastic properties,” *Mechanics of Materials,* vol. 20(4), pp. 351-368, 1995.

[26] E. Andreassen, B. S. Lazarov and O. Sigmund, “Design of manufacturable 3D extremal elastic microstructure,” *Mechanics of Materials,* vol. 69(1), pp. 1-10, 2014.

[27] E. N. Silva, J. O. Fonseca and N. Kikuchi, “Optimal design of piezoelectric microstructures,” *Computational mechanics,* vol. 19(5), pp. 397-410, 1997.

[28] C. F. Hvejsel and E. Lund, “Material interpolation schemes for unified topology and multi-material optimization,” *Structural and Multidisciplinary Optimization,* vol. 43(6), pp. 811-825, 2011.

[29] Z. Hashin and S. Shtrikman, “A variational approach to the theory of the effective magnetic permeability of multiphase materials,” *Journal of applied Physics,* vol. 33(10), pp. 3125-3131, 1962.

[30] O. Sigmund, “A 99 line topology optimization code written in Matlab,” *Structural and multidisciplinary optimization,* vol. 21, no. 2, pp. 120-127., 2001.

[31] G. Allaire, F. Jouve and A. M. Toader, “Structural optimization using sensitivity analysis and a level-set method,” *Journal of computational physics,* vol. 194(1), pp. 363-393, 2004.

[32] M. P. Bendsøe, “Optimization of structural topology, shape, and material,” vol. 414, Berlin, Heidelberg, New York, Springer, 1995.

[33] K. Svanberg, “The method of moving asymptotes - a new method for structural optimization,” *International journal for numerical methods in engineering,* vol. 24, no. 2, pp. 359-373, 1987.

[34] K. Svanberg, “MMA and GCMMA, versions September 2007,” *Optimization and Systems Theory,* vol. 104, 2007.

[35] P. L. Gould, Introduction to linear elasticity, New York: Springer, 1994.

[36] J. N. Reddy, An introduction to the finite element method, New York: McGraw-Hill, 1993.

[37] Z. Hashin, “Analysis of composite materials - A survey,” *Journal of Applied Mechanics,* vol. 50(2), pp. 481-505, 1983.

[38] W. Zhang, G. Dai, F. Wang, S. Sun and H. Bassir, “Using strain energy-based prediction of effective elastic properties in topology optimization of material microstructures,” *Acta Mechanica Sinica,* vol. 23(1), pp. 77-89, 2007.

[39] W. Zhang, F. Wang, G. Dai and S. Sun, “Topology Optimal Design of Material Microstructures Using Strain Energy-based Method,” *Chinese Journal of Aeronautics,* vol. 20(4), pp. 320-326, 2007.

[40] J. C. Michel, H. Moulinec and P. Suquet, “Effective properties of composite materials with periodic microstructure: A computational approach,” *Computer methods in applied mechanics and engineering,* Vols. 172(1-4), pp. 109-143, 1999.

[41] Z. Xia, Y. Zhang and F. Ellyin, “A unified periodical boundary conditions for representative volume elements of composites and applications,” *International Journal of Solids and Structures,* vol. 40(8), pp. 1907-1921, 2003.

[42] Z. Xia, C. Zhou, Q. Yong and X. Wang, “On selection of repeated unit cell model and application of unified periodic boundary conditions in micro-mechanical analysis of composites,” *International Journal of Solids and Structures,* vol. 43(2), pp. 266-278, 2006.

[43] L. Xia and P. Breitkopf, “Design of materials using topology optimization and energy-based homogenization approach in Matlab,” *Structural and multidisciplinary optimization,* vol. 52(6), pp. 1229-1241, 2015.

[44] B. Hassani and E. Hinton, “A review of homogenization and topology opimization II—analytical and numerical solution of homogenization equations,” *Computers & structures,* vol. 69(6), pp. 719-738, 1998.

[45] S. Amstutz, S. M. Giusti, A. A. Novotny and E. A. Souza Neto, “Topological derivative for multi-scale linear elasticity models applied to the synthesis of microstructures,” *International Journal for Numerical Methods in Engineering,* vol. 84(6), pp. 733-756, 2010.

[46] F. Wang, O. Sigmund and J. S. Jensen, “Design of materials with prescribed nonlinear properties,” *Journal of the Mechanics and Physics of Solids,* vol. 69, pp. 156-174, 2014.

[47] O. Sigmund, “A new class of extremal composites,” *Journal of the Mechanics and Physics of Solids,* vol. 48(2), pp. 397-428, 2000.

[48] L. V. Gibiansky and O. Sigmund, “Multiphase composites with extremal bulk modulus,” *Journal of the Mechanics and Physics of Solids,* vol. 48(3), pp. 461-498, 2000.